Blind Received Signal Strength Difference Based Source Localization with System Parameter Error and Sensor Position Uncertainty

by

Hannan Lohrasbipeydeh

A Dissertation Submitted in Partial Fulfillment of the
Requirements for the Degree of

DOCTOR OF PHILOSOPHY

in the Department of Electrical and Computer Engineering

Augest 2014
University of Victoria

Blind Received Signal Strength Difference Based Source Localization with System Parameter Error and Sensor Position Uncertainty

by

Hannan Lohrasbipeydeh

Supervisory Committee

Dr. T. Aaron Gulliver, Supervisor
(Department of Electrical and Computer Engineering)

Dr. Fayez Gebali, Departmental Member
(Department of Electrical and Computer Engineering)

Dr. George Tzanetakis, Outside Member
(Department of Computer Science)

ABSTRACT

Passive source localization in wireless sensor networks (WSNs) is an important field of research with numerous applications in signal processing and wireless communications. One purpose of a WSN is to determine the position of a signal emitted from a source. This position is estimated based on received noisy measurements from sensors (anchor nodes) that are distributed over a geographical area. In most cases, the sensor positions are assumed to be known exactly, which is not always reasonable. Even if the sensor positions are measured initially, they can change over time.

Due to the sensitivity of source location estimation accuracy with respect to the *a priori* sensor position information, the source location estimates obtained can vary significantly regardless of the localization method used. Therefore, the sensor position uncertainty should be considered to obtain accurate estimates. Among the many localization approaches, signal strength based methods have the advantages of low cost and simple implementation. The received signal energy mainly depends on the transmitted power and path loss exponent which are often unknown in practical scenarios.

In this dissertation, three received signal strength difference (RSSD) based methods are presented to localize a source with unknown transmit power. A nonlinear RSSD-based model is formulated for systems perturbed by noise. First, an effective low complexity constrained weighted least squares (CWLS) technique in the presence of sensor uncertainty is derived to obtain a least squares initial estimate (LSIE) of the source location. Then, this estimate is improved using a computationally efficient Newton method. The Cramér-Rao lower bound (CRLB) is derived to determine the effect of sensor location uncertainties on the source location estimate. Results are presented which show that the proposed method achieves the CRLB when the signal to noise ratio (SNR) is sufficiently high.

Least squares (LS) based methods are typically used to obtain the location estimate that minimizes the data vector error instead of directly minimizing the unknown parameter estimation error. This can result in poor performance, particularly in noisy environments, due to bias and variance in the location estimate. Thus, an efficient two stage estimator is proposed here. First, a minimax optimization problem is developed to minimize the mean square error (MSE) of the proposed RSSD-based model. Then semidefinite relaxation is employed to transform this nonconvex and nonlinear problem into a convex optimization problem. This can be solved efficiently to obtain

the optimal solution of the corresponding semidefinite programming (SDP) problem. Performance results are presented which confirm the efficiency of the proposed method which achieves the CRLB.

Finally, an extended total least squares (ETLS) method is developed for blind localization which considers perturbations in the system parameters as well as the constraints imposed by the relation between the observation matrix and data vector. The corresponding nonlinear and nonconvex RSSD-based localization problem is then transformed to an ETLS problem with fewer constraints. This is transformed to a convex semidefinite programming (SDP) problem using relaxation. The proposed ETLS-SDP method is extended to the case with an unknown path loss exponent. The mean squared error (MSE) and corresponding CRLB are derived as performance benchmarks. Performance results are presented which show that the RSSD-based ETLS-SDP method attains the CRLB for a sufficiently large SNR.

Contents

List of Tables

List of Figures

ABBREVIATIONS

AOA	Angle of arrival
BLUE	Best linear unbiased estimator
CLS	Constrained least squares
CRLB	Cramér-Rao lower bound
CWLS	Constrained weighted least squares
ETLS	Extended total least squares
FIM	Fisher information matrix
FLOP	Floating point operation
GTRS	Generalized trust region subproblem
iid	Independent and identically distributed
LCJE	Low complexity joint estimator
LLS	Linear least squares
LMI	Linear matrix inequalities
LS	Least squares
LSIE	Least squares initial estimation
LSIE-NM	Least squares initial estimation - Newton method
MAP	Maximum *a posteriori*
MLE	Maximum likelihood
ML	Maximum likelihood estimator
MSE	Mean squared error
NLS	Nonlinear least squares
NM	Newton method
PD	Positive definite
PDF	Probability density function
PLE	Path loss exponent

PSD	Positive semidefinite
RMSE	Root mean squared error
RSS	Received signal strength
RSSD	Received signal strength difference
RTLS	Regularized total least squares
SDP	Semidefinite programming
SDR	Semidefinite relaxation
SNR	Signal to noise ratio
TDOA	Time difference of arrival
TLS	Total least squares
TOA	Time of arrival
UAV	Unmanned aerial vehicle
UT	Unscented transformation
WLS	Weighted least squares
WSN	Wireless sensor network

ACKNOWLEDGEMENTS

First and foremost, I would like to thank **God**, the Almighty, for giving me the strength, motivation and courage to do this work. Thank you for being the best teacher I have ever had as your patience and foresight are beyond measure.

I would like to express my gratitude to **Dr. T. Aaron Gulliver**, my supervisor, for his extremely constructive and detailed comments during my PhD study. Moreover, I would like to thank him for the patient guidance, encouragement and advice he has provided throughout my time as his student. He helped me to be a better and more professional researcher.

I would also like to express my deep gratitude to my MASc supervisor, **Dr. Hamidreza Amindavar**, who cared deeply about me and my work. I thank him for all his valuable suggestions and comments during my MASc and PhD programs and wish the best for him 'inshaallah'.

I also owe many thanks to **Dr. Fayez Gebali** for his support and kind consideration both as department chair and supervisory committee member. I would also like to thank the staff members of the Department of Electrical and Computer Engineering for their help during my studies. Further, I would like to thank **Dr. George Tzanetakis** and **Dr. Payman Arabshahi** for their many excellent comments and suggestions on my work.

I would like also to thank **Mrs. Zahra Mortazavi** for all her kind support and scarification during my PhD study.

Finally, a very special thanks to **Tom Dakin**, my supervisor at Ocean Networks Canada (ONC) for both his scientific help and encouragement during my PhD study. It was my pleasure and great honour to work at ONC. I would also like to thank **Scott McLean** for his kind support.

Learn from yesterday, live for today, hope for tomorrow.
The important thing is to not stop questioning.
Albert Einstein, Relativity: The Special and the General Theory

DEDICATION

I dedicate this dissertation to my family, especially my Dad and Mom who passed away during my PhD study for instilling the importance of hard work and higher education and all their encouragement.

Chapter 1

Introduction

1.1 Source Localization with a Wireless Sensor Network

The localization problem in wireless sensor networks (WSNs) has received significant attention over the past two decades [1]-[6]. Wireless communication technological progress in hardware and software have led to numerous applications of wireless networks for industrial, commercial and personal use.

Positioning an unknown source (sensor node) in a WSN has a wide range of applications in many fields such as emergency services, mobile communications, public safety and intelligent transportation [7]-[12]. As an example, the signals sent to the central monitoring system in a wireless network of sensor should include the location information of the corresponding phenomenon. The main purpose of a WSN is to determine the position of a signal emitted from a source based on received noisy measurements from sensors (anchor nodes) that are distributed over a geographical area.

Sensors are typically small, inexpensive devices with limited communication and processing capabilities [2],[6]. As a result, the measured values from the WSN are sent to a signal processing center in order to estimate the unknown source location. In addition, *a priori* information of the sensor positions (node or anchor) can affect the efficiency of the network in terms of the accuracy of the estimated location.

Figures 1.1 and 1.2 present some of the energy based source localization scenarios which respectively can be considered for wireless or underwater applications. In most cases the transmitted power is not known *a priori* which makes the localization

Figure 1.1: Wireless energy based source localization applications.

problem more complex. As an example, in marine mammal and ship tracking cases, the transmitted power changes from one case to another depending on the transmitted source energy. Furthermore, the sensor location can have position errors.

Due to the accuracy of *a priori* sensor position information, the source location estimates obtained can vary significantly regardless of the localization method used. In most cases, the sensor positions are assumed to be known exactly, which is not reasonable. Even if the sensor positions are measured initially, they can change over time. For example, unmanned aerial vehicles (UAVs) are employed in several emerging applications and are constantly in motion. Therefore, sensor position uncertainty should be considered when developing practical location estimation techniques.

1.2 Example of Energy based Data

In this section, three examples of real signals are described which are applications of the energy based model. First, a sperm whale acoustic sound model is described as an example of marine mammal localization. Next, a diver acoustic signal is presented

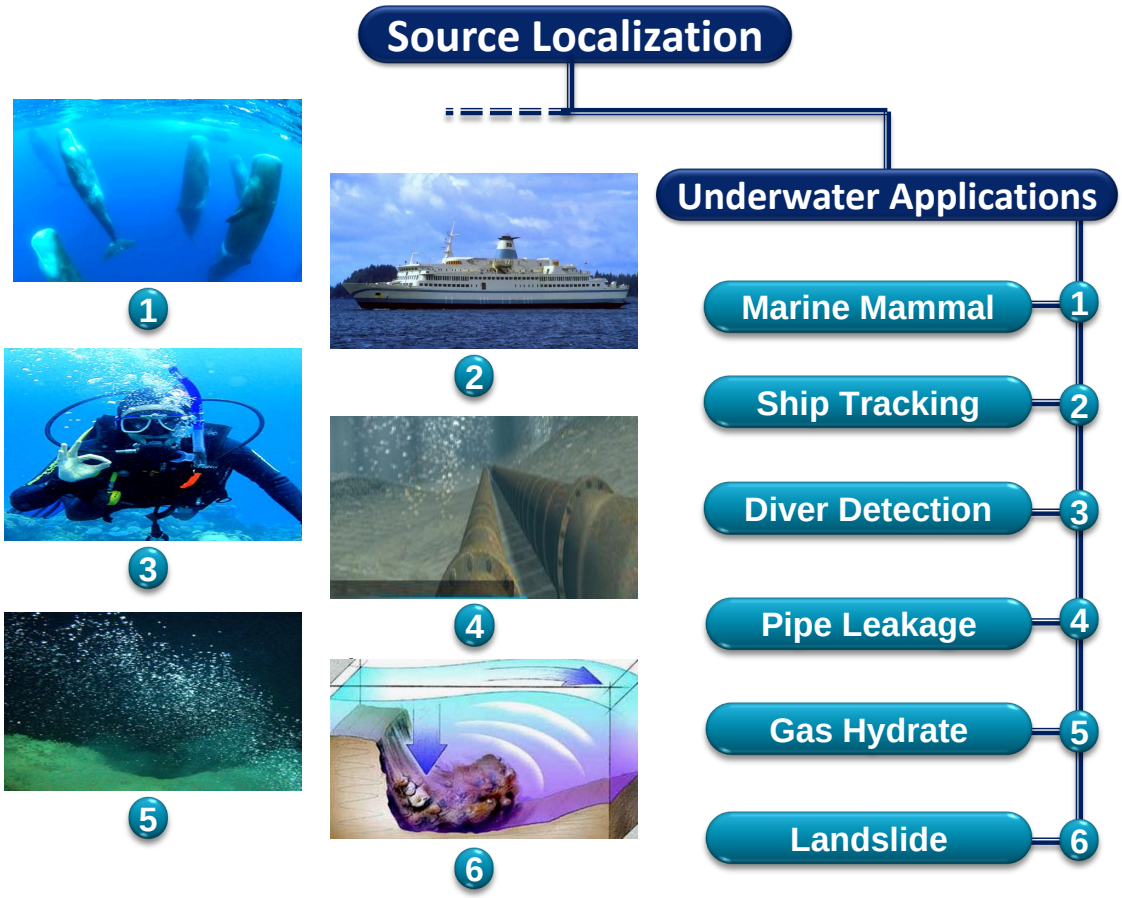

Figure 1.2: Underwater energy based source localization applications.

which was recorded in the ocean. Finally, pipe leakage experimental data is shown which was recorded at the Marine Technology Center (MTC).

1.2.1 Sperm Whale Acoustic Data

Sperm whales (Physeter macrocephalus) are prodigious divers and can reach vertical depths of up to 2 km in search of food such as squid and fish. They remain on the sea surface for approximately 10 min for breathing and then dive from 30 to 90 min before returning to the sea surface. They generate a train of impulsive acoustic signals called clicks that can be categorized as usual click or creak clicks. These clicks are used for echolocation purposes and communication with other sperm whales [13]-[19]. Echolocation signals can be used to investigate the behaviour of sperm whales. They produce these signals primarily when diving and searching for prey. If prey are present, the click rate is increased to approximately 10 clicks per second. The

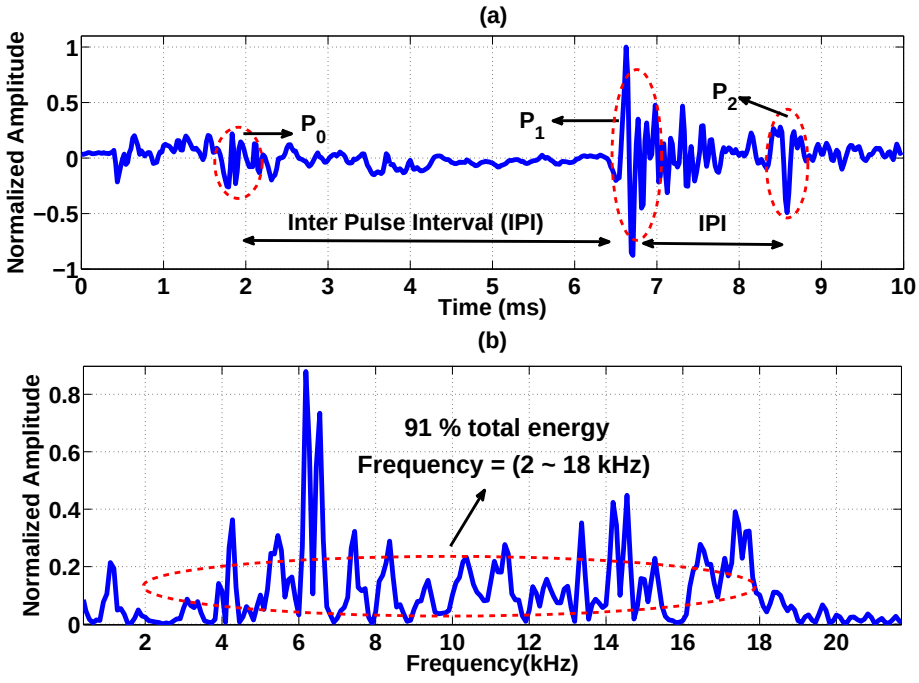

Figure 1.3: Click structure (a) time domain, and (b) power spectral density (PSD).

duration of these signals depends on the sperm whale size and varies from 10 to 20 ms. They are generated using the spermaceti compartments and passages located in the head of the whale. The corresponding signals are shown in Fig. 1.3. Note that the signal structure is obtained from real sperm whale data provided by the Atlantic Undersea Test and Evaluation Center (AUTEC).

The museau de signe in the sperm whale head forces air through the right nasal passage which generates the click signals. A small portion of the signal energy is released immediately producing an initial pulse P_0. The frontal sac lies near the cranium and acts like a reflector sending signals back through the junk, which creates a second pulse P_1. A portion of the signal energy is reflected back to the distal air sac from the spermaceti organ, resulting in a third pulse P_2. Hence, each click has a pattern consisting of several pulses with short time intervals between them as it is shown in Fig. 1.3. The power spectral density of the click shows that the most of the click signal energy (approximately 91% in this example), is located between 2 kHz and 18 kHz.

1.2.2 Diver Acoustic Signal

Protection of commercial and military harbour facilities from malicious divers has been an important challenge for several decades. In fact, these divers can cause serious damage to coastal infrastructure such as ports, power plants, oil tanks, refineries, and bridges. In commercial applications, diver health is an important consideration and thus monitoring heart rates and stress levels is of considerable interest. Passive acoustic methods are an important and useful class of techniques for processing underwater signals. They can be used to detect, estimate and classify divers based on the acoustic signals generated by diver breathing underwater. These signals can propagate over very long distances and thus can be observed from far away. The problem of vessel engine and biological signal detection has been examined in the literature, but diver signals have very different characteristics and they typically have lower power levels. In this section, an experimental presentation of the acoustic signal from a diver is shown. Data was recorded for vertical and horizontal dives in the Sannich Inlet near Victoria, BC, Canada over a period of two hours in July, 2013. The vertical diving was done for depths from 5 to 25 m depth at 5m intervals. The horizontal diving was done at 4 different distances at a depth of 5 m. Accurate low and high frequency hydrophones were employed to capture the signals created by the

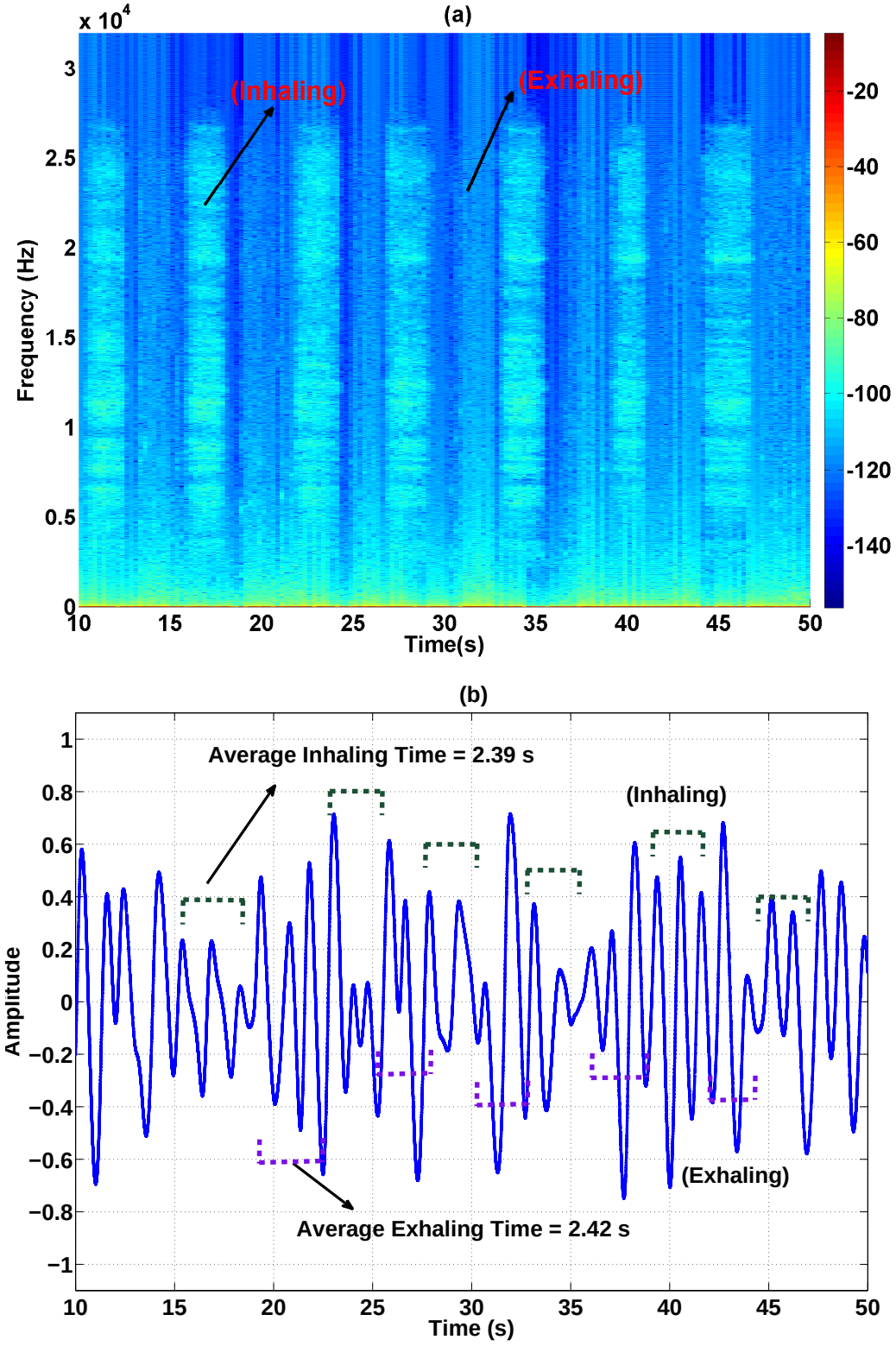

Figure 1.4: A typical (a) spectrogram of the acoustic signal from a diver in the ocean, and (b) time domain characteristics of the inhaling and exhaling signals.

open breathing system of the diver.

Figure 1.4.(a) presents the time-frequency spectrogram of the diver data recorded using each hydrophone separately over a one hour diving period. The time domain acoustic signal due to breathing can be considered to be periodic with low and high frequency characteristics as shown in Fig. 1.4.(b). This signal is produced by the inhaling and exhaling of the diver and so the periodicity is due to the breathing rate. Figure 1.4 shows that there is less acoustic energy when a diver is inhaling than when exhaling. The high frequency components of the signal are mainly due to air flowing from the tank to the regulator valve, while the low frequency components are due to the release of compressed air into the water when exhaling.

1.2.3 Pipe Leakage Experimental Data

The behaviour of bubbles in water is an important research topic that is applicable to engineering and marine projects such as gas hydrate detection and underwater source localization. These bubbles come from different sources such as breaking waves, natural ocean sources and cavitation produced by ship or submarine propellers. The bubble surface oscillation produces an acoustic signal which can be characterized as a damped sinusoid. The damping coefficients of this signal consists of radiation, viscosity and thermal coefficients. The signal produced by a single bubble has low energy, but a train of bubbles has a much larger signal level which is suitable for passive sensing applications. The bubbles can be generated in a controlled way by a nozzle, or in an uncontrolled manner by a leaking underwater gas line or a natural source. In order to develop a model for pipe leakage detection, controlled bubble experiments were conducted underwater. The bubbles were generated using a horizontal pipe with a number of holes drilled into it. A low frequency hydrophone was located two meters perpendicular from the center of the pipe.

The experiments were conducted in a pool of depth 4 m at the Marine Technology Center (MTC) of Ocean Networks Canada (ONC). Each experiment was conducted twice to ensure the accuracy of the measurement results. A single bubble injected into water generates an acoustic signal due to its surface oscillations and volume pulsations. The acoustic signal generated by this bubble can be expressed as

$$s(t) = Ke^{-2\pi\beta f_0 t}\sin(2\pi f_0 t), \qquad 0 \leq t \leq T, \tag{1.1}$$

where K is the amplitude, T is the effective time interval during which the bubble

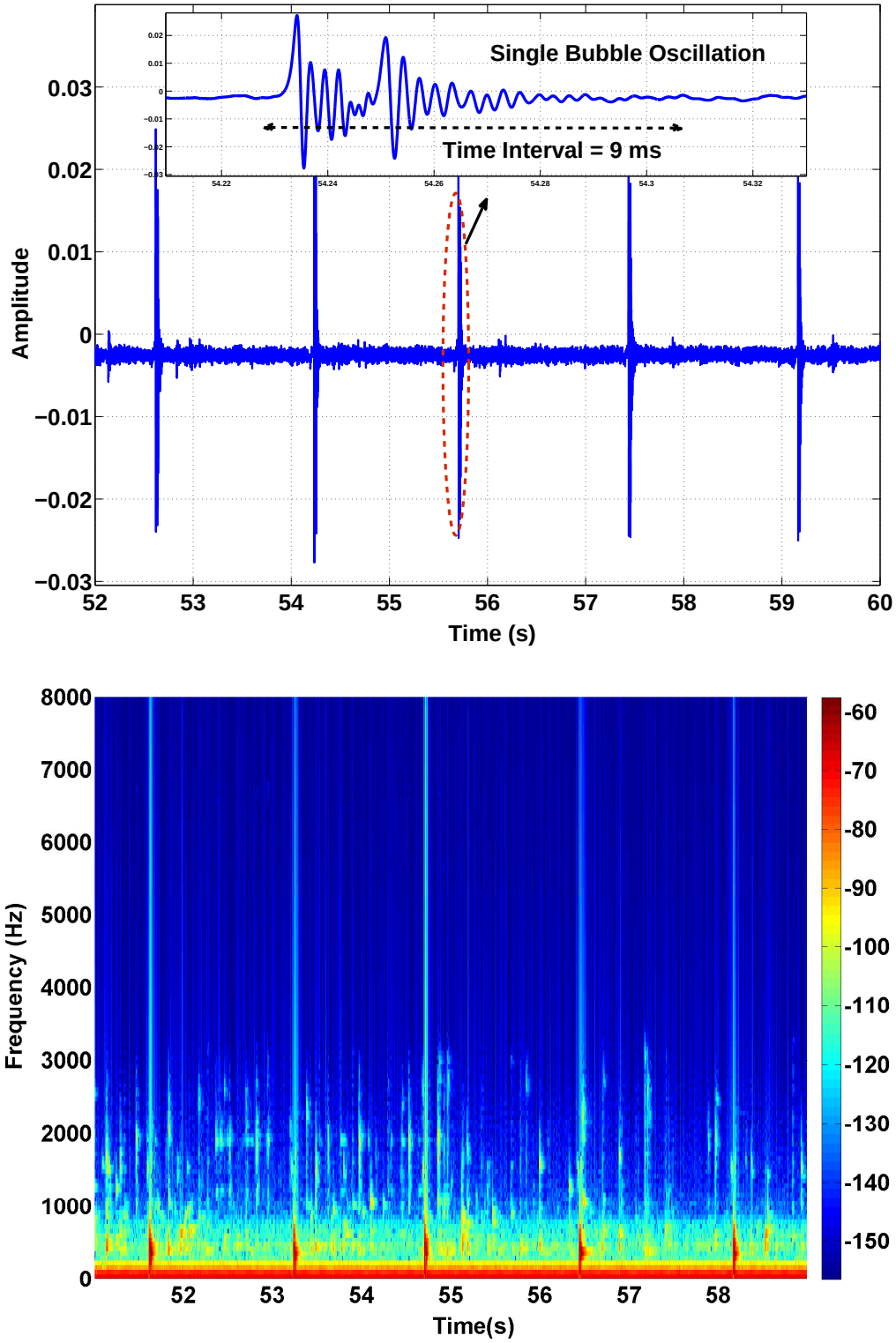

Figure 1.5: Time domain signal and spectrogram of a single bubble injected in water from a hole with diameter 5/32 in.

oscillates, β is the damping factor and f_0 is the central frequency of the oscillations known as the Minnaert volume oscillation frequency. This frequency is given by

$$f_0 = \frac{1}{2\pi r}\sqrt{\frac{3\gamma P}{\rho}}, \tag{1.2}$$

where ρ is the density of the liquid, r is the bubble radius, γ is the specific heat ratio of the air inside the bubble to that of the surrounding water, and P is the ambient pressure. Figure 1.5 shows the time domain signal and spectrogram of a single bubble injected from a hole with diameter 5/32 in. These results indicate that most of the signal energy is present at frequencies below 1500 Hz. Thus a filter can be designed for detection purposes that passes only the predominant frequencies.

Figure 1.5 shows that the bubble produces a damped sinusoidal signal with an interval of approximately 9 ms which matches the acoustic signal model in (1.1). The time domain signal and spectrogram of a train of bubbles injected from a hole with diameter 5/32 in is presented in Fig. 1.6. Increasing the number of holes results in a significant increase in the received signal energy. This will provide better detection in an underwater environment. Note that most of the energy in the train of bubbles is located below 1500 Hz as shown in Fig. 1.6.

1.3 Contributions

The contributions of this dissertation are summarized as follow:

1. The problem of RSSD-based source localization is formulated and the results are extended to the RSSD-based measurement model in presence of sensor position uncertainty.

2. The CRLB of the RSSD-based measurement model is derived and the results are extended to the case of correlated measurements. Furthermore, the CRLB of the RSSD-based model is extended to the general case with sensor position uncertainty.

3. A new LSIE-NM algorithm is developed for source localization in an unknown channel for both the near field and far field cases considering the sensor position uncertainty.

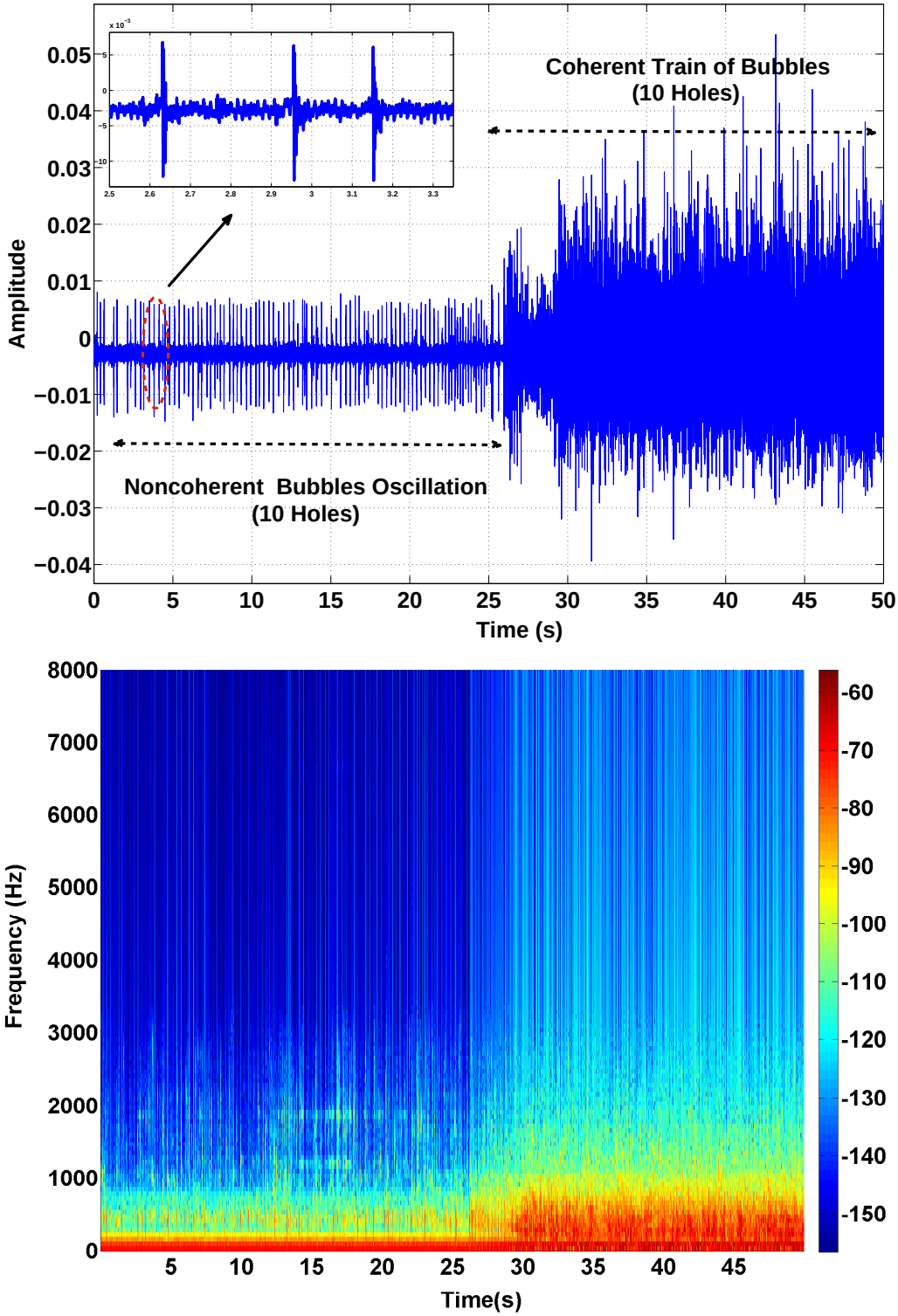

Figure 1.6: Time domain signal and spectrogram of a trains of bubbles injected in water from a hole with diameter 5/32 in.

4. The performance of the proposed LSIE-NM is analysed by deriving the bias of the system and simulation results are obtained considering the effect of the number of sensors, path loss exponent and noise power.

5. A new Minimax-MSE method is developed for RSSD localization for the near field scenario with improved accuracy and this is extended to the blind channel case.

6. A new ETLS-SDP localization algorithm is developed for the near field scenario with high accuracy for the blind channel case considering the system parameter error.

7. The ETLS-SDP method is extended to the unknown channel case with random and deterministic path loss exponents.

8. The performance of the ETLS-SDP method is analysed by developing the MSE analysis and also considering the effect of higher order error terms. The results are compared through simulation in terms of the path loss exponent and noise power.

9. The complexity of the proposed LSIE-NM, ETLS-SDP and minimax-SDP methods are obtained analytically and compared with state of the art methods in the literature.

1.4 Scope and Dissertation Outline

Chapter 2 In this chapter, the background of the energy based model is described. The motivation for energy based localization is given and the time and energy based models are compared in terms of the complexity and efficiency. The related energy based methods in the literature are also considered in this section and their drawbacks are described.

Chapter 3 In this chapter, an RSSD measurement model is formulated for source localization in the presence of sensor position errors. Since only RSSD measurements are employed in the proposed approach, *a priori* knowledge of the source transmit power is not required. The received power is assumed to follow an exponential decay model that is a function of the path loss, transmit power

and distance between the sensor and source [4]. The source location is estimated using a set of nonlinear geometry-based equations based on the RSSD measurements and the nominal sensor positions.

The proposed set of nonlinear equations are converted via an intermediate variable into a set of linear equations which can be expressed as $\mathbf{A}\boldsymbol{\theta} = \mathbf{b}$. The CRLB for signal strength difference based location estimation methods has been derived without considering sensor position errors, and the performance of these methods was presented based on this bound, which is not practical. As will be shown, the CRLB differs significantly when these errors are considered. The CRLB analysis presented here incorporates the inaccuracy in the sensor locations, and thus is a more realistic bound. Further, it shows that the localization accuracy is degraded by sensor position uncertainty.

Chapter 4 In this chapter two different methods are considered for the proposed problem. The least squares initial estimate (LSIE) of the source position is obtained using an efficient constrained weighted least squares (CWLS) method. A low complexity iterative Newton method is then used with the LSIE as the initial point to improve the accuracy and efficiency. Note that no transmit power estimation is required, and the proposed RSSD approach improves the location accuracy compared to methods that employ this estimation. For simplicity, the proposed two stage method is denoted as LSIE-NM.

The goal of the proposed least squares (LS) based method is to obtain the location estimate $\hat{\boldsymbol{\theta}}$ that minimizes the data vector error $\mathbf{b} - \hat{\mathbf{b}}$ where $\mathbf{A}\hat{\boldsymbol{\theta}} = \hat{\mathbf{b}}$, instead of directly minimizing the unknown parameter estimation error $\hat{\boldsymbol{\theta}} - \boldsymbol{\theta}$. This can result in poor performance, particularly in very noisy environments, due to the bias and variance of the location estimate. Hence, a minimax optimization technique is developed to directly minimize the mean squared error (MSE) of the unknown parameter estimation error in the corresponding localization problem without sensor uncertainty. This is extended to the case of localization with sensor position error.

Semidefinite relaxation (SDR) [20]-[21] is used to relax the nonconvex minimax optimization problem into a convex semidefinite programming (SDP) problem [20]-[21]. This problem can be efficiently solved using standard SDP solvers such as SeDuMi or SDPT3 [22],[23] which employ the interior point method to obtain a globally optimal solution. The proposed approach converges quickly

with a worst case computational complexity of $O(N^{4.5})$ where N is the number of sensors.

Chapter 5 In this chapter the problem of RSSD-based source localization considering the system parameter error is formulated. The total least squares (TLS) estimator has been shown to be efficient when errors exist in the system parameters as it compensates for both observation matrix and data vector errors [24]-[28]. As a consequence, it provides performance superior to conventional LS-based methods. It was shown that this method performs well when there is no linear dependence between the observation matrix and data vector. Therefore, any dependencies should be added as constraints by reformulating the TLS cost function. The contributions of this chapter are as follows:

1. RSSD-based source localization with unknown transmit power is generalized and extended using the total least squares (ETLS) method. An RSSD-based ETLS method is developed which considers errors in the data as well as the constraints due to the relationship between the observation and data matrices.
2. Semidefinite relaxation (SDR) is used to relax the nonconvex ETLS cost function to obtain a convex semidefinite programming (SDP) cost function. This yields a global solution of the relaxed localization problem which is nonconvex and difficult to solve [20]-[21]. The proposed ETLS-SDP method is extended to the localization problem with unknown path loss exponent.
3. The mean squared error (MSE) and the Cramér-Rao lower bound (CRLB) of the ETLS-based method are derived, and the performance of the ETLS-SDP method is compared with the CRLB as well as existing RSS- and RSSD-based methods.

Chapter 6 For future work, four topics are proposed for the RSSD-based source localization problem. These are as follows:

- The proposed ETLS-SDP method will be extended to the problem of RSSD-based localization considering the sensor position uncertainty.
- The regularized and recursive version of the proposed TLS method will be derived to improve the accuracy and computational complexity.

- The proposed Minimax-SDP method will be extended to the case of unknown path loss exponent and a new kernel recursive total least square algorithm will be developed.
- Finally, the proposed blind RSSD based method will be extended to the cooperative source localization case with unknown path loss exponent.

1.5 Publications

Several recent publications in this field are given below:

- H. Lohrasbipeydeh, T.A. Gulliver and H. Amindavar, **RSSD Based Source Localization with Unknown Transmit Power and Sensor Position Uncertainly,** submitted to *IEEE Trans. Wireless Commun.*, Jan. 2014.
- H. Lohrasbipeydeh, T.A. Gulliver and H. Amindavar, **A Minimax SDP Method for Energy Based Source Localization with Unknown Transmit Power**, *IEEE Wireless Commun Letter.*, May. 2014.
- H. Lohrasbipeydeh, T.A. Gulliver and H. Amindavar, **Blind received signal strength difference based source localization with system parameter errors**, *IEEE Trans. Signal Process.*, Jun. 2014.
- H. Lohrasbipeydeh, T.A. Gulliver and H. Amindavar, **Efficient RSSD based source positioning with unknown transmit power for wireless sensor networks**, *IEEE VTC Conf.*, Mar. 2014.
- H. Lohrasbipeydeh, T.A. Gulliver and H. Amindavar, **Unknown transmit power energy-based source localization in wireless sensor networks**, *IEEE VTC Conf.*, Mar. 2014.
- H. Lohrasbipeydeh, T. Dakin, T. A. Gulliver, C. D. Grasse, **Passive acoustic energy based diver detection and depth estimation** , *IEEE Ocean Conf.*, Sep. 2014.

Chapter 2

Background

2.1 Motivation of Energy Based Localization

There are several well known techniques which can be used for the problem of source localization to obtain the location estimate. However, signal energy based localization is a promising approach considering the constraints and assumptions in the corresponding localization problem. Energy based localization is motivated in this section by comparing it with other measurements models in the literature.

2.1.1 Time Based Measurement Models

Most wireless sensor network (WSN) localization techniques rely on distance estimates obtained using the time of arrival (TOA), time difference of arrival (TDOA), angle of arrival (AOA) to estimate the direction of the received signal or a combination of these methods [29]-[41]. Energy based techniques such as received signal strength (RSS) and received signal strength difference (RSSD) have also been employed [42]-[48].

The geometries of the time based and energy based measurement models are shown in Fig. 2.1. Note that relative based models like TDOA and RSSD require at least 4 sensors to obtain the requisite measurement data for source localization in three dimensions. As shown in Fig. 2.1, the models can be combined to provide addiitonal measurement data at the expense fo greater complexity and cost.

There is an inherent trade off between these methods considering the implementation cost and localization accuracy. For example, complex TOA, TDOA and AOA methods are used in wireless networks to obtain precise location information, while RSS and RSSD measurements are used in low complexity techniques to provide rea-

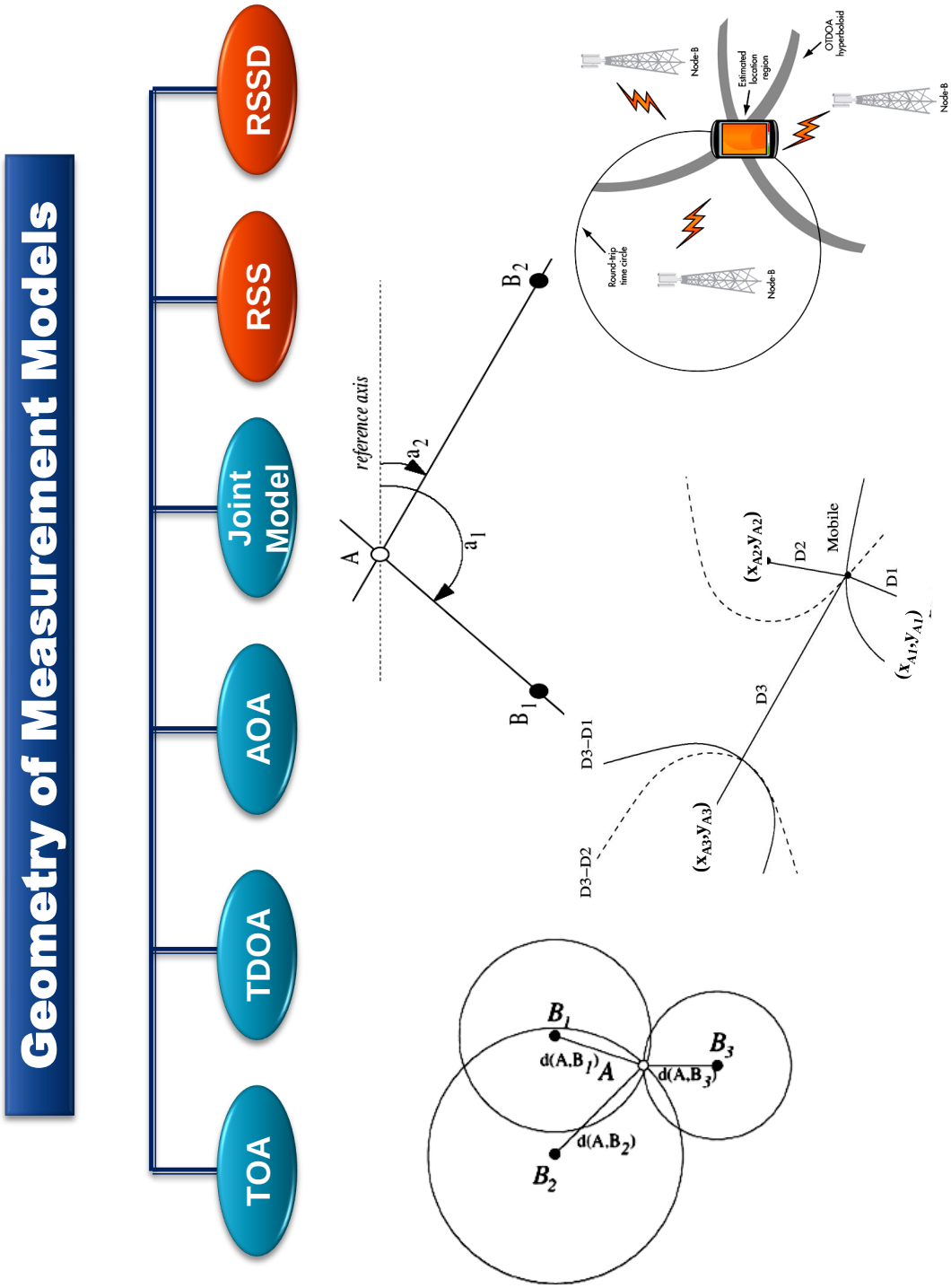

Figure 2.1: Different time based and energy based localization measurement models

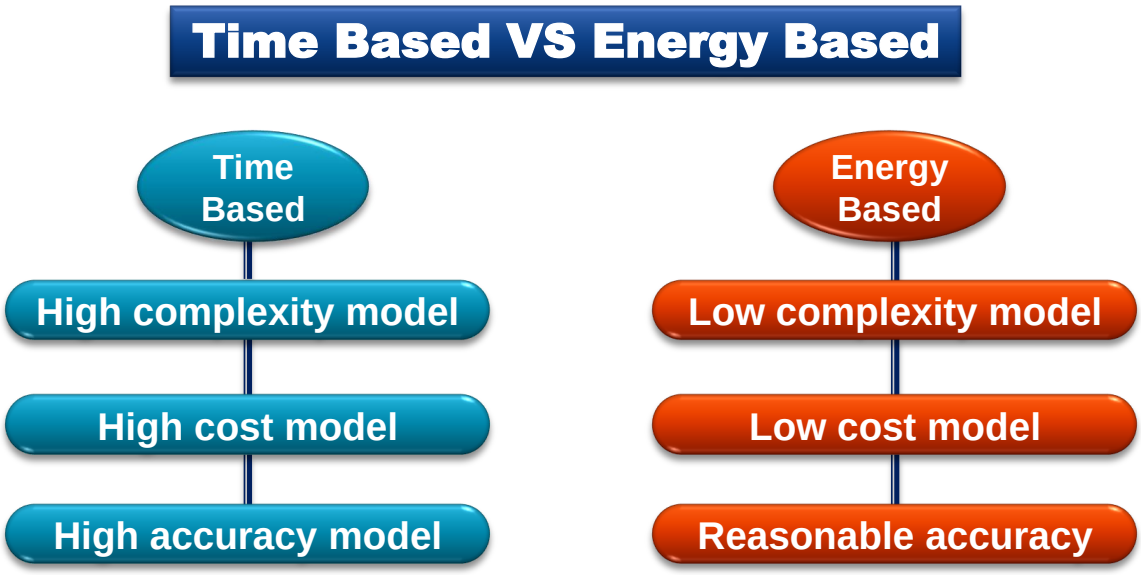

Figure 2.2: Comparison of the time and energy based measurement models.

sonable accuracy [49]-[53]. Energy based methods are low cost and simple to implement compared to TDOA, TOA and AOA methods.

Energy based solutions can be implemented on existing infrastructure with very little modification to the software and hardware, while other methods such as TOA, TDOA and AOA require additional hardware to obtain a location estimate. In addition, TOA, TDOA and AOA techniques have the following inherent limitations:

1. TOA-based methods require *a priori* information of the amplitude and phase of the transmitted signal to obtain the time interval between the source and sensors. If this information is not available, the time must be transmitted for source location estimation purposes. This means that TOA methods require synchronization between the source and sensors and high-precision timing [31],[36].

2. Unlike TOA methods, TDOA-based techniques do not require *a priori* information about the transmitted signal. However, TDOA methods require that the receivers be synchronized to estimate the time delay between the signals received at the sensors. Therefore, obtaining an accurate source location estimate requires precise timing and synchronization which necessitates the use of very accurate clocks, increasing the cost and complexity of implementation. In addition, TDOA techniques use the correlation of the received signals to estimate the time delay, which can be complex [12].

3. AOA-based localization techniques need the angle information of the received signal from the corresponding source. This information can be obtained using an antenna array at the receiver which adds to the hardware complexity. Signal processing is also required with these methods to overcome the effects of multipath, which also adds to the complexity [29],[33].

2.1.2 Energy Based Measurement Models

Energy based models are easy to implement on existing infrastructure with minimal modifications to the software or hardware. There are two major energy based models which use RSS or RSSD measurements. In the RSS model, the transmitted power is typically considered to be known and the source localization is done using LS or ML based methods. Recently the joint estimation of the location and transmit power was considered for RSS based localization in the case of unknown transmit power. This has some drawbacks which are discussed in the related work section. The RSSD based measurement model does not require transmit power information which is often the case. This model has recently been developed and the related literature is discussed in the next section.

As mentioned above, energy based models are low complexity models compared to time based models. These models also provide reasonable accuracy for sufficient signal to noise ratios. A comparison of time and energy based models is presented in Fig. 1.

2.2 Related Work

The estimators used to obtain an unknown source position using energy based measurements can be divided into two categories: 1) maximum likelihood (ML) and 2) least squares (LS).

2.2.1 Maximum Likelihood Based Methods

The ML estimator is asymptotically optimal when the noise statistics are known [54]-[55], but is difficult to implement due to the highly nonconvex cost function. This results in multiple local minima or maxima and as a consequence has high computational complexity [43],[47]. Recently, the problem of RSS-based source localization

with unknown transmit power and path loss exponent has been studied. Vaghefi et al. presented an ML estimator and solved the proposed RSS-based problem by relaxing it to a convex optimization problem. The global solution of this problem was then obtained using semidefinite programming [62],[63]. In [49], a high complexity ML estimator was used with known transmit power to jointly estimate the source location and path loss exponent. Salman et al. [50] reformulated the problem to obtain a low complexity joint estimator (LCJE).

2.2.2 Least Squares Based Methods

LS based estimators have been developed to overcome the problems with ML estimators by transforming the original nonlinear equations into linear equations. For example, spherical interpolation (SI) [56], weighted least squares (WLS) [57] and the best linear unbiased estimator (BLUE) [58] are well known RSS-based LS estimators. Spherical interpolation is a low complexity least squares based method, but it has poor accuracy. The BLUE and WLS can be used for RSS-based positioning, however the performance with the proposed approaches is poor due to the significant bias and variance in noisy environments. Further, in practical situations the channel parameters are not known which results in a degradation in the estimation accuracy.

A suboptimal algorithm was developed in [64] to improve the ML estimator which was developed in [62],[63] by formulating the original problem as a general trust region subproblem. This was solved using numerical optimization [65] under mild conditions.

A linear LS (LLS) method with known transmit power and unknown path loss exponent was proposed in [51] to estimate the unknown source location based on RSS measurements. Wang et al. considered the weighted least squares (WLS) method based on the unscented transformation (UT) to solve a noncooperative localization problem, however global estimates cannot be obtained due to the unknown weights [52]. Recently, this WLS problem was reformulated by estimating the weights and solving the problem using an alternative approach, but this degrades the performance, particularly at low signal to noise ratios [53].

2.2.3 RSSD Versus RSS Localization

Unlike RSS based localization, the RSSD based problem has not been adequately investigated. The problem of source localization with unknown transmit power based on RSSD measurements has been of interest recently to improve the degradation in

performance due to the use of transmit power estimation. An RSSD method has been proposed for source localization [59] which uses a simple hyperbolic positioning technique. However, the performance of this approach can be poor because the quality of the sensor information and the problem geometry are not included in the optimization problem. A distance correction factor was employed in [60] to improve the estimation accuracy. A nonlinear least squares (NLS) method has also been developed, but it has significant bias and low efficiency compared to the LLS solution [61]. The complexity of the NLS method is also high due to the large search space required to find the optimal solution.

Unfortunately, the proposed least squares based methods only provide a suboptimal solution due to the fact that they only consider errors in the data vector due to noise, and assume there are no errors in the observation matrix [24]-[26]. This leads to poor accuracy and biased estimates of the unknown parameters due to observation matrix errors [26]-[28]. Furthermore, none of the existing RSS- and RSSD-based techniques consider the effect of sensor position errors. The accuracy can be degraded significantly in the presence of sensor uncertainties. The Cramér-Rao lower bound (CRLB) can be achieved by some of these techniques in high signal to noise ratio cases when the sensor position errors are not considered, but as will be shown, these errors have a significant effect on the CRLB.

Chapter 3

RSSD Based Problem Formulation

3.1 System Model with Sensor Uncertainty

In this section, RSSD measurements are used for source location estimation. The anchor nodes are assumed to be sensors with known positions and the target is a source with unknown location. To avoid solution ambiguity, the sensors are assumed to not be deployed in a straight line, which is reasonable. Let $\mathbf{u} = [\mathbf{x}, \mathbf{y}]^{\mathbf{T}}$ be the unknown source position to be determined in a two-dimensional space and $\mathbf{u}_i = [x_i, y_i]^T$, $i = 1, 2, \ldots, N$, be the actual coordinates of the sensors where $(\ )^T$ denotes matrix transpose and N is the number of sensors. Source localization requires at least four sensors, $(N > 3)$, to provide a minimum of three RSSD values. The distance between the source and the ith sensor is given by

$$r_i = \|\mathbf{u} - \mathbf{u}_i\| = \sqrt{(x - x_i)^2 + (y - y_i)^2}, \ \ i = 1, 2, \ldots, N. \tag{3.1}$$

The received signal power at the ith sensor can be expressed as

$$P_i = K_0 \frac{P_t}{r_i^{\gamma}}, \quad i = 1, 2, \ldots, N, \tag{3.2}$$

where P_t denotes the source transmit power, γ is the path loss exponent and K_0 is the path loss for the reference distance which is typically taken as 1 m [4]. The path loss exponent γ is a function of the wireless environment and can vary from 1 to 6 [4], In free space, $\gamma = 2$, and this is assumed to be the a priori value for the RSSD measurements. Although γ is typically unknown, it can easily be estimated [51],[53].

Assuming a log-normal distribution for P_i, (3.2) can be rewritten as

$$P_i(dB) - P_t(dB) = K_0(dB) - 10\gamma \log_{10}(r_i) + \varepsilon_i, \tag{3.3}$$

where ε_i is the measurement noise at the ith sensor which is assumed to be Gaussian distributed with zero mean and variance σ_i^2. To determine the RSSD, one of the N sensor must be chosen as the reference. It will be shown in the next section that the CRLB is independent of the choice of the reference sensor. Therefore, let Sensor 1 be the reference sensor. The RSSD between the first and ith sensor is $\Delta P_{1i}(dB) = P_1(dB) - P_i(dB)$, which from (3.3) can be expressed as

$$\Delta P_{1i}(dB) = 10\gamma \log_{10}\left(\frac{r_i}{r_1}\right) + \upsilon_{1i}, \tag{3.4}$$

where $\upsilon_{i1} \sim N(0, \sigma_i^2 + \sigma_1^2)$ is the RSSD measurement noise and ε_1 and ε_i, $i = 2, \ldots, N$, are assumed to be independent [43]. Therefore, the unknown source coordinates can be estimated from the difference values ΔP_{1i}. From (3.4), the ith distance is given by

$$r_i = 10^{\left(\frac{\Delta \tilde{P}_{1i}(dB)}{10\gamma}\right)} r_1, \quad i = 2, \ldots, N. \tag{3.5}$$

where $\Delta \tilde{P}_{1i}$ is the noise free RSSD measurement with respect to the first sensor. To convert the RSSD measurements into a set of linear equations, the following intermediate variable is introduced

$$r_1^2 = (x - x_1)^2 + (y - y_1)^2. \tag{3.6}$$

Squaring both sides of (3.1) and substituting (3.5) and (3.6) yields

$$\begin{aligned} \left(10^{\frac{\Delta \tilde{P}_{1i}(dB)}{5\gamma}} - 1\right) r_1^2 = x_i^2 + y_i^2 - x_1^2 - y_1^2 + \\ 2x(x_1 - x_i) + 2y(y_1 - y_i), \quad i = 2, \ldots, N. \end{aligned} \tag{3.7}$$

Defining $k_{1i} = 10^{\left(\frac{\Delta\tilde{P}_{1i}(dB)}{5\gamma}\right)} - 1$, (3.7) can be simplified as

$$\begin{aligned} k_{1i}{r_1}^2 &= x_i^2 + y_i^2 - (x_1^2 + y_1^2) + 2(x - x_1)(x_1 - x_i) \\ &\quad + 2(y - y_1)(y_1 - y_i) + 2x_1(x_1 - x_i) + 2y_1(y_1 - y_i) \\ &= x_i^2 + y_i^2 + (x_1^2 + y_1^2) - 2(x_1 x_i + y_1 y_i) \\ &\quad - 2\left((x_i - x_1)(x - x_1) + (y_i - y_1)(y - y_1)\right) \\ &= \mathbf{u}_i^T\mathbf{u}_i + \mathbf{u}_1^T\mathbf{u}_1 - 2(\mathbf{u}_i - \mathbf{u}_1)^T\widehat{\mathbf{u}} - 2\mathbf{u}_i^T\mathbf{u}_1, \\ &\qquad i = 2, \ldots, N. \end{aligned} \tag{3.8}$$

where $\widehat{\mathbf{u}} = [x - x_1, y - y_1]^T$. Equation (3.8) can be employed for localization without sensor location uncertainty. Let $\tilde{\mathbf{u}}_i = [\tilde{x}_i, \tilde{y}_i]^T$ and $\Delta\mathbf{u}_i = [\Delta x_i, \Delta y_i]^T$ be the assumed location and the position error of the ith sensor, respectively, so that $\tilde{\mathbf{u}}_i = \Delta\mathbf{u}_i + \mathbf{u}_i$. Substituting these values into (3.8) and ignoring the second-order error terms gives

$$\begin{aligned} \delta_i &= 2(\tilde{\mathbf{u}}_1 + \tilde{\mathbf{u}} - \tilde{\mathbf{u}}_i)^T\Delta\mathbf{u}_1 + 2(\tilde{\mathbf{u}}_i - \tilde{\mathbf{u}} - \tilde{\mathbf{u}}_1)^T\Delta\mathbf{u}_i \\ &= \tilde{\mathbf{u}}_i^T\tilde{\mathbf{u}}_i + \tilde{\mathbf{u}}_1^T\tilde{\mathbf{u}}_1 - 2(\tilde{\mathbf{u}}_i - \tilde{\mathbf{u}}_1)^T\tilde{\mathbf{u}} - 2\tilde{\mathbf{u}}_i^T\tilde{\mathbf{u}}_1 - k_{1i}r_1^2, \end{aligned} \tag{3.9}$$

where $\tilde{\mathbf{u}} = [x - \tilde{x}_1, y - \tilde{y}_1]^T$ and δ_i is the ith, $i = 2, 3, \ldots, N$, sensor location error which includes the position error due to sensor uncertainty and measurement noise.

$$\begin{aligned} \boldsymbol{\delta} &= \mathbf{C}\Delta\mathbf{s}, \\ \mathbf{C} &= \begin{cases} C_{(i-1),1} = -C_{(i-1),(2i-1)} = 2(x - \tilde{x}_i) & i = 2, \ldots, N \\ C_{(i-1),2} = -C_{(i-1),(2i)} = 2(y - \tilde{y}_i) & i = 2, \ldots, N \end{cases}, \\ \Delta\mathbf{s} &= [\Delta x_1, \Delta y_1, \ldots, \Delta x_N, \Delta y_N]^T. \end{aligned} \tag{3.10}$$

Let $\boldsymbol{\delta} = [\delta_2, \delta_3, \ldots, \delta_N]^T$, which is given by (3.10) where $\mathbf{C}$ is an $(N-1) \times (2N)$ matrix. Let $\tilde{R}_i^2 = \tilde{x}_i^2 + \tilde{y}_i^2$, so that (3.9) can be written as

$$\mathbf{A}\boldsymbol{\theta} - \mathbf{b} = \boldsymbol{\delta}, \tag{3.11}$$

where

$$\mathbf{A} = \begin{bmatrix} \tilde{x}_2 - \tilde{x}_1 & \tilde{y}_2 - \tilde{y}_1 & k_{12}/2 \\ \vdots & \vdots & \vdots \\ \tilde{x}_N - \tilde{x}_1 & \tilde{y}_N - \tilde{y}_1 & k_{1N}/2 \end{bmatrix}, \tag{3.12}$$

$$\boldsymbol{\theta} = \begin{bmatrix} x - \tilde{x}_1 & y - \tilde{y}_1 & r_1^2 \end{bmatrix}^T, \tag{3.13}$$

and

$$\mathbf{b} = \begin{bmatrix} (\tilde{R}_2^2 + \tilde{R}_1^2) - (\tilde{x}_2\tilde{x}_1 + \tilde{y}_2\tilde{y}_1)/2 \\ \vdots \\ (\tilde{R}_N^2 + \tilde{R}_1^2) - (\tilde{x}_N\tilde{x}_1 + \tilde{y}_N\tilde{y}_1)/2 \end{bmatrix}. \tag{3.14}$$

The proposed RSSD measurement model will be used in the next chapter to estimate the source location in the presence of sensor position uncertainty. Before we start the location estimation problem, lets analyse the effect of sensor position uncertainty on the CRLB which is derived below.

3.2 Cramér-Rao Lower Bound Analysis

In this section, the CRLB of the proposed RSSD based measurement without considering the sensor position error and in presence of sensor position uncertainty is analysed. The independence of the proposed CRLB in the presence of sensor uncertainty with respect to the reference sensor is also derived. The result shows a significant change in CRLB in the presence of sensor position error.

3.2.1 CRLB without Sensor Uncertainty

In this section, the Cramér-Rao lower bound (CRLB) is derived for the RSSD based measurements without sensor uncertainty. It provides a lower limit on the covariance matrix of an unbiased estimator of the unknown parameter. Let

$$\mathbf{\Delta P} = [\Delta P_{12},\ \ldots,\ \Delta P_{1N}]^T, \tag{3.15}$$

be the vector of $(N-1)$ RSSD values, with ΔP_{1i} as defined in (3.4). Considering the independent Gaussian distributed measurement noise, $\upsilon_{i1} \sim N(0, \sigma_i^2 + \sigma_1^2)$, the joint probability density function (pdf) of $\mathbf{\Delta P}$ conditioned on $\mathbf{u}$ is

$$\begin{aligned} g(\mathbf{\Delta P}; \mathbf{u}) = \prod_{i=2}^{N} \frac{\eta 10^{\frac{\Delta P_{1i}}{10}}}{\sqrt{2\pi(\sigma_i^2 + \sigma_1^2)}} \\ \times \exp\left\{ -\frac{\left(\Delta P_{1i} + 10\gamma \log_{10}\left(\frac{d_1}{r_i}\right)\right)^2}{2(\sigma_i^2 + \sigma_1^2)} \right\}, \end{aligned} \tag{3.16}$$

where $\eta = \frac{10}{\ln 10}$. The covariance matrix of an unbiased estimator of $\mathbf{s}$ satisfies

$$\text{cov}(\mathbf{s}) \geq \mathbf{F}^{-1}, \tag{3.17}$$

where $\mathbf{F}$ is the Fisher information matrix (FIM) [55]. The CRLB of $\mathbf{s}$ is then $\mathbf{F}^{-1}$. The covariance matrix in (3.17) can be derived as

$$E\{(\tilde{\mathbf{u}} - \mathbf{s})(\tilde{\mathbf{u}} - \mathbf{s})^T\} = \begin{bmatrix} \sigma_{\tilde{x}}^2 & \sigma_{\tilde{x}\tilde{y}}^2 \\ \sigma_{\tilde{y}\tilde{x}}^2 & \sigma_{\tilde{y}}^2 \end{bmatrix}. \tag{3.18}$$

The diagonal elements are the mean square errors of the unknown source location $\mathbf{u}$, and the off-diagonal elements are the covariances between them. The FIM can then be expressed as

$$\mathbf{F} = \begin{bmatrix} F_{xx} & F_{xy} \\ F_{yx} & F_{yy} \end{bmatrix}. \tag{3.19}$$

The FIM components are obtained using the log likelihood function of (3.16), $\ln(g(\mathbf{\Delta P}; \mathbf{u}))$, which gives

$$[\mathbf{F}]_{kj} = -E\left[\frac{\partial^2 \ln g(\mathbf{\Delta P}; \mathbf{u})}{\partial u_k \partial u_j}\right], \quad k, j = 1, 2. \tag{3.20}$$

where $\mathbf{u} = [u_1, u_2]^T = [x, y]^T$. Substituting (3.16) into (3.20) yields the FIM components

$$F_{xx} = \sum_{i=2}^{N} \left(\frac{\eta\gamma}{\sigma_{1i}}\right)^2 \left(\frac{x - x_1}{\|\mathbf{u} - \mathbf{u}_1\|^2} + \frac{x_i - x}{\|\mathbf{u}_i - \mathbf{u}\|^2}\right)^2, \tag{3.21}$$

$$F_{yy} = \sum_{i=2}^{N} \left(\frac{\eta\gamma}{\sigma_{1i}}\right)^2 \left(\frac{y - y_1}{\|\mathbf{u} - \mathbf{u}_1\|^2} + \frac{y_i - y}{\|\mathbf{u}_i - \mathbf{u}\|^2}\right)^2, \tag{3.22}$$

and

$$\begin{aligned} \left[\tilde{\mathbf{F}}\right]_{xy} &= \sum_{i=2}^{N} \left(\frac{\eta\gamma}{\sigma_{1i}}\right)^2 \left\{ \left(\frac{(x - x_1)\|\mathbf{u}_i - \mathbf{u}\|^2}{\|\mathbf{u} - \mathbf{u}_1\|^4} \right.\right. \\ &\quad \left.\left. + \frac{(x_i - x)}{\|\mathbf{u} - \mathbf{u}_1\|^2} \right) \left(\frac{(y - y_1)\|\mathbf{u}_i - \mathbf{u}\|^2}{\|\mathbf{u}_i - \mathbf{u}\|^4} + \frac{(y_i - y)}{\|\mathbf{u}_i - \mathbf{u}\|^2} \right) \right\}. \\ &= \left[\tilde{\mathbf{F}}\right]_{yx}. \end{aligned} \tag{3.23}$$

The CRLB is then obtained by calculating the FIM components in (3.21)-(3.23) and substituting them in (3.17).

3.2.2 CRLB with Sensor Uncertainty

In this section, the CRLB in the presence of sensor uncertainty is derived for the RSSD-based technique. This can be used to evaluate the degradation in performance due to errors in the sensor positions. Define the measurement and sensor error vectors as $\boldsymbol{\vartheta} = [\upsilon_{12}, \upsilon_{13}, \ldots, \upsilon_{1N}]^T$ and $\Delta\mathbf{u} = [\Delta\mathbf{u}_1{}^T, \Delta\mathbf{u}_2{}^T, \ldots, \Delta\mathbf{u}_N{}^T]^T$, respectively, which are assumed to be independent Gaussian distributed random variables. Define $\mathbf{Q}_\upsilon = E\{\boldsymbol{\upsilon}\boldsymbol{\upsilon}^T\}$ and $\mathbf{Q}_{\Delta u} = E\{\boldsymbol{\Delta}\mathbf{u}\boldsymbol{\Delta}\mathbf{u}^T\}$ as the covariance matrices of the measurement noise and sensor position errors, respectively. The joint pdf of the measurement noise and sensor position errors is obtained from (3.16) as

$$g(\boldsymbol{\chi};\boldsymbol{\beta}) = \frac{\eta^{(N-1)} 10^{\sum_{i=2}^{N} \frac{\Delta P_{1i}}{10}}}{(2\pi)^{\frac{3(N-1)}{2}} |\mathbf{Q}_{\Delta\mathbf{u}}|^{\frac{1}{2}} |\mathbf{Q}_{\vartheta}|^{\frac{1}{2}}} \times \exp\left(-\frac{(\Delta\mathbf{u}^T\mathbf{Q}_{\Delta\mathbf{u}}^{-1}\Delta\mathbf{u} + \vartheta^T\mathbf{Q}_{\vartheta}^{-1}\vartheta)}{2}\right) \tag{3.24}$$

where $|\,|$ denotes determinant, $\mathbf{u}_s = [\mathbf{u}_2, \ldots, \mathbf{u}_N]^T$, $\boldsymbol{\chi} = \begin{bmatrix} \boldsymbol{\Delta}\mathbf{P}^T & \tilde{\mathbf{u}}_s^T \end{bmatrix}^T$ and $\boldsymbol{\beta} = \begin{bmatrix} \boldsymbol{\beta}_1 & \boldsymbol{\beta}_2 \end{bmatrix} = \begin{bmatrix} \mathbf{u}^T & \mathbf{u}_s^T \end{bmatrix}^T$.

Substituting (3.24) into (3.19), and taking the natural log and differentiating, the FIM in the presence of sensor position errors, $\tilde{\mathbf{F}}$, can be obtained. The elements of this matrix are given by

$$\left[\tilde{\mathbf{F}}\right]_{kj} = -E\left[\frac{\partial^2 \ln g(\boldsymbol{\chi};\boldsymbol{\beta})}{\partial\boldsymbol{\beta}_k \partial\boldsymbol{\beta}_j}\right], \quad k, j = 1, 2. \tag{3.25}$$

Therefore, the FIM components can be obtained by substituting (3.24) into (3.25) which gives

$$\tilde{\mathbf{F}}_{\mathbf{uu}} = \left(\frac{\partial\Delta\tilde{\mathbf{P}}}{\partial\mathbf{u}}\right)^T \mathbf{Q}_\upsilon^{-1} \left(\frac{\partial\Delta\tilde{\mathbf{P}}}{\partial\mathbf{u}}\right) = \mathbf{F} \tag{3.26}$$

$$\tilde{\mathbf{F}}_{\mathbf{uu_s}} = \left(\frac{\partial\Delta\tilde{\mathbf{P}}}{\partial\mathbf{u}}\right)^T \mathbf{Q}_\upsilon^{-1} \left(\frac{\partial\Delta\tilde{\mathbf{P}}}{\partial\mathbf{u}_s}\right) \tag{3.27}$$

$$\tilde{\mathbf{F}}_{\mathbf{u}_s\mathbf{u}_s} = \left(\frac{\partial\Delta\tilde{\mathbf{P}}}{\partial\mathbf{u}_s}\right)^T \mathbf{Q}_\upsilon^{-1} \left(\frac{\partial\Delta\tilde{\mathbf{P}}}{\partial\mathbf{u}_s}\right) + \mathbf{Q}_{\Delta\mathbf{u}}^{-1} \tag{3.28}$$

where $\Delta\tilde{\mathbf{P}}$ denotes $\Delta\mathbf{P}$ without noise.

The partitioned matrix inversion given in [66] can be used to invert $\tilde{\mathbf{F}}$ giving

$$\tilde{\mathbf{F}}^{-1} = (\mathbf{F} - \tilde{\mathbf{F}}_{\mathbf{uu_s}}\tilde{\mathbf{F}}^{-1}_{\mathbf{u_s u_s}}\tilde{\mathbf{F}}^{T}_{\mathbf{u_s u}})^{-1}.$$

$\tilde{\mathbf{F}}^{-1}$ is the CRLB in the presence of sensor uncertainty. The increase in the CRLB due to sensor location errors is then $\mathbf{\Delta}_{CRLB(u)} = \tilde{\mathbf{F}}^{-1} - \mathbf{F}^{-1}$, which is given by

$$\begin{aligned}\mathbf{\Delta}_{CRLB(\mathbf{u})} = \mathbf{F}^{-1}\tilde{\mathbf{F}}_{\mathbf{uu_s}}(\tilde{\mathbf{F}}_{\mathbf{u_s u_s}} - \tilde{\mathbf{F}}^{T}_{\mathbf{u_s u}}\mathbf{F}^{-1}\tilde{\mathbf{F}}_{\mathbf{uu_s}}) \\ \times\tilde{\mathbf{F}}_{\mathbf{uu_s}}\mathbf{F}^{-1}.\end{aligned} \tag{3.29}$$

Equation (3.29) shows the sensitivity of the source location estimation accuracy to the sensor position errors. This difference in the CRLB was the motivation for developing the localization algorithm given in this paper.

The variances of the coordinates of the source location estimate $(\tilde{x}, \tilde{y})$ are

$$\begin{aligned}\sigma^2_{\tilde{x}} &= E\{(\tilde{x} - x)^2\} \geq [\mathbf{F}^{-1}]_{11}, \\ \sigma^2_{\tilde{y}} &= E\{(\tilde{y} - y)^2\} \geq [\mathbf{F}^{-1}]_{22}.\end{aligned} \tag{3.30}$$

Their sum is the mean square error (MSE) of the source location $\mathbf{u}$. Equations (3.21)-(3.23) show that the CRLB and the MSE depend on the sensor positions, the number of sensors and the propagation model. The sensors position change the distances and also the geometry of the sensors, and thus the CRLB. For example, the worst case occurs when the sensors are located in a straight line with respect to the source, which leads to a singular FIM. The CRLB is decreased by increasing the number of sensors, N, or an increased path loss exponent γ, while it is increased with larger RSSD variances, σ_{1i}.

3.2.3 Independence of the CRLB in the Presence of Sensor Uncertainty with Respect to the Reference Sensor

To investigate the independence of the FIM components given in (3.26)-(3.28), consider $\tilde{\mathbf{F}}^{(i)}_{\mathbf{uu}}$, $\tilde{\mathbf{F}}^{(i)}_{\mathbf{uu_s}}$ and $\tilde{\mathbf{F}}^{(i)}_{\mathbf{u}_s\mathbf{u}_s}$ with respect to sensor i. Define

$$\Delta\mathbf{P}^{(i)} = [\Delta P_{i1}, ..., \Delta P_{i,i-1}, \Delta P_{i,i+1}, \ldots, \Delta P_{i,N}]^T \tag{3.31}$$

as the vector of received signal strength differences when the ith sensor, $i = 2, \ldots, N$, is the reference sensor. Using $\Delta P_{i,i-1} = P_i - P_{i-1}$, (3.31) can be represented in terms

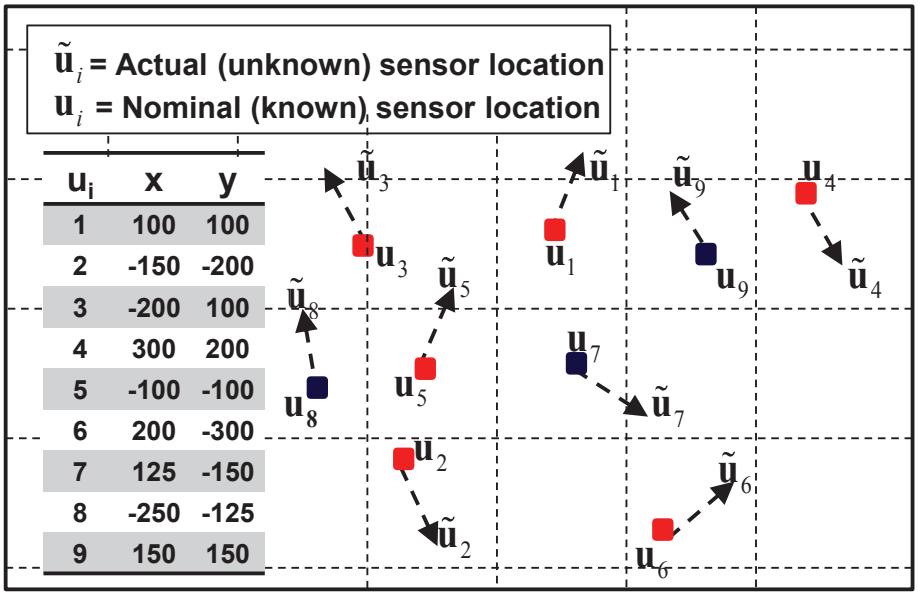

$\mathbf{u}_i$	x	y
1	100	100
2	-150	-200
3	-200	100
4	300	200
5	-100	-100
6	200	-300
7	125	-150
8	-250	-125
9	150	150

Figure 3.1: The sensor locations $\mathbf{u}_i$ and the locations due to position uncertainty $\tilde{\mathbf{u}}_i$.

of $\Delta\mathbf{P}^{(1)}$ as

$$\Delta\mathbf{P}^{(i)} = \mathbf{Q}_i \Delta\mathbf{P}^{(1)}, i = 2, \ldots, N, \tag{3.32}$$

where $\mathbf{Q}_i$, $i = 2, \ldots, N$ is an $(N-1) \times (N-1)$ square matrix given by

$$\mathbf{Q}_i = \begin{cases} Q_{n,n-1} = 1 & n = 2, \ldots, i-1 \\ Q_{n,i-1} = -1 & n = 1, \ldots, N-1 \\ Q_{n,n} = 1 & n = i, \ldots, N-1 \end{cases} \tag{3.33}$$

The measurement noise covariance matrix of $\Delta\mathbf{P}^{(i)}$ can be obtained from (3.32) as

$$\mathbf{Q}_v^{(i)} = \mathbf{Q}_i \mathbf{Q}_v^{(1)} \mathbf{Q}_i^T, i = 2, \ldots, N. \tag{3.34}$$

The FIM components when sensor i is the reference sensor are then given by

$$\begin{aligned} \tilde{\mathbf{F}}_{kj}^{(i)} &= \left(\frac{\partial \Delta\widetilde{\mathbf{P}}^{(i)}}{\partial k}\right)^T \left\{\mathbf{Q}_v^{(i)}\right\}^{-1} \left(\frac{\partial \Delta\widetilde{\mathbf{P}}^{(i)}}{\partial j}\right) + c\mathbf{Q}_{\Delta\mathbf{u}}^{-1} \\ &= \left(\frac{\partial \Delta\widetilde{\mathbf{P}}^{(i)}}{\partial k}\right)^T \mathbf{Q}_i^{-T} \left\{\mathbf{Q}_v^{(1)}\right\}^{-1} \mathbf{Q}_i^{-1} \\ &\times \left(\frac{\partial \Delta\widetilde{\mathbf{P}}^{(i)}}{\partial j}\right) + c{\mathbf{Q}_{\Delta\mathbf{u}}}^{-1}, \end{aligned} \tag{3.35}$$

where $k, j \in \{\mathbf{u}, \mathbf{u}_s\}$,

$$c = \begin{cases} 1 & k = j = \mathbf{u}_s, \\ 0 & \text{otherwise;} \end{cases}$$

and $\Delta\widetilde{\mathbf{P}}^{(i)}$ is the noise free version of (3.31) with respect to reference sensor i. Taking the derivative of (3.32) with respect to k and j gives

$$\left(\frac{\partial \Delta\widetilde{\mathbf{P}}^{(i)}}{\partial k}\right)^T = \left(\frac{\partial(\mathbf{Q}_i \Delta\widetilde{\mathbf{P}}^{(1)})}{\partial k}\right)^T = \left(\frac{\partial \Delta\widetilde{\mathbf{P}}^{(1)}}{\partial k}\right)^T \mathbf{Q}_i^T, \tag{3.36}$$

and

$$\left(\frac{\partial \Delta\widetilde{\mathbf{P}}^{(i)}}{\partial j}\right) = \left(\frac{\partial(\mathbf{Q}_i \Delta\widetilde{\mathbf{P}}^{(1)})}{\partial j}\right) = \mathbf{Q}_i \left(\frac{\partial \Delta\widetilde{\mathbf{P}}^{(1)}}{\partial j}\right). \tag{3.37}$$

Substituting (3.36) and (3.37) into (3.35) gives

$$\begin{aligned} \tilde{\mathbf{F}}_{kj}^{(i)} = &\left(\frac{\partial \Delta\widetilde{\mathbf{P}}^{(1)}}{\partial k}\right)^T \mathbf{Q}_i^T \mathbf{Q}_i^{-T} \left\{\mathbf{Q}_v^{(1)}\right\}^{-1} \mathbf{Q}_i^{-1} \mathbf{Q}_i \\ &\times \left(\frac{\partial \Delta\widetilde{\mathbf{P}}^{(1)}}{\partial j}\right) + c\mathbf{Q}_{\Delta\mathbf{u}}^{-1} = \tilde{\mathbf{F}}_{kj}^{(1)}, \end{aligned} \tag{3.38}$$

where $\tilde{\mathbf{F}}_{kj}^{(1)}$ denotes the FIM components given in (3.26)-(3.28) when the first sensor is considered as the reference. This shows that the FIM and thus the CRLB is independent of the choice of the reference sensor.

3.3 CRLB Performance Evaluation

$\Delta CRLB$ is defined as the difference in the CRLB with and without sensor uncertainty. In this section, the sensitivity of $\Delta CRLB$ is examined with respect to the measurement noise, number of sensors, and path loss exponent.

Both near field and far field source locations are considered. The geometry of the source and sensor locations including the sensor errors is shown in Fig. 3.1. The near field and far field source location coordinates are $(400, 450)$ and $(2500, 2100)$, respectively. The change in CRLB due to sensor uncertainty is defined by ΔCRLB. The first six sensors shown in red are considered so that $N = 6$.

For simplicity, the sensor position error variances are assumed to be equal and

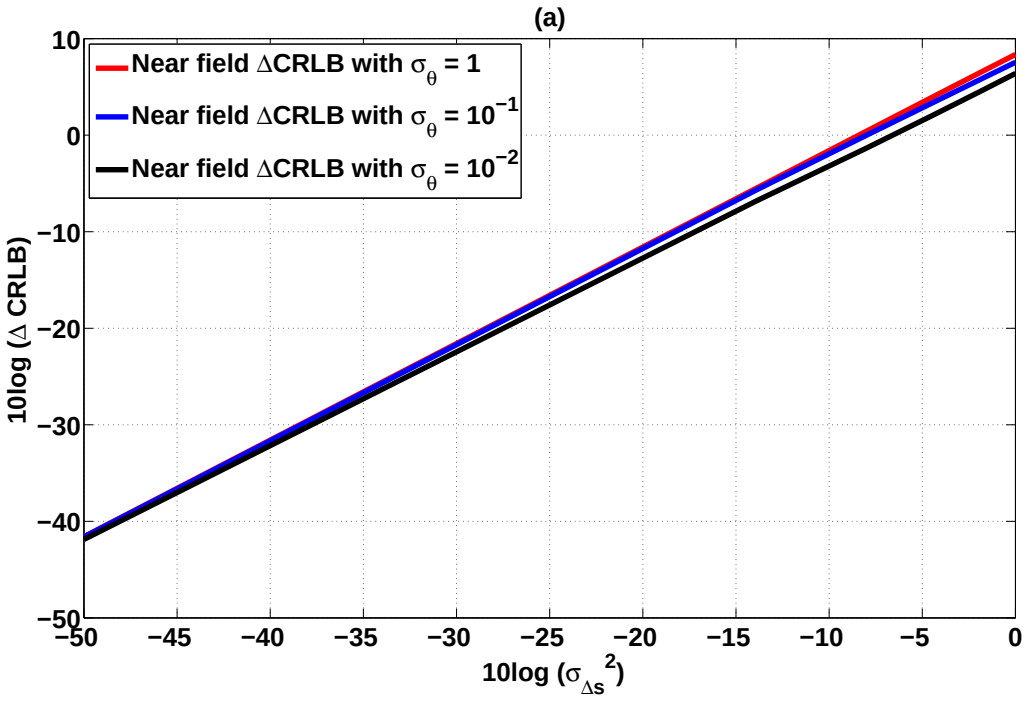

Figure 3.2: Near field $\Delta CRLB$ versus sensor error variance ${\sigma_{\Delta s}}^2$ for different measurement noise variances ${\sigma_\theta}^2$ with $N = 6$ sensors.

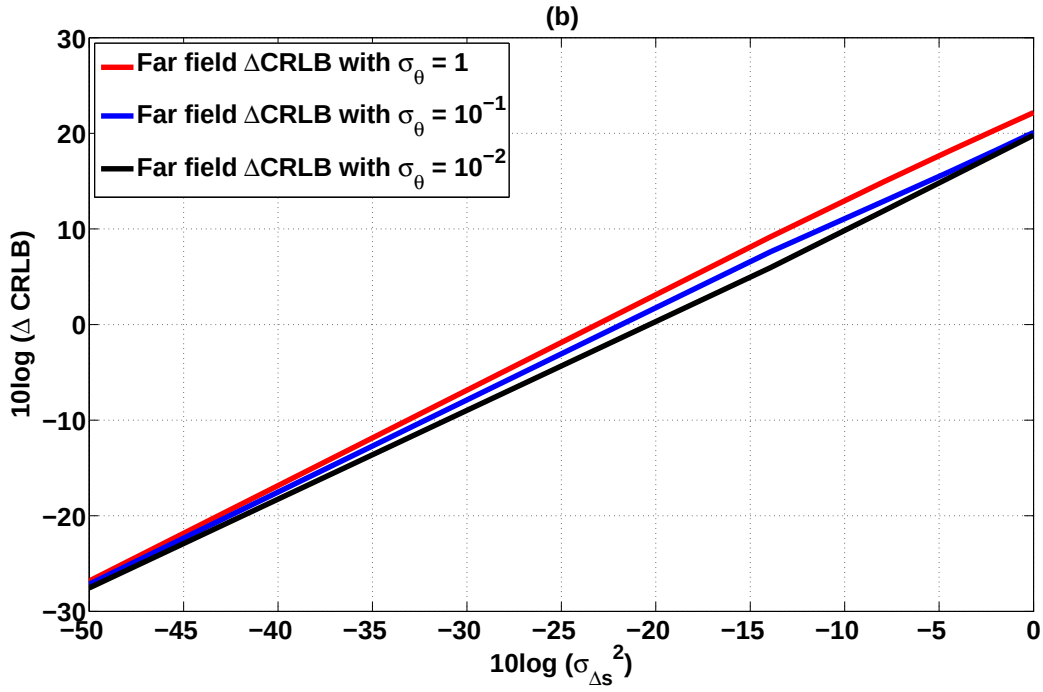

Figure 3.3: Far field $\Delta CRLB$ versus sensor error variance ${\sigma_{\Delta s}}^2$ for different measurement noise variances ${\sigma_\theta}^2$ with $N = 6$ sensors.

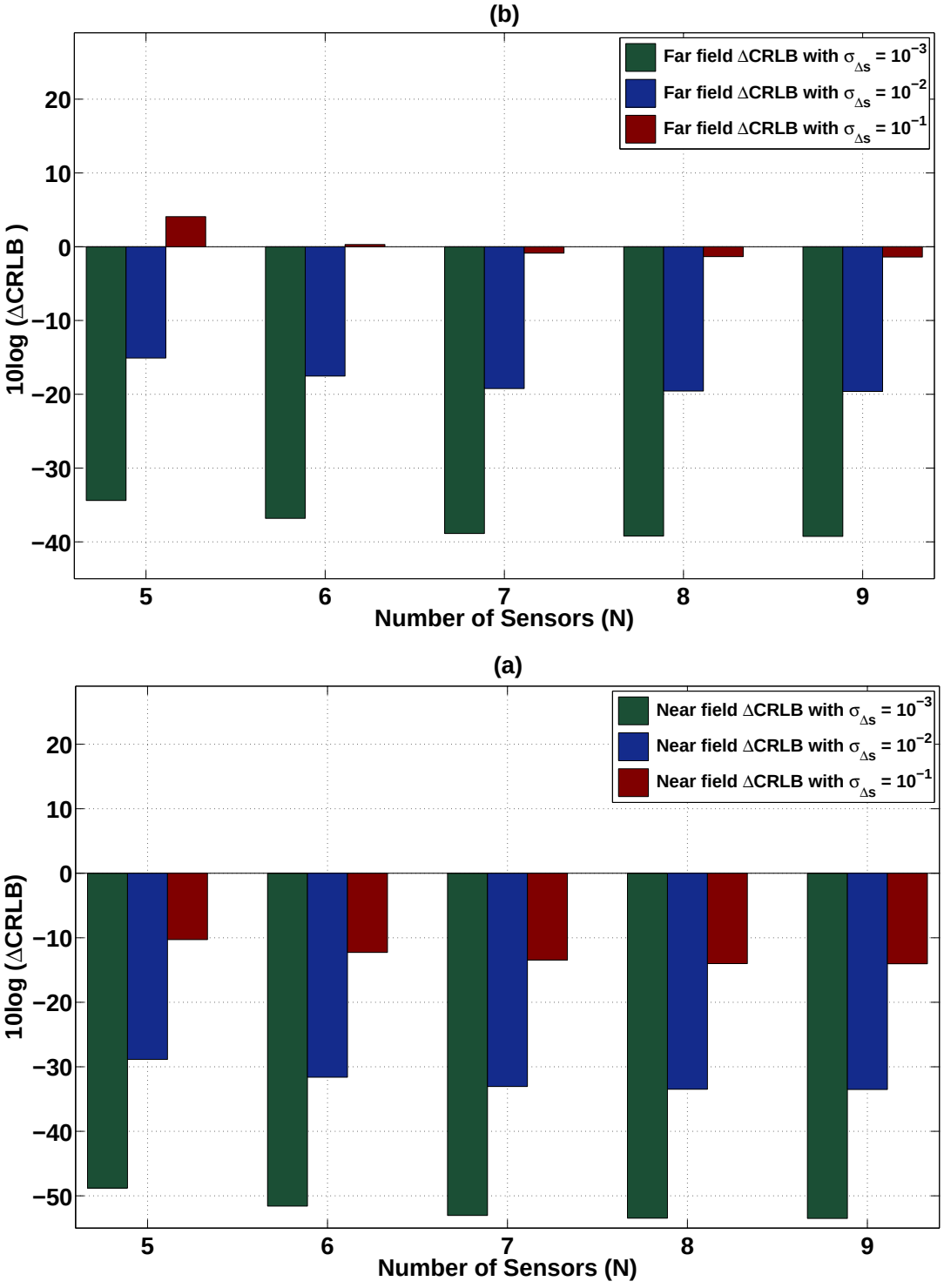

Figure 3.4: $\Delta CRLB$ versus the number of sensors N for different values of ${\sigma_\theta}^2$ for the (a) far field, and (b) near field cases.

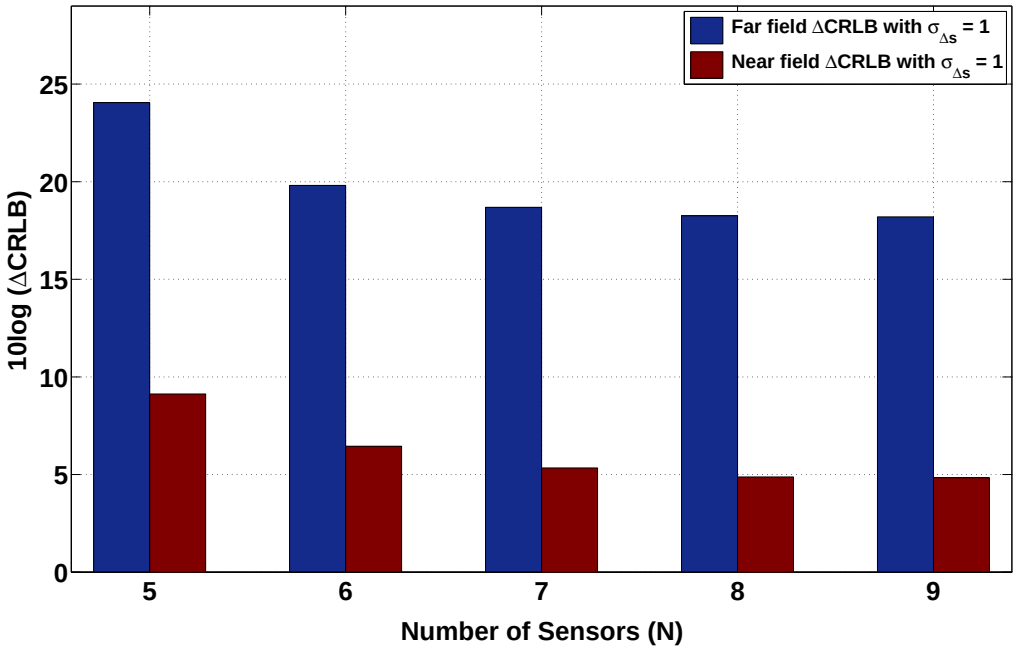

Figure 3.5: $\Delta CRLB$ for the near field and far field cases with $\sigma_\theta = 1$, $\sigma_{\Delta \mathbf{s}} = 1$ and $N = 5$ to 9 sensors.

given by $\sigma^2_{\Delta \mathbf{s}}$. This can easily be extended to the case of unequal variances. Figures 3.2 and 3.3 show that $\Delta CRLB$ is increased as $\sigma^2_{\Delta \mathbf{s}}$ increases for the near and far field cases, respectively. Figure 3.3 also indicates that this increase is higher in the far field case. The effect of increasing the measurement noise variance ${\sigma_\theta}^2$ is also given in these figures. This shows that σ_θ has a minimal effect on ΔCRLB in the near field case, but a considerable effect in the far field case when $\sigma^2_{\Delta \mathbf{s}}$ is large. As an example, for $\sigma^2_{\Delta \mathbf{s}} = 10^{-2}$, the increase in $\Delta CRLB$ between $\sigma_\theta = 10^{-2}$ and $\sigma_\theta = 1$ for the far field case is about 2.8 dB.

Figure 3.4 illustrates the effect of the number of sensors on $\Delta CRLB$ for the far field (a) and near field (b) cases with different values of ${\sigma_\theta}^2$. This shows that increasing the number of sensors decreases $\Delta CRLB$. For example, with $\sigma_\theta = 10^{-2}$ and $\sigma_{\Delta \mathbf{s}} = 10^{-2}$, increasing N from 5 to 9 reduces $\Delta CRLB$ by 2.2 and 3.7 dB for the near and far field cases, respectively. In addition, for $N \geq 8$ the improvement in $\Delta CRLB$ is negligible. Even when the sensor position error variance is high, i.e., $\sigma_{\Delta \mathbf{s}} = 10^{-1}$, the change in $\Delta CRLB$ between $N = 8$ and $N = 9$ sensors is only 0.05 dB for a far field source.

The source location estimate is worse in the far field case compared to the near

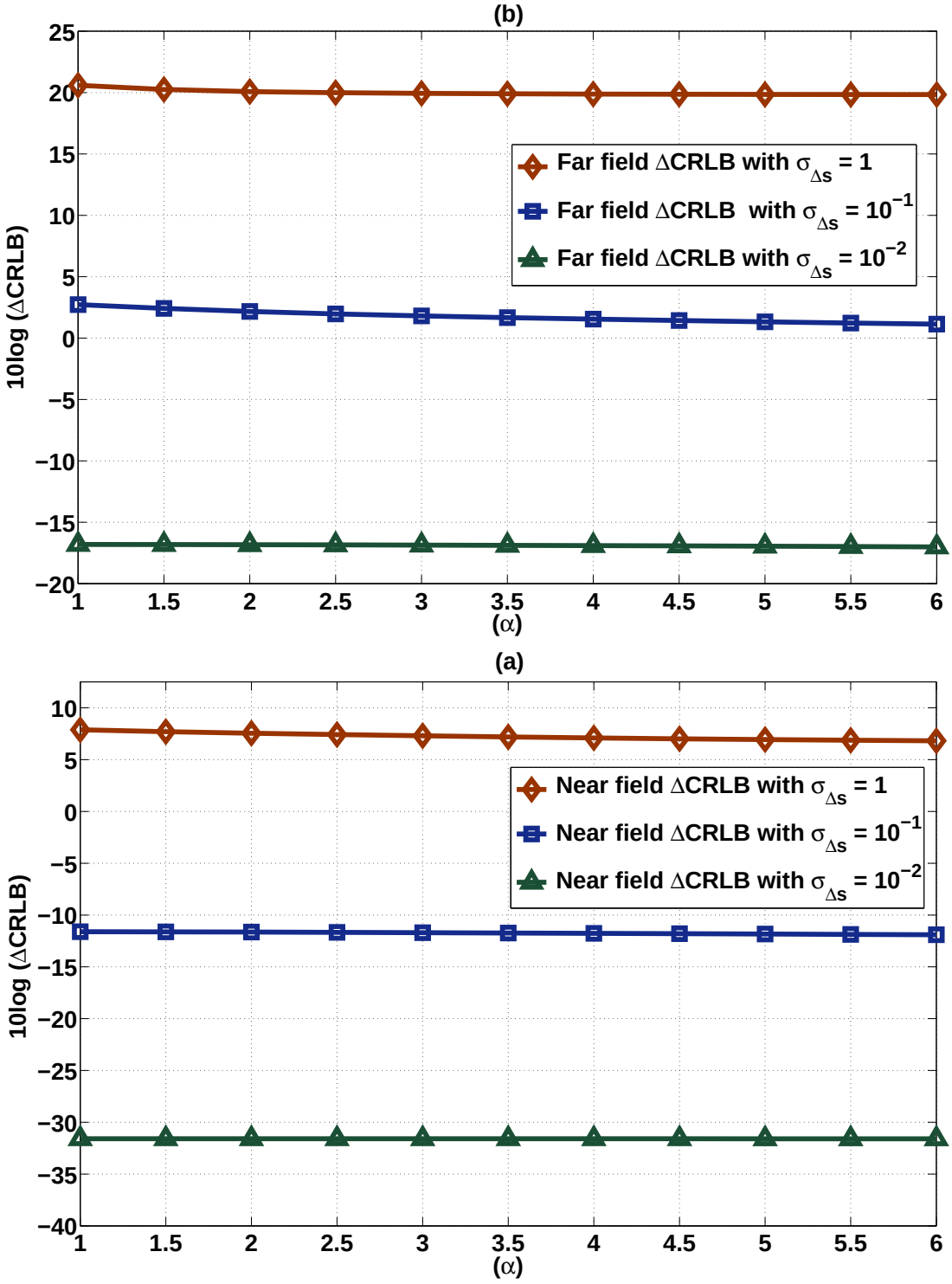

Figure 3.6: $\Delta CRLB$ versus path loss exponent γ for different values of $\sigma^2_{\Delta s}$ with $N = 6$ sensors for the (a) far field case, and (b) near field case.

field due to the increased path loss. Figure 3.5 compares $\Delta CRLB$ for the near field and far field cases with $\sigma_\theta = 10^{-2}$, $\sigma_{\Delta s} = 1$ and $N = 5$ to 9 sensors.

This shows that the rate that $\Delta CRLB$ decreases is lower in the far field case (16%), compared to the near field case (47%), when the number of sensors is increased from $N = 5$ to 9. The sensitivity of $\Delta CRLB$ with respect to the path loss exponent γ is depicted in Fig. 3.6 for the near field (a) and far field (b) cases with different sensor position error variances $\sigma^2_{\Delta \mathbf{s}}$.

In both cases, changing γ has a minimal effect on $\Delta CRLB$. Even for high sensor position uncertainty (e.g. $\sigma_{\Delta \mathbf{s}} = 1$), $\Delta CRLB$ decreases by 1.1 dB and 0.76 dB when γ increases from 1 to 6 for the near field and far field cases, respectively. This corresponds to a change in $\Delta CRLB$ of 14% percent and 3.7%, respectively. This rate of change decreases as $\sigma_{\Delta \mathbf{s}}$ decreases in both cases. As an example, the reduction in $\Delta CRLB$ for $\sigma_{\Delta \mathbf{s}} = 10^{-2}$ is 0.21 dB for the far field case, (corresponding to a 1.3% reduction in $\Delta CRLB$), as γ increases from 1 to 6. Therefore, variations in γ have little effect on $\Delta CRLB$.

Chapter 4

LSIE-NM and Minimax-MSE Methods

In this chapter the RSSD-based measurements are utilized to obtain the source location estimate with unknown transmitted power. Two methods are considered to this end. First, a constrained weighted least squares (CWLS) based method is utilized to obtain the location estimate in presence of the sensor uncertainty. The results are compared with other corresponding methods showing the efficiency of the proposed method. Next, a linear estimator based on the minimax optimization is developed for the case of known sensor location without sensor position uncertainty and the global source location estimate is obtained by converting the proposed problem into a semidefinite programming (SDP) problem. As will be discussed in the next chapter, the result will be extended to the case of sensor position uncertainty for future work.

4.1 Least Squares Initial Estimate-Newton Method

Let $\boldsymbol{\theta}_0$ be the initial value of $\boldsymbol{\theta}$. The constrained weighted least squares (CWLS) method can be used to obtain $\boldsymbol{\theta}_0$ from (2.11) by minimizing the constrained cost function

$$f(\boldsymbol{\theta}_0) = (\mathbf{A}\boldsymbol{\theta}_0 - \mathbf{b})^T \boldsymbol{\Phi}^{-\mathbf{1}} (\mathbf{A}\boldsymbol{\theta}_0 - \mathbf{b}), \tag{4.1}$$

where $\boldsymbol{\theta}_0 = \begin{bmatrix} x - \tilde{x}_1 & y - \tilde{y}_1 & r_1^2 \end{bmatrix}^T$ is the optimization variable vector and $\boldsymbol{\Phi}^{-1}$ is the corresponding weighting matrix that is found subject to the intermediate variable constraint r_1^2 as

$$\boldsymbol{\Lambda}^T \boldsymbol{\theta}_0 + {\boldsymbol{\theta}_0}^T \boldsymbol{\Psi} \boldsymbol{\theta}_0 = 0, \tag{4.2}$$

such that

$$\mathbf{\Lambda} = \begin{bmatrix} 0 & 0 & -1 \end{bmatrix}^T, \tag{4.3}$$

and

$$\mathbf{\Psi} = diag\{1, 1, 0\}. \tag{4.4}$$

The best linear unbiased estimator (BLUE) [58], can be used to obtain the optimum weighting matrix, $\mathbf{\Phi}^{-1}$, which is equal to the inverse of the covariance matrix of $\boldsymbol{\delta}$

$$\mathbf{\Phi}^{-1} = E[\boldsymbol{\delta}\boldsymbol{\delta}^T]^{-1} = (\mathbf{C}\mathbf{Q}_{\Delta\mathbf{u}}\mathbf{C}^T)^{-1}, \tag{4.5}$$

where $\mathbf{Q}_{\Delta\mathbf{u}}$ is the covariance matrix of the sensor position errors. Determining $\mathbf{C}$ in (2.10) requires the source location, which is not known. The simple initial choice based on BLUE [58] can be used and is given by $\mathbf{\Phi}_0 = diag\left\{\sigma^2_{\Delta\mathbf{u_2}}, \sigma^2_{\Delta\mathbf{u_3}}, \ldots, \sigma^2_{\Delta\mathbf{u_N}}\right\}$ where $\sigma^2_{\Delta\mathbf{u_i}} = \sigma^2_{\Delta\mathbf{x_i}} + \sigma^2_{\Delta\mathbf{y_i}}$. Then, the CWLS method can be used to obtain an initial source location estimate. The weights are iteratively updated using (4.5) to find the optimum weights, $\mathbf{\Phi}^{-1}$.

Minimizing (4.1) subject to (4.2) is equivalent to minimizing the Lagrangian cost function [68]-[69] using the corresponding Lagrange multipliers, λ, as

$$L(\boldsymbol{\theta_0}, \lambda) = f(\boldsymbol{\theta_0}) + \lambda(\boldsymbol{\theta_0}^T\mathbf{\Psi} + \mathbf{\Lambda}^T)\boldsymbol{\theta_0}. \tag{4.6}$$

The Lagrangian cost function $L(\boldsymbol{\theta_0}, \lambda)$ can be minimized by differentiating with respect to $\boldsymbol{\theta_0}$ giving

$$\frac{L(\boldsymbol{\theta_0}, \lambda)}{\partial\boldsymbol{\theta_0}} = \widehat{\mathbf{A}}\boldsymbol{\theta_0} - \widehat{\mathbf{b}}^{'} \tag{4.7}$$

where

$$\widehat{\mathbf{A}} = \mathbf{A}^T{\mathbf{\Phi_0}}^{-1}\mathbf{A} + \lambda\mathbf{\Psi}, \tag{4.8}$$

and

$$\widehat{\mathbf{b}} = \mathbf{A}^T{\mathbf{\Phi_0}}^{-1}\mathbf{b} - \lambda\mathbf{\Lambda}/2. \tag{4.9}$$

Equating (4.7) to zero gives $\widehat{\mathbf{A}}\boldsymbol{\theta}_0 = \widehat{\mathbf{b}}$ which yields the CWLS estimate

$$\hat{\boldsymbol{\theta}}_0 = (\mathbf{A}^T{\mathbf{\Phi_0}}^{-1}\mathbf{A} + \lambda\mathbf{\Psi})^{-1}(\mathbf{A}^T{\mathbf{\Phi_0}}^{-1}\mathbf{b} - 0.5\lambda\mathbf{\Lambda}), \tag{4.10}$$

where λ is a real root of a degree 5 equation obtained by taking the differentiation of (4.6) with respect to λ and equating the result to zero. Substituting the resulting values of λ into (4.10) yields the possible solutions, and the CWLS solution is the one

which results in the smallest value of (4.1).

Due to the non-convex cost function in (4.1), the initial estimate may yield only a locally optimal solution. Thus the Newton method (NM) is employed here to improve the accuracy of the initial estimate $\hat{\boldsymbol{\theta}}_0$ using the optimum weighting matrix (4.5). This algorithm has order-two convergence if the function to be minimized has a continuous second derivative. Let $\mathbf{A} = \begin{bmatrix} \mathbf{A}_2 & \mathbf{A}_3 \end{bmatrix}$ where $\mathbf{A}_2$ and $\mathbf{A}_3$ are the first two columns and the third column of matrix $\mathbf{A}$, respectively. Then the minimum of the nonlinear unconstrained problem

$$f(\mathbf{s}) = \boldsymbol{\alpha}^T \boldsymbol{\Phi}^{-1} \boldsymbol{\alpha}, \tag{4.11}$$

is required where $\mathbf{s}$ and $\boldsymbol{\alpha}$ are defined as

$$\mathbf{s} = \begin{bmatrix} x - \tilde{x}_1 & y - \tilde{y}_1 \end{bmatrix}^T, \tag{4.12}$$

and

$$\boldsymbol{\alpha} = \mathbf{A}_2 \mathbf{s} + \mathbf{A}_3 (\mathbf{s}^T \mathbf{s})^{1/2} - \mathbf{b}. \tag{4.13}$$

The solution can be obtained using the quadratic approximation of the Taylor series expansion of (4.1) which can be written as

$$\begin{aligned} f(\mathbf{s}_k) \approx f(\mathbf{s}_{k-1}) + (\mathbf{s}_k - \mathbf{s}_{k-1})^T \mathbf{G}_{k-1} + \\ \frac{1}{2} (\mathbf{s}_k - \mathbf{s}_{k-1})^T \mathbf{H}_{k-1} (\mathbf{s}_k - \mathbf{s}_{k-1}), \end{aligned} \tag{4.14}$$

where

$$\mathbf{G}_{k-1} = \left. \frac{\partial f(\mathbf{s})}{\partial \mathbf{s}} \right|_{\mathbf{s}=\mathbf{s}_{k-1}},$$

and

$$\mathbf{H}_{k-1} = \left. \frac{\partial^2 f(\mathbf{s})}{\partial \mathbf{s} \partial \mathbf{s}^T} \right|_{\mathbf{s}=\mathbf{s}_{k-1}}.$$

The gradient $\mathbf{G}_{k-1}$ and Hessian $\mathbf{H}_{k-1}$ matrices of $f(\mathbf{s})$ at $\mathbf{s}_{k-1}$ can be obtained from the first and second order derivatives of (4.11), respectively.

To minimize $f(\mathbf{s})$, let $\mathbf{G}_k = 0$, which from (4.14) gives

$$\frac{\partial f(\mathbf{s}_k)}{\partial \mathbf{s}_k} = \mathbf{G}_{k-1} + \mathbf{H}_{k-1} (\mathbf{s}_k - \mathbf{s}_{k-1}) = 0. \tag{4.15}$$

The Newton iteration is then

$$\mathbf{s}_k = \mathbf{s}_{k-1} - {\mathbf{H}_{k-1}}^{-1}\mathbf{G}_{k-1}, \tag{4.16}$$

where $\mathbf{s}_0$ is obtained from the CWLS estimate $\hat{\boldsymbol{\theta}}_0$ given by (4.10). Therefore, the solution can be obtained by calculating $\mathbf{G}_{k-1}$ and $\mathbf{H}_{k-1}$ at $\mathbf{s}_{k-1}$. Taking the first and second derivatives of (4.11) with respect to $\mathbf{s}$ yields the gradient and Hessian of $f(\mathbf{s})$ as

$$\begin{aligned}\frac{\partial f(\mathbf{s})}{\partial \mathbf{s}} &= \frac{\partial \boldsymbol{\alpha}^T}{\partial \mathbf{s}}\boldsymbol{\Phi}^{-1}\boldsymbol{\alpha} + \boldsymbol{\alpha}^T\frac{\partial(\boldsymbol{\Phi}^{-1}\boldsymbol{\alpha})}{\partial \mathbf{s}} \\ &= \boldsymbol{\mu}(\boldsymbol{\Phi}^{-1} + \boldsymbol{\Phi}^{-T})\boldsymbol{\alpha},\end{aligned} \tag{4.17}$$

and

$$\frac{\partial^2 f(\mathbf{s})}{\partial \mathbf{s}\partial \mathbf{s}^T} = \boldsymbol{\alpha}^T(\boldsymbol{\Phi}^{-1} + \boldsymbol{\Phi}^{-T})\mathbf{A}_3 + 2\boldsymbol{\mu}(\boldsymbol{\Phi}^{-1} + \boldsymbol{\Phi}^{-T})\boldsymbol{\mu}^T, \tag{4.18}$$

respectively, where $\boldsymbol{\mu} = \mathbf{A}_2^T + (\mathbf{s}^T\mathbf{s})^{-1/2}\mathbf{s}\mathbf{A}_3^T$ and $()^{-T}$ denotes inverse transpose. The

Algorithm 1 Least Squares Initial Estimate-Newton Method (LSIE-NM)

1: Calculate the inverse of the weighting matrix $\boldsymbol{\Phi}^{-1}$ using (4.5).
2: Calculate the Lagrange multiplier λ by differentiating (4.6).
3: Calculate the initial location estimate $\hat{\boldsymbol{\theta}}_0$ using (4.10).
4: Set *iter* as the number of iterations (*iter* = 2 is used here)
5: **for** $1 \leq k \leq iter$ **do**
6: $\quad\boldsymbol{\alpha} = \mathbf{A_2}\mathbf{s_{k-1}} + \mathbf{A_3}(\mathbf{s_{k-1}^T}\mathbf{s_{k-1}})^{\mathbf{1/2}} - \mathbf{b}$
7: $\quad\boldsymbol{\mu} = \mathbf{A}_2^T + (\mathbf{s}_{k-1}^T\mathbf{s_{k-1}})^{-1/2}\mathbf{s_{k-1}}\mathbf{A}_3^T$
8: $\quad$Calculate the gradient $\mathbf{G}_{k-1}$ and Hessian $\mathbf{H}_{k-1}$ using (4.17) and (4.18).
9: $\quad$**if** ($\mathbf{H}_{k-1}$ is not positive definite) **then**
10: $\quad\quad$Calculate the modified Hessian $\hat{\mathbf{H}}_{k-1}$ using [69]
11: $\quad$**end if**
12: $\quad\mathbf{s}_k = \mathbf{s}_{k-1} - {\mathbf{H}_{k-1}}^{-1}\mathbf{G}_{k-1}$
13: **end for**

Hessian matrix $\mathbf{H}_{k-1}$ used in (4.16) must be positive definite in each iteration of the Newton method [69]. To ensure this, a modified Hessian matrix $\hat{\mathbf{H}}_{k-1}$ can be employed. A practical method to modify $\mathbf{H}_{k-1}$ has been developed which is based on Gaussian elimination [68]-[69]. The LSIE-NM algorithm is summarized in Algorithm 1. The major weakness of the Newton algorithm is that convergence cannot be guaranteed. If the noise is very small or very large, the standard least squares or BLUE [58], respectively, can be used to obtain $\mathbf{s_0}$. The CWLS method is used here

to obtain $\mathbf{s_0}$, as it provides a more accurate estimate compared to the other methods. The performance improvement is illustrated in Section 4.2. The LSIE algorithm provides a good initial estimate so that non-convergence seldom arises (it was never encountered during the simulations). In addition, it was found that two iterations are sufficient to obtain an accurate estimate of $\mathbf{s}$.

4.1.1 Bias Analysis

The bias of the proposed method is analysed in this section using the first order perturbation technique. The second order noise term was ignored due to the fact that the corresponding noise power is not large. The bias is defined as

$$E\left\{\delta_{\mathbf{s}}\right\} = E\left\{\tilde{\mathbf{u}} - \mathbf{s}\right\}, \tag{4.19}$$

where $\boldsymbol{\delta}_{\mathbf{s}}$ is the error term, and $E\{\ \}$ denotes expectation. Let $\left[\begin{array}{cc} \mathbf{A}_2 & \mathbf{A}_3 \end{array}\right] = \left[\begin{array}{cc} \widehat{\mathbf{A}}_2 + \boldsymbol{\delta}_2 & \widehat{\mathbf{A}}_3 + \boldsymbol{\delta}_3 \end{array}\right]$ and $\mathbf{b} = \widehat{\mathbf{b}} + \boldsymbol{\delta}_{\mathbf{b}}$ where $\boldsymbol{\delta}_2$, $\boldsymbol{\delta}_3$ and $\boldsymbol{\delta}_{\mathbf{b}}$ represent the noise perturbations in $\mathbf{A_2}$, $\mathbf{A_3}$ and $\mathbf{b}$, respectively, and $\widehat{\mathbf{A}}_2$, $\widehat{\mathbf{A}}_3$ and $\widehat{\mathbf{b}}$ denote the corresponding true values. Considering the linear perturbation terms, (4.17) can be written as

$$\frac{\partial f(\mathbf{s})}{\partial \mathbf{s}} = \boldsymbol{\mu}^o(\boldsymbol{\Phi}^{-1} + \boldsymbol{\Phi}^{-T})\boldsymbol{\alpha}^o, \tag{4.20}$$

where

$$\begin{aligned} \boldsymbol{\mu}^o = &\left((\mathbf{s}+\boldsymbol{\delta}_{\mathbf{s}})^T(\mathbf{s}+\boldsymbol{\delta}_{\mathbf{u}})\right)^{-1/2}(\mathbf{s}+\boldsymbol{\delta}_{\mathbf{s}}) \\ &\times\left(\widehat{\mathbf{A}}_3+\boldsymbol{\delta}_3\right)^T + (\widehat{\mathbf{A}}_2+\boldsymbol{\delta}_2)^T, \end{aligned} \tag{4.21}$$

and

$$\begin{aligned} \boldsymbol{\alpha}^o = &\left(\widehat{\mathbf{A}}_2+\boldsymbol{\delta}_2\right)(\mathbf{s}+\boldsymbol{\delta}_{\mathbf{s}}) + \left(\widehat{\mathbf{A}}_3+\boldsymbol{\delta}_3\right) \\ &\times\left((\mathbf{s}+\boldsymbol{\delta}_{\mathbf{s}})^T(\mathbf{s}+\boldsymbol{\delta}_{\mathbf{s}})\right)^{1/2} - \left(\widehat{\mathbf{b}}+\boldsymbol{\delta}_{\mathbf{b}}\right). \end{aligned} \tag{4.22}$$

Substituting

$$\left((\mathbf{s}+\boldsymbol{\delta}_{\mathbf{s}})^T(\mathbf{s}+\boldsymbol{\delta}_{\mathbf{s}})\right)^{1/2} \simeq \left(\mathbf{s}^T\mathbf{s}\right)^{-1/2}\mathbf{s}^T\boldsymbol{\delta}_{\mathbf{s}} + \left(\mathbf{s}^T\mathbf{s}\right)^{1/2} \tag{4.23}$$

into (4.22) and considering that $\boldsymbol{\delta}_2 = \boldsymbol{\delta}_{\mathbf{b}} = \mathbf{0}$ as there are no perturbations in $\mathbf{A_2}$ and $\mathbf{b}$, gives

$$\begin{aligned}\boldsymbol{\alpha}^o &= \left(\widehat{\mathbf{A}}_3 + \boldsymbol{\delta}_3\right)\left\{\left(\mathbf{s}^T\mathbf{s}\right)^{-1/2}\mathbf{s}^T\boldsymbol{\delta}_{\mathbf{s}} + \left(\mathbf{s}^T\mathbf{s}\right)^{1/2}\right\} \\ &\quad + \widehat{\mathbf{A}}_2\left(\mathbf{s} + \boldsymbol{\delta}_{\mathbf{s}}\right) - \widehat{\mathbf{b}} \\ &\simeq \widehat{\mathbf{A}}_2\boldsymbol{\delta}_{\mathbf{s}} + \widehat{\mathbf{A}}_3\mathbf{s}^T\boldsymbol{\delta}_{\mathbf{s}}\left(\mathbf{s}^T\mathbf{s}\right)^{-1/2} + \boldsymbol{\delta}_3\left(\mathbf{s}^T\mathbf{s}\right)^{1/2} \\ &\simeq \mathbf{P}\boldsymbol{\delta}_{\mathbf{s}} + \boldsymbol{\delta}_3\left(\mathbf{s}^T\mathbf{s}\right)^{1/2},\end{aligned} \tag{4.24}$$

where

$$\mathbf{P} = \widehat{\mathbf{A}}_2 + \widehat{\mathbf{A}}_3\left(\mathbf{s}^T\mathbf{s}\right)^{-1/2}\mathbf{s}^T.$$

Note that $\boldsymbol{\delta_3}$ corresponds to the zero mean noise in $\mathbf{A_3}$ so that $E\{\boldsymbol{\delta}_3\} = \mathbf{0}$. Using (4.24), (4.20) can be expressed as

$$\mathbf{P}^T(\boldsymbol{\Phi}^{-1} + \boldsymbol{\Phi}^{-T})\left(\mathbf{P}\boldsymbol{\delta}_{\mathbf{s}} + \boldsymbol{\delta}_3\left(\mathbf{s}^T\mathbf{s}\right)^{1/2}\right) = \mathbf{0} \tag{4.25}$$

and then solving (4.25) gives

$$\begin{aligned}\boldsymbol{\delta}_{\mathbf{s}} &= \left\{\mathbf{P}^T\left(\boldsymbol{\Phi}^{-1} + \boldsymbol{\Phi}^{-T}\right)^{-1}\mathbf{P}\right\}^{-1}\mathbf{P}^T\left(\boldsymbol{\Phi}^{-T} + \boldsymbol{\Phi}^{-1}\right)^{-1}\boldsymbol{\delta}_3\left(\mathbf{s}^T\mathbf{s}\right)^{1/2} \\ &= \mathbf{P}^{-1}\left(\boldsymbol{\Phi}^{-1} + \boldsymbol{\Phi}^{-T}\right)\mathbf{P}^{-T}\mathbf{P}^T\left(\boldsymbol{\Phi}^{-1} + \boldsymbol{\Phi}^{-T}\right)^{-1}\boldsymbol{\delta}_3\left(\mathbf{s}^T\mathbf{s}\right)^{1/2} \\ &= \mathbf{P}^{-1}\boldsymbol{\delta}_3\left(\mathbf{s}^T\mathbf{s}\right)^{1/2}.\end{aligned} \tag{4.26}$$

Thus, the bias defined in (4.19) can be obtained by taking the expectation of (4.26) which gives

$$\begin{aligned}E\left\{\boldsymbol{\delta}_{\mathbf{s}}\right\} &= E\left\{\mathbf{P}^{-1}\boldsymbol{\delta}_3\left(\mathbf{s}^T\mathbf{s}\right)^{1/2}\right\} \\ &= \mathbf{P}^{-1}E\left\{\boldsymbol{\delta}_3\right\}\left(\mathbf{s}^T\mathbf{s}\right)^{1/2} = \mathbf{0}.\end{aligned} \tag{4.27}$$

This shows that the proposed estimator is unbiased when the noise is not large.

4.2 LSIE-NM Simulation Results

In this section, the performance of the proposed LSIE-NM algorithm is evaluated to verify the theoretical analysis. Both near and far field cases are considered in the presence of sensor location uncertainty in which the near field denotes the source to

be close to the sensor networks while the far field denotes the source is in far distance with respect to the sensor networks. The geometry of the actual and nominal sensor locations is given in Fig. 3.1. The nominal and unknown sensor coordinates are

Table 4.1: Far Field ΔMSE after k Iterations

Iteration	$\Delta MSE(dB)$ $\sigma^2 = 10^{-1}$	$\Delta MSE(dB)$ $\sigma^2 = 1$
k = 3	0.31	0.92
k = 5	0.40	1.45
k = 7	0.51	1.65
k = 9	0.62	1.68

denoted by $\mathbf{u}_i$ and $\tilde{\mathbf{u}}_i$, respectively. Fig. 4.1 shows the mean square error (MSE) of the proposed algorithm for different numbers of iterations versus $10\log(\sigma^2_{\Delta\mathbf{s}})$ with $\sigma_{\Delta\mathbf{s}} \in [0.001, 1]$. The near field source is located at $[400, 450]^T$ and results are given for $k = 1$ and $k = 2$ iterations with $\sigma^2_\theta = 10^{-2}$ and $\gamma = 2$. The corresponding CRLB is also shown for comparison purposes. For the near field case, the MSE is close to the CRLB after the first iteration for a small measurement noise variance, but the difference increases to 3.4 dB at $\sigma^2_{\Delta\mathbf{s}} = 1$. After the second iteration, the CRLB is essentially achieved for all values of $\sigma^2_{\Delta\mathbf{s}}$. For the far field case, there is a considerable difference between the results for the first and second iterations even with a small measurement noise variance. At $\sigma^2_{\Delta\mathbf{s}} = 10^{-4}$, this difference is about 2.6 dB. The second iteration provides a significant improvement as it achieves the CRLB for $\sigma^2_{\Delta\mathbf{s}} \leq 10^{-2}$. The worst case difference is 4.2 dB at $\sigma^2_{\Delta\mathbf{s}} = 1$. Further, the third iteration provides a very small improvement in the MSE compared to the second iteration in the far field case. Table 3.1 shows the change in far field MSE for different numbers of iterations with respect to the second iteration, defined as

$$\Delta MSE(dB) = MSE_k(dB) - MSE_2(dB),$$

where MSE_k denotes the far field MSE for the kth iteration. This shows that two iterations are sufficient in this case, so two iterations are used in the next section to evaluate the proposed method.

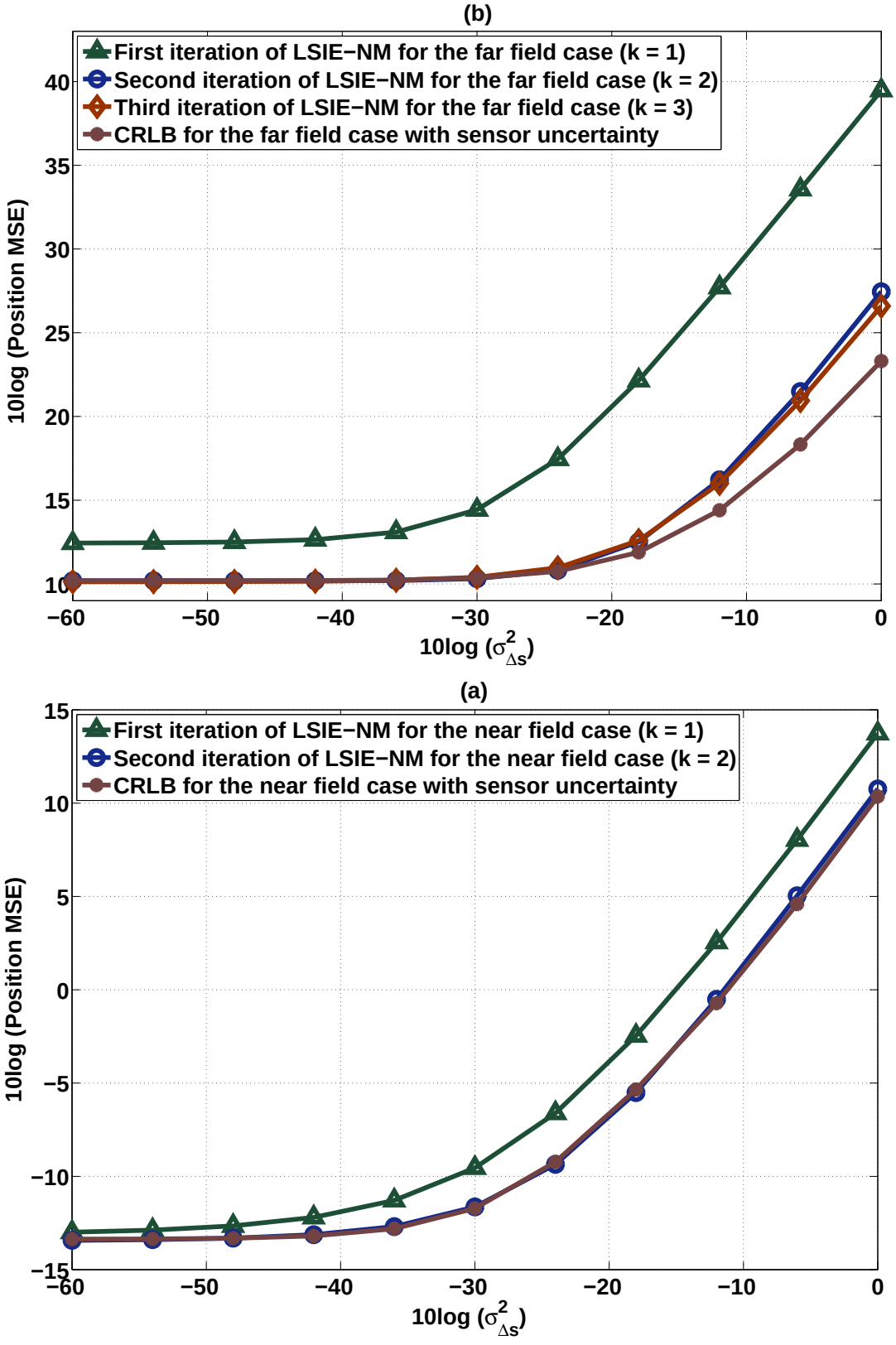

Figure 4.1: Source position MSE versus $\sigma^2_{\Delta \mathbf{s}}$ using the LSIE-NM algorithm for different numbers of iterations with $N = 6$ sensors for the (a) far field, and (b) near field cases.

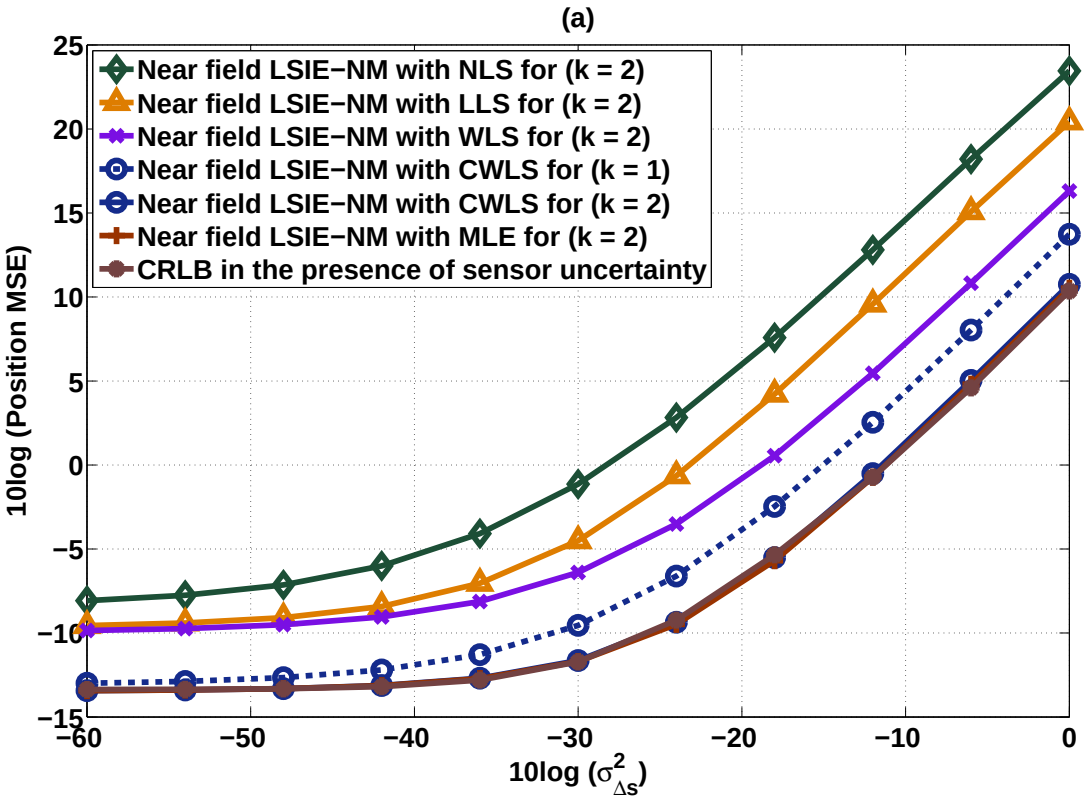

Figure 4.2: MSE for different values of $\sigma^2_{\Delta \mathbf{s}}$ for the near field case with $N = 6$ sensors and $\sigma^2_{\boldsymbol{\theta}} = 0.01$.

4.2.1 LSIE-NM with Different Methods for the Initial Estimate

In this section, the performance of the proposed method is compared to the performance of the maximum likelihood estimator (MLE) [43], WLS [46] LLS [45] and NLS [61] methods. The CRLB with sensor uncertainty is also considered as a benchmark for comparison. As the performance of the proposed method depends on the initial estimate, different methods are considered to obtain the initial estimate to compare the effect of this value on the final estimate. Figures 4.2 and 4.3 present the MSE of the source location estimate in the near field (NF) and far field (FF) cases for the first ($k = 1$) and second ($k = 2$) iterations of the proposed, MLE, WLS, LLS and NLS methods versus $\sigma^2_{\Delta \mathbf{s}}$. Figure 4.2 shows that the ML and CWLS techniques provide the best performance for the near field case as the CRLB is achieved. The NLS method has the worst performance, with a significant degradation even for a small sensor position error variance.

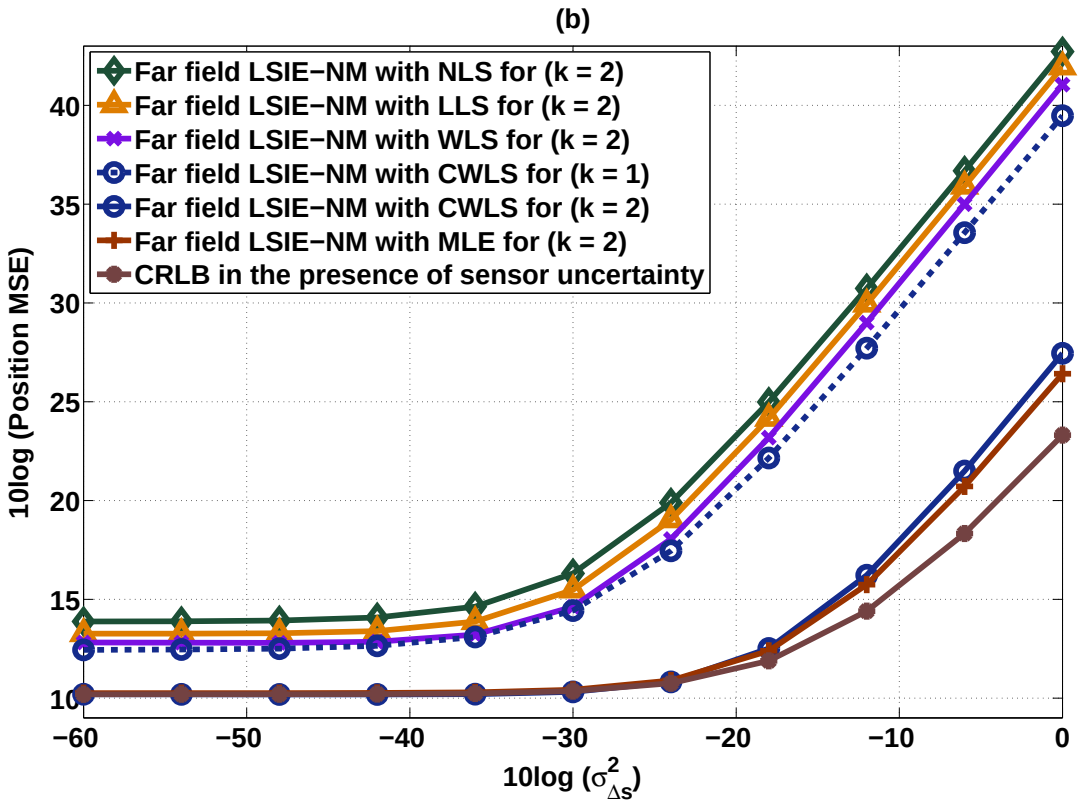

Figure 4.3: MSE for different values of $\sigma^2_{\Delta \mathbf{s}}$ for the far field case with and $N = 6$ sensors and $\sigma^2_{\boldsymbol{\theta}} = 0.01$.

The WLS method has better performance compared to the LLS and NLS methods, but there is still a significant difference compared to the ML and CWLS techniques. In the far field case, both the ML and CWLS methods are degraded compared to the CRLB for large values of $\sigma^2_{\Delta \mathbf{s}}$, as shown in Fig. 3.3. The difference is approximately 1.7 dB at $\sigma^2_{\Delta \mathbf{s}} = 0.1$. The WLS method is again better than the LLS and NLS methods. Further, the second iteration of the CWLS technique shows a significant performance improvement. The performance after two iterations with $\sigma_{\Delta \mathbf{s}} = 0.1$ for the near field and far field cases are shown in Tables 4.2 and 4.3, respectively. Figures 4.4 and 4.5 also depict the performance of the proposed and other RSSD methods for the near field and far field source location estimates, respectively. This shows that in both scenarios, LSIE-NM provides the best performance which is closest to the CRLB. The NLS method has the worst performance. The poor performance with the LS based RSSD method in [59] is due to not employing weights as well as constraints in the optimization. For example, at $\sigma^2_{\Delta \mathbf{s}} = 0.01$ there is approximately a 10.1 dB and 11.8 dB difference with respect to the CRLB for the near field and

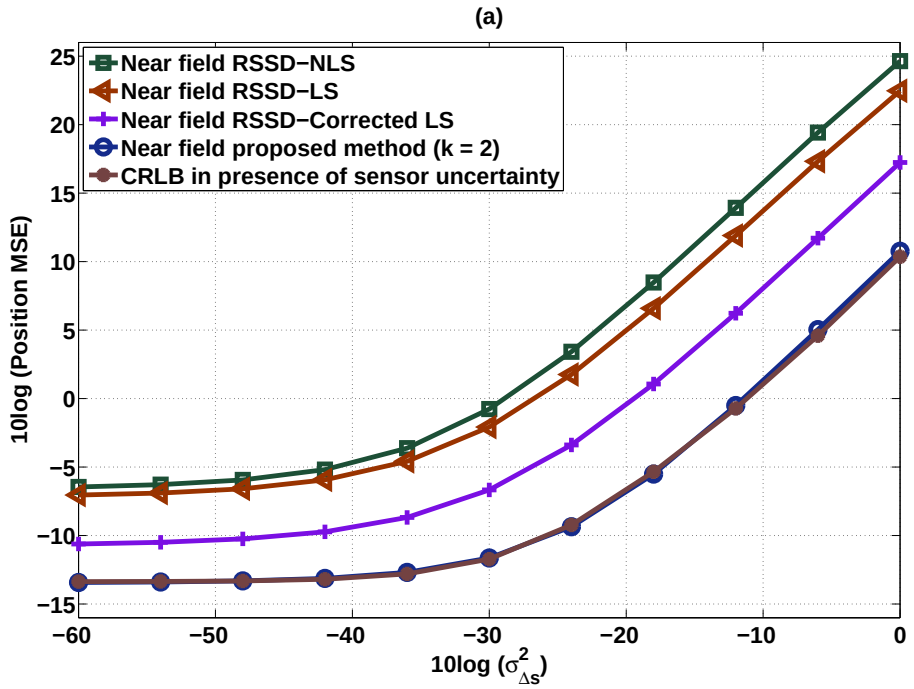

Figure 4.4: MSE versus $\sigma^2_{\Delta \mathbf{s}}$ for different RSSD based localization algorithms with $N = 6$ sensors and $\sigma^2_{\boldsymbol{\theta}} = 0.01$ in the near field case.

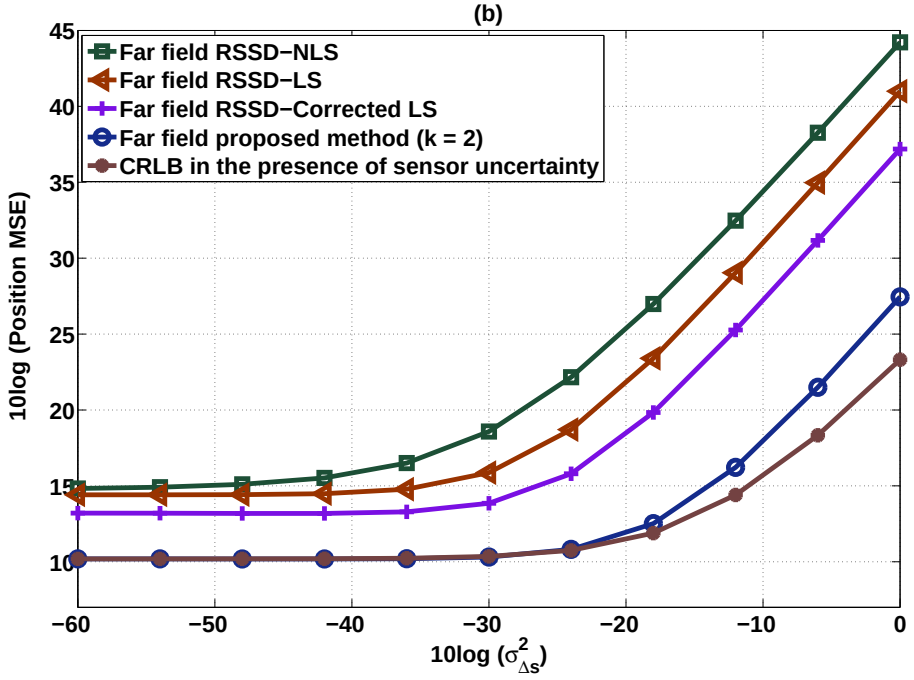

Figure 4.5: MSE versus $\sigma^2_{\Delta \mathbf{s}}$ for different RSSD based source localization algorithms with $N = 6$ sensors and $\sigma^2_{\boldsymbol{\theta}} = 0.01$ in the far field case.

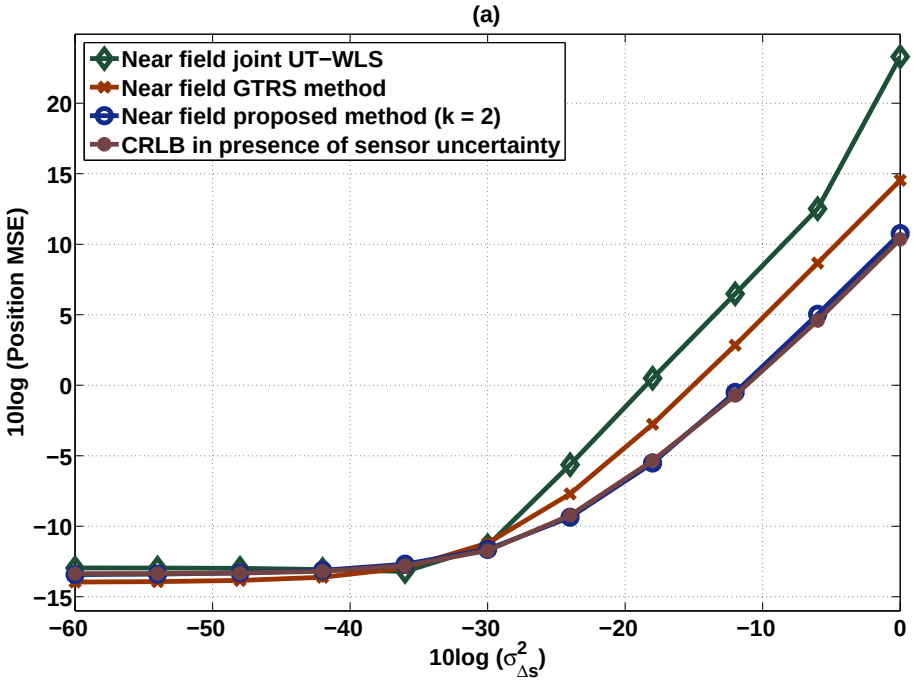

Figure 4.6: Comparison of different joint methods with $N = 6$ sensors and $\sigma_{\theta}^2 = 0.01$ in the near field case.

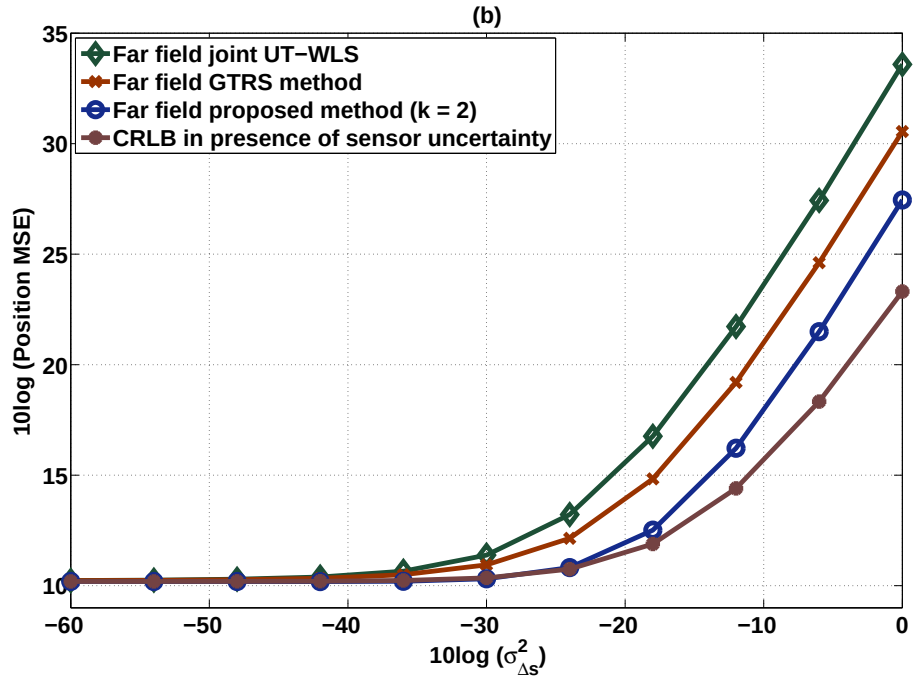

Figure 4.7: Comparison of different joint methods with $N = 6$ sensors and $\sigma_{\theta}^2 = 0.01$ in the far field case.

far field cases, respectively. Considering the error correction technique in [60], the performance of the LS based RSSD method in [59] is improved by approximately 4.5 dB and 3.8 dB at $\sigma^2_{\Delta\mathbf{s}} = 0.01$ for the near field and far field cases, respectively. Thus the degradation in performance of this method with respect to the CRLB is still considerable, particularly in the far field case. This is due to the fact that these RSSD based methods do not consider the effect of sensor uncertainty.

The proposed LSIE-NM method is next compared with the UT-WLS method [53] and the generalized trust region subproblem (GTRS) solution [64], which were recently developed based on joint RSS estimators. Fig. 6 and Fig. 7 present the performance of LSIE-NM and these methods for the near field and far field cases with $N = 6$ and $\sigma^2_{\boldsymbol{\theta}} = 0.01$. This shows that for sufficiently large SNRs, the UT-WLS and GTRS methods have performance comparable to the proposed approach, but for small SNRs, the proposed method provides better performance. For example, at $\sigma^2_{\Delta\mathbf{s}} = 0.01$ there is approximately a 2.2 dB and 5 dB difference for the GTRS and UT-WLS methods with respect to the proposed method for the near field case, and a corresponding difference of 3.1 dB and 6.2 dB for the far field case.

4.2.2 Complexity Analysis

In this section, the computational complexity of the proposed CWLS estimator is compared with the MLE, LLS, NLS and WLS estimators. The complexity is evaluated based on the number of floating point operations (flops). Each multiplication, sum and square root is considered as one flop. Let $\mathbf{R} = \mathbf{A}^T{\boldsymbol{\Phi}_\mathbf{0}}^{-1}\mathbf{A} + \lambda\boldsymbol{\Psi}$ and $\mathbf{S} = \mathbf{A}^T{\boldsymbol{\Phi}_\mathbf{0}}^{-1}\mathbf{b} - 0.5\lambda\boldsymbol{\Lambda}$. From (4.10), the initial estimate with the proposed method can be written as $\boldsymbol{\theta}_0 = \mathbf{R}^{-1}\mathbf{S}$. The number of flops required to obtain $\mathbf{R^{-1}}$ and $\mathbf{S}$ are given by

$$\mathbf{R}^{-1} = \overbrace{\underbrace{(\underbrace{\mathbf{A}^T{\boldsymbol{\Phi}_\mathbf{0}}^{-1}}_{3(2N^2-5N+3)}\mathbf{A} + \lambda\boldsymbol{\Psi})}^{6N^2-3N+18}{}^{-1}}^{3(2N^2+N+15)}, \tag{4.28}$$

and

$$\mathbf{S} = \underbrace{(\underbrace{\mathbf{A}^T{\boldsymbol{\Phi}_\mathbf{0}}^{-1}\mathbf{b}}_{6N^2-9N} - 0.5\lambda\boldsymbol{\Lambda})}_{3(2N^2-3N+2)+1}, \tag{4.29}$$

where N is the number of sensors. Therefore, the complexity of the CWLS estimator given by (4.10) is

$$\text{flops}_{CWLS} = 6(N^2 - N) + 67, \tag{4.30}$$

so the complexity has order $O(N^2)$ flops. From [43], and considering the cost function in (4.1), the computational complexity of the ML and NLS estimators is $O(N^3)$ flops, which is much higher than the proposed estimator. The complexity of the LLS and WLS estimators is $O(N)$ and $O(N^2)$, respectively [46],[45]. However, as shown by the results in this section, the performance of these estimators is very poor.

Table 4.2: Performance of Several Localization Methods in the Near Field with Sensor Uncertainty

	MLE	CWLS	WLS	LLS	NLS
Nominal Source Location	$\mathbf{x}_{NF} = 400$ $\mathbf{y}_{NF} = 450$	$\mathbf{x}_{NF} = 400$ $\mathbf{y}_{NF} = 450$	$\mathbf{x}_{NF} = 400$ $\mathbf{y}_{NF} = 450$	$\mathbf{x}_{NF} = 400$ $\mathbf{y}_{NF} = 450$	$\mathbf{x}_{NF} = 400$ $\mathbf{y}_{NF} = 450$
LSIE-NM ($k = 2$ iterations)	$\hat{\mathbf{x}} = 400.56$ $\hat{\mathbf{y}} = 450.13$	$\hat{\mathbf{x}} = 400.54$ $\hat{\mathbf{y}} = 449.88$	$\hat{\mathbf{x}} = 402.62$ $\hat{\mathbf{y}} = 450.53$	$\hat{\mathbf{x}} = 405.73$ $\hat{\mathbf{y}} = 454.48$	$\hat{\mathbf{x}} = 409.18$ $\hat{\mathbf{y}} = 445.44$
Bias Error (|Nominal-Estimated|)	$\boldsymbol{\varepsilon}_{MLE} = 0.57$	$\boldsymbol{\varepsilon}_{CWLS} = 0.55$	$\boldsymbol{\varepsilon}_{WLS} = 2.67$	$\boldsymbol{\varepsilon}_{LLS} = 7.27$	$\boldsymbol{\varepsilon}_{NLS} = 10.67$
$10\log($|Nominal-Estimated|$)$	$\boldsymbol{\varepsilon}(dB) = -2.44$	$\boldsymbol{\varepsilon}(dB) = -2.57$	$\boldsymbol{\varepsilon}(dB) = 4.26$	$\boldsymbol{\varepsilon}(dB) = 8.61$	$\boldsymbol{\varepsilon}(dB) = 10.28$

Table 4.3: Performance of Several Localization Methods in the Far Field with Sensor Uncertainty

	MLE	CWLS	WLS	LLS	NLS
Nominal Source Location	$\mathbf{x}_{FF} = 2500$ $\mathbf{y}_{FF} = 2100$	$\mathbf{x}_{FF} = 2500$ $\mathbf{y}_{FF} = 2100$	$\mathbf{x}_{FF} = 2500$ $\mathbf{y}_{FF} = 2100$	$\mathbf{x}_{FF} = 2500$ $\mathbf{y}_{FF} = 2100$	$\mathbf{x}_{FF} = 2500$ $\mathbf{y}_{FF} = 2100$
LSIE-NM ($k = 2$ iterations)	$\hat{\mathbf{x}} = 2502.5$ $\hat{\mathbf{y}} = 2095.9$	$\hat{\mathbf{x}} = 2503.3$ $\hat{\mathbf{y}} = 2095.7$	$\hat{\mathbf{x}} = 2531.9$ $\hat{\mathbf{y}} = 2057.5$	$\hat{\mathbf{x}} = 2532.3$ $\hat{\mathbf{y}} = 2057.1$	$\hat{\mathbf{x}} = 2552.7$ $\hat{\mathbf{y}} = 2077.6$
Bias Error (|Nominal-Estimated|)	$\boldsymbol{\varepsilon}_{MLE} = 4.80$	$\boldsymbol{\varepsilon}_{CWLS} = 5.42$	$\boldsymbol{\varepsilon}_{WLS} = 53.54$	$\boldsymbol{\varepsilon}_{LLS} = 53.71$	$\boldsymbol{\varepsilon}_{NLS} = 57.45$
$10\log($|Nominal-Estimated|$)$	$\boldsymbol{\varepsilon}(dB) = 6.81$	$\boldsymbol{\varepsilon}(dB) = 7.34$	$\boldsymbol{\varepsilon}(dB) = 17.29$	$\boldsymbol{\varepsilon}(dB) = 17.30$	$\boldsymbol{\varepsilon}(dB) = 17.59$

4.3 Minimax SDP Localization

In this section, a Minimax SDP approach is developed for the RSSD problem without sensor position uncertainty with sufficiently large SNR. Considering the RSSD based model developed in chapter 2, the system model without sensor position uncertainty can be reformulated using (2.7). Lets define $c_{1i} = 10^{\frac{\Delta \tilde{P}_{1i}}{5\gamma}}$ which can be approximated using a first-order Taylor series for sufficiently small noise levels as $c_{1i} = \eta_{1i}\left(\frac{5\gamma}{\ln 10} + \upsilon_{i1}\right)$, where $\eta_{1i} = \frac{\ln 10}{5\gamma} 10^{\frac{\Delta P_{1i}}{5\gamma}}$. Thus, considering the intermediate variable $R^2 = x^2 + y^2$, the RSSD measurement in (2.7) without sensor position uncertainty can be reformulated in matrix format as

$$\mathbf{A}\boldsymbol{\theta} = \mathbf{b}, \tag{4.31}$$

where

$$\mathbf{A} = \begin{bmatrix} 2(c_{12}x_1 - x_2) & 2(c_{12}y_1 - y_2) & 1 - c_{12} \\ \vdots & \vdots & \vdots \\ 2(c_{1N}x_1 - x_N) & 2(c_{1N}y_1 - y_N) & 1 - c_{1N} \end{bmatrix},$$

$$\boldsymbol{\theta} = \begin{bmatrix} x & y & R^2 \end{bmatrix}^T,$$

and

$$\mathbf{b} = \begin{bmatrix} c_{12}(x_1^2 + y_1^2) - (x_2^2 + y_2^2) \\ \vdots \\ c_{1N}(x_1^2 + y_1^2) - (x_N^2 + y_N^2) \end{bmatrix}.$$

Define the data matrices as $\tilde{\mathbf{A}}$ and $\tilde{\mathbf{b}}$, and the perturbation matrices as $\boldsymbol{\Delta}\mathbf{A}$ and $\boldsymbol{\Delta}\mathbf{b}$. Thus, (4.31) can be expressed in matrix form as

$$\left(\tilde{\mathbf{A}} + \boldsymbol{\Delta}\mathbf{A}\right)\boldsymbol{\theta} = \left(\tilde{\mathbf{b}} + \boldsymbol{\Delta}\mathbf{b}\right) \tag{4.32}$$

where

$$\tilde{\mathbf{A}} = \begin{bmatrix} 2\left(\frac{5\eta_{12}}{\ln 10}\gamma x_1 - x_2\right) & 2\left(\frac{5\eta_{12}}{\ln 10}\gamma y_1 - y_2\right) & 1 - \frac{5\eta_{12}}{\ln 10}\gamma \\ \vdots & \vdots & \vdots \\ 2\left(\frac{5\eta_{1N}}{\ln 10}\gamma x_1 - x_N\right) & 2\left(\frac{5\eta_{1N}}{\ln 10}\gamma y_1 - y_N\right) & 1 - \frac{5\eta_{1N}}{\ln 10}\gamma \end{bmatrix},$$

$$\boldsymbol{\Delta}\mathbf{A} = \begin{bmatrix} 2\eta_{12}x_1\upsilon_{21} & 2\eta_{12}y_1\upsilon_{21} & -\eta_{12}\upsilon_{21} \\ \vdots & \vdots & \vdots \\ 2\eta_{1N}x_1\upsilon_{N1} & 2\eta_{1N}y_1\upsilon_{N1} & -\eta_{1N}\upsilon_{N1} \end{bmatrix},$$

$$\tilde{\mathbf{b}} = \begin{bmatrix} \frac{5\eta_{12}}{\ln 10}\gamma R_1^2 - R_2^2 \\ \vdots \\ \frac{5\eta_{1N}}{\ln 10}\gamma R_1^2 - R_N^2 \end{bmatrix}, \quad \boldsymbol{\Delta}\mathbf{b} = R_1^2 \begin{bmatrix} \eta_{12}\upsilon_{21} \\ \vdots \\ \eta_{1N}\upsilon_{N1} \end{bmatrix}.$$

$\tilde{\mathbf{A}} \in \Re^{(N-1)\times 3}$ and $\tilde{\mathbf{b}} \in \Re^{(N-1)}$ are data matrices, $\boldsymbol{\Delta}\mathbf{A} \in \Re^{(N-1)\times 3}$ and $\boldsymbol{\Delta}\mathbf{b} \in \Re^{(N-1)}$ are perturbation matrices, and $R_i^2 = x_i^2 + y_i^2$. Hence, (4.31) can be expressed as $\mathbf{A}\boldsymbol{\theta} = \mathbf{b}$, where $\mathbf{A} = \tilde{\mathbf{A}} + \boldsymbol{\Delta}\mathbf{A}$ and $\mathbf{b} = \tilde{\mathbf{b}} + \boldsymbol{\Delta}\mathbf{b}$. Note that both $\mathbf{A}$ and $\mathbf{b}$ contain perturbation error terms.

4.3.1 MSE Problem Formulation

The problem of estimating the unknown parameter vector $\boldsymbol{\theta}$ from (4.32) is considered in this section. It is assumed that $\boldsymbol{\theta}$ satisfies the upper bound constraint $\|\boldsymbol{\theta}\|^2 = \boldsymbol{\theta}^T\boldsymbol{\theta} \leq \mu$ where μ is a positive scaler and $\|\cdot\|$ denotes the norm. Let $\hat{\boldsymbol{\theta}}$ be the linear estimate of $\boldsymbol{\theta}$ given by

$$\hat{\boldsymbol{\theta}} = \boldsymbol{\Upsilon}\tilde{\mathbf{b}}, \tag{4.33}$$

where $\boldsymbol{\Upsilon} \in \Re^{3\times(M-1)}$ is the unknown estimation matrix. Considering (4.32) and (4.33), $\hat{\boldsymbol{\theta}}$ can be obtained by minimizing the mean square error (MSE) which is given by the following optimization problem

$$\min_{\hat{\boldsymbol{\theta}}} \; E\left\{\left(\hat{\boldsymbol{\theta}} - \boldsymbol{\theta}\right)^T\left(\hat{\boldsymbol{\theta}} - \boldsymbol{\theta}\right)\right\}, \tag{4.34}$$

where $E\{\cdot\}$ denotes expected value. Using (4.32) and (4.33), the MSE in (4.34) can be written as

$$\begin{aligned} \text{MSE} &= E\left\{\left\|\hat{\boldsymbol{\theta}} - \boldsymbol{\theta}\right\|^2\right\} = E\left\{\left(\boldsymbol{\Upsilon}\tilde{\mathbf{b}} - \boldsymbol{\theta}\right)^T\left(\boldsymbol{\Upsilon}\tilde{\mathbf{b}} - \boldsymbol{\theta}\right)\right\} \\ &= E\left\{\left(\boldsymbol{\Upsilon}\left(\tilde{\mathbf{A}}\boldsymbol{\theta} + \boldsymbol{\Delta}\mathbf{A}\boldsymbol{\theta} - \boldsymbol{\Delta}\mathbf{b}\right) - \boldsymbol{\theta}\right)^T\left(\boldsymbol{\Upsilon}\left(\tilde{\mathbf{A}}\boldsymbol{\theta}\right.\right.\right. \\ &\quad \left.\left.\left. + \; \boldsymbol{\Delta}\mathbf{A}\,\boldsymbol{\theta} - \boldsymbol{\Delta}\mathbf{b}\right) - \boldsymbol{\theta}\right)\right\} = \mathbf{M}_{\mathbf{b}} + \tilde{\mathbf{M}} + \mathbf{M}_{\mathbf{A}} \end{aligned} \tag{4.35}$$

where

$$\mathbf{M}_{\mathbf{b}} = E\left\{\boldsymbol{\Delta}\mathbf{b}^T\boldsymbol{\Upsilon}^T\boldsymbol{\Upsilon}\boldsymbol{\Delta}\mathbf{b}\right\},$$

$$\tilde{\mathbf{M}} = -E\left\{\boldsymbol{\theta}^T\mathbf{A}^T\boldsymbol{\Upsilon}^T\boldsymbol{\Upsilon}\boldsymbol{\Delta}\mathbf{b} + \boldsymbol{\Delta}\mathbf{b}^T\boldsymbol{\Upsilon}^T\boldsymbol{\Upsilon}\mathbf{A}\boldsymbol{\theta}\right\},$$

$$\mathbf{M}_{\mathbf{A}} = \boldsymbol{\theta}^T\left\{\boldsymbol{\Lambda}^T\boldsymbol{\Lambda} + E\left(\boldsymbol{\Delta}\mathbf{A}^T\left(\boldsymbol{\Upsilon}^T\boldsymbol{\Upsilon}\right)\boldsymbol{\Delta}\mathbf{A}\right)\right\}\boldsymbol{\theta},$$

in which $\mathbf{\Lambda} = \mathbf{\Upsilon}\tilde{\mathbf{A}} - \mathbf{I}$. The terms $\mathbf{M_A}$, $\tilde{\mathbf{M}}$ and $\mathbf{M_b}$ can be calculated as follows. Define $\mathbf{Q_b} = E\left\{\mathbf{\Delta b}\mathbf{\Delta b}^T\right\}$ as the covariance matrix of the perturbation vector $\mathbf{\Delta b}$. Then

$$\mathbf{M_b} = \mathbf{Tr}\left(\mathbf{\Upsilon} E\left\{\mathbf{\Delta b}\mathbf{\Delta b}^T\right\}\mathbf{\Upsilon}^T\right) = \mathbf{Tr}\left(\mathbf{\Upsilon}\mathbf{Q_b}\mathbf{\Upsilon}^T\right), \tag{4.36}$$

where $\mathbf{Tr}\left(\cdot\right)$ denotes trace. The pth element of the vector $\mathbf{\Phi} = -\mathbf{A}^T\mathbf{\Upsilon}^T\mathbf{\Upsilon}\mathbf{\Delta b}$ in $\tilde{\mathbf{M}}$ can be written as

$$\mathbf{\Phi}_p = \sum_{k=1}^{N-1}\left(\sum_{m=1}^{N-1} -\mathbf{\Delta b}_m\left(\mathbf{\Upsilon}^T\mathbf{\Upsilon}\right)_{km}\right)\mathbf{\Delta A}_{pk}^T, \tag{4.37}$$

where $\mathbf{\Delta b}_m$ is the mth element of the corresponding vector and $\mathbf{\Phi} \in \Re^{3\times 1}$. Then from (4.37) we have

$$\begin{aligned} E\left\{\mathbf{\Phi}\right\} &= \sum_{k=1}^{N-1}\sum_{m=1}^{N-1} -\left(\mathbf{\Upsilon}^T\mathbf{\Upsilon}\right)_{(mk)} E\left\{\mathbf{\Delta A}_{kp}\mathbf{\Delta b}_m\right\} \\ &= \sum_{m,k=1}^{N-1} \mathbf{q}_m\left(\mathbf{\Upsilon}^T\mathbf{\Upsilon}\right)_{(mk)}, \end{aligned} \tag{4.38}$$

where $\mathbf{q}_m = -E\left\{\overset{[m]}{\mathbf{\Delta A}}\,\mathbf{\Delta b}_m\right\}$ and $\overset{[m]}{\mathbf{\Delta A}}$ denotes the mth column of the perturbation matrix $\mathbf{\Delta A}^T$. Then using (4.38) we obtain

$$\tilde{\mathbf{M}} = \boldsymbol{\theta}^T E\left\{\mathbf{\Phi}\right\} + E\left\{\mathbf{\Phi}\right\}^T\boldsymbol{\theta} = 2\boldsymbol{\theta}^T E\left\{\mathbf{\Phi}\right\}. \tag{4.39}$$

Defining $\mathbf{\Psi} = \mathbf{\Delta A}^T\mathbf{\Upsilon}^T\mathbf{\Upsilon}\mathbf{\Delta A}$, then

$$\mathbf{\Psi}_{(pq)} = \sum_{k=1}^{N-1}\left(\sum_{m=1}^{N-1}\mathbf{\Delta A}_{(pm)}^T\left(\mathbf{\Upsilon}^T\mathbf{\Upsilon}\right)_{mk}\right)\mathbf{\Delta A}_{kp}, \tag{4.40}$$

where $\mathbf{\Psi} \in \Re^{3\times 3}$. Using (4.40) and $\mathbf{Q_A}[mk] = E\left\{\overset{[m]}{\mathbf{\Delta A}}\ \overset{[k]}{\mathbf{\Delta A}}\right\}$, which is the covariance matrix between the mth and kth columns of $\mathbf{\Delta A}^T$, we obtain

$$\begin{aligned} E\left\{\mathbf{\Psi}\right\} &= \sum_{k=1}^{N-1}\sum_{m=1}^{N-1} E\left\{\overset{[m]}{\mathbf{\Delta A}}\ \overset{[k]}{\mathbf{\Delta A}}\right\}\left(\mathbf{\Upsilon}^T\mathbf{\Upsilon}\right)_{mk} \\ &= \sum_{m=1}^{N-1} \mathbf{Q_A}[mk]\left(\mathbf{\Upsilon}^T\mathbf{\Upsilon}\right)_{mk} \end{aligned} \tag{4.41}$$

Note that $\tilde{\mathbf{M}}$ and $\mathbf{M_A}$ depend on the parameter vector $\boldsymbol{\theta}$, so it is not possible to directly estimate $\mathbf{\Upsilon}$ for the minimization problem in (4.34), while $\mathbf{M_b}$ is independent of $\boldsymbol{\theta}$. Considering $\boldsymbol{\theta}^T\boldsymbol{\theta} \leq \mu$, an optimization problem can be developed which minimizes the worst case MSE in (4.35) so that (4.34) can be reformulated as

$$\begin{aligned} \mathbf{\Upsilon} &= \arg\min \max_{\boldsymbol{\theta}^T\boldsymbol{\theta}\leq\Psi} E\left\{\left(\hat{\boldsymbol{\theta}}-\boldsymbol{\theta}\right)^T\left(\hat{\boldsymbol{\theta}}-\boldsymbol{\theta}\right)\right\} \\ &= \arg\min \max_{\boldsymbol{\theta}^T\boldsymbol{\theta}\leq\Psi} \mathbf{M_b} + \tilde{\mathbf{M}} + \mathbf{M_A} \\ &= \arg\min \left\{\mathbf{M_b} + \max_{\boldsymbol{\theta}^T\boldsymbol{\theta}\leq\Psi}\left(\tilde{\mathbf{M}} + \mathbf{M_A}\right)\right\}. \end{aligned} \tag{4.42}$$

From (4.39) and (4.41), the term $\max\left(\tilde{\mathbf{M}} + \widehat{\mathbf{M}}_{\mathbf{A}}\right)$ in (4.42) can be reformulated as the following minimization problem

$$\max_{\boldsymbol{\theta}^T\boldsymbol{\theta}\leq\Psi} \boldsymbol{\theta}^T\left(\mathbf{\Lambda}^T\mathbf{\Lambda} + E\left\{\mathbf{\Psi}\right\}\right)\boldsymbol{\theta} + 2\boldsymbol{\theta}^T E\left\{\mathbf{\Phi}\right\} =$$

$$\begin{aligned} &\min_{\tau}\ \mu\tau + 2\mu^{1/2} E\left\{\mathbf{\Phi}\right\} \\ &\mathbf{s.t.}\quad \tau\mathbf{I} - \left\{\mathbf{\Lambda}^T\mathbf{\Lambda} + E\left\{\mathbf{\Psi}\right\}\right\} \succeq 0, \end{aligned} \tag{4.43}$$

where $\mathbf{G} \succeq 0$ denotes that $\mathbf{G}$ is positive semidefinite and $\mu_{\max}[\cdot]$ denotes the maximum eigenvalue. Substituting (4.38) and (4.41) in the MSE based minimax optimization problem in (4.42) gives

$$\begin{aligned} &\min_{\tau,\mathbf{\Lambda}}\ \mathbf{M_b} + \mu\tau + 2\mu^{1/2}\sum_{m,k=1}^{N-1}\mathbf{q}_m\left(\mathbf{\Upsilon}^T\mathbf{\Upsilon}\right)_{(mk)} \\ &\mathbf{s.t.}\ \tau\mathbf{I} - \left\{\sum_{m=1}^{N-1}\mathbf{Q_A}[mk]\left(\mathbf{\Upsilon}^T\mathbf{\Upsilon}\right)_{mk} + \mathbf{\Lambda}^T\mathbf{\Lambda}\right\} \succeq 0, \end{aligned} \tag{4.44}$$

4.3.2 RSSD Based Localization via SDR

In this section, the RSSD based optimization problem given by (4.44) is reformulated as a convex optimization problem using semidefinite programming (SDP) [20]. This allows a globally optimum solution to be obtained efficiently using SDP solvers such as SDPT3 and SeDuMi [22],[23] that employ the interior point method [20]. Because of $\mathbf{M_b}$, the objective function of the optimization problem in (4.44) is nonlinear in terms of the unknown term $\boldsymbol{\Upsilon}$. Define the auxiliary variables $\mathbf{U} = \boldsymbol{\Upsilon}^T\boldsymbol{\Upsilon}$ and $\mathbf{V} = \boldsymbol{\Upsilon}\mathbf{Q_b}\boldsymbol{\Upsilon}^T$ with$\mathbf{U} \in \Re^{(M-1)\times(M-1)}$ and $\mathbf{V} \in \Re^{3\times 3}$. Using semidefinite relaxation (SDR) [20], we obtain

$$\begin{aligned} &\mathbf{U} - \boldsymbol{\Upsilon}^T\boldsymbol{\Upsilon} \succeq 0, \\ &\mathbf{V} - \boldsymbol{\Upsilon}\mathbf{Q_b}\boldsymbol{\Upsilon}^T \succeq 0. \end{aligned} \tag{4.45}$$

The inequality constraints in (4.44) and (4.45) can be reformulated into linear matrix inequalities using Schur's Complement Lemma [66]-[67] which is defined as follows.

Lemma 1. *Define a symmetric matrix as*

$$\mathbf{T} = \begin{bmatrix} \mathbf{H} & \mathbf{R} \\ \mathbf{R}^T & \mathbf{L} \end{bmatrix},$$

where $\mathbf{L}$ *is a positive definite matrix* ($\mathbf{L} \succ 0$). *Then the Schur complement of* $\mathbf{L}$ *defined as*

$$\tilde{\mathbf{L}} = \mathbf{H} - \mathbf{R}\mathbf{L}^{-1}\mathbf{R}^T,$$

is positive semi-definite ($\tilde{\mathbf{L}} \succeq \mathbf{0}$) *if and only if* $\mathbf{T}$ *is positive semi-definite* ($\mathbf{T} \succeq \mathbf{0}$).

Hence, the inequality constraints in (4.44) and (4.45) can be expressed as

$$\begin{aligned} &\begin{bmatrix} \mathbf{U} & \boldsymbol{\Upsilon}^T \\ \boldsymbol{\Upsilon} & \mathbf{I} \end{bmatrix} \succeq 0, \quad \begin{bmatrix} \mathbf{V} & \boldsymbol{\Upsilon} \\ \boldsymbol{\Upsilon}^T & \mathbf{Q_b}^{-1} \end{bmatrix} \succeq 0, \\ &\begin{bmatrix} \tau\mathbf{I} - \left(\sum_{m,k=1}^{N-1} \mathbf{Q_A}\left[mk\right](\mathbf{U})_{(mk)} \right) & \boldsymbol{\Lambda}^T \\ \boldsymbol{\Lambda} & \mathbf{I} \end{bmatrix} \succeq 0. \end{aligned} \tag{4.46}$$

Then the minimax optimization problem given by (4.44) can be expressed as an SDP problem based on the corresponding linear matrix inequalities in (4.46) which yields

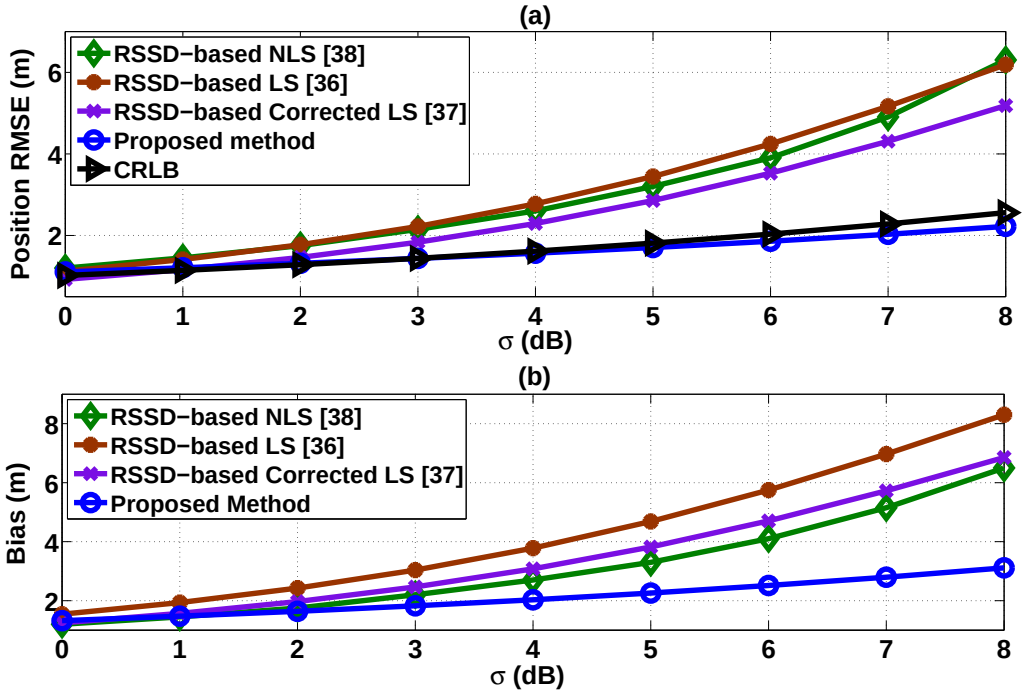

Figure 4.8: Comparison of several RSSD based source location estimation algorithms with $\gamma = 2$ and $N = 7$ sensors, (a) position RMSE, and (b) bias.

$$\min_{\mathbf{U},\mathbf{V},\boldsymbol{\Upsilon},\tau} \quad \mu\tau + 2\mu^{1/2} \sum_{m,k=1}^{N-1} \mathbf{q}_m(\mathbf{U})_{(mk)} + \mathbf{Tr}\{\mathbf{V}\}$$

$$\mathbf{s.t.} \quad \begin{bmatrix} \mathbf{V} & \boldsymbol{\Upsilon} \\ \boldsymbol{\Upsilon}^T & \mathbf{Q}_\mathbf{b}^{-1} \end{bmatrix} \succeq 0, \begin{bmatrix} \mathbf{U} & \boldsymbol{\Upsilon}^T \\ \boldsymbol{\Upsilon} & \mathbf{I} \end{bmatrix} \succeq 0 \tag{4.47}$$

$$\begin{bmatrix} \tau\mathbf{I} - \left(\sum_{m,k=1}^{N-1} \mathbf{Q}_\mathbf{A}[mk] (\mathbf{U})_{(mk)} \right) & \tilde{\mathbf{A}}^T\boldsymbol{\Upsilon}^T - \mathbf{I} \\ \boldsymbol{\Upsilon}\tilde{\mathbf{A}} - \mathbf{I} & \mathbf{I} \end{bmatrix} \succeq 0.$$

This is a convex optimization problem for which a globally optimal solution can be calculated efficiently using SDP solvers.

4.4 Minimax SDP Performance Evaluation

In this section, simulation results are presented to evaluate the performance of the proposed RSSD based minimax SDP method. We set $\gamma = 2$ and distribute $N = 7$ sensors within the 2D geometry with known coordinates $(1, 1)$, $(5, 5)$, $(5, 15)$, $(15, 5)$,

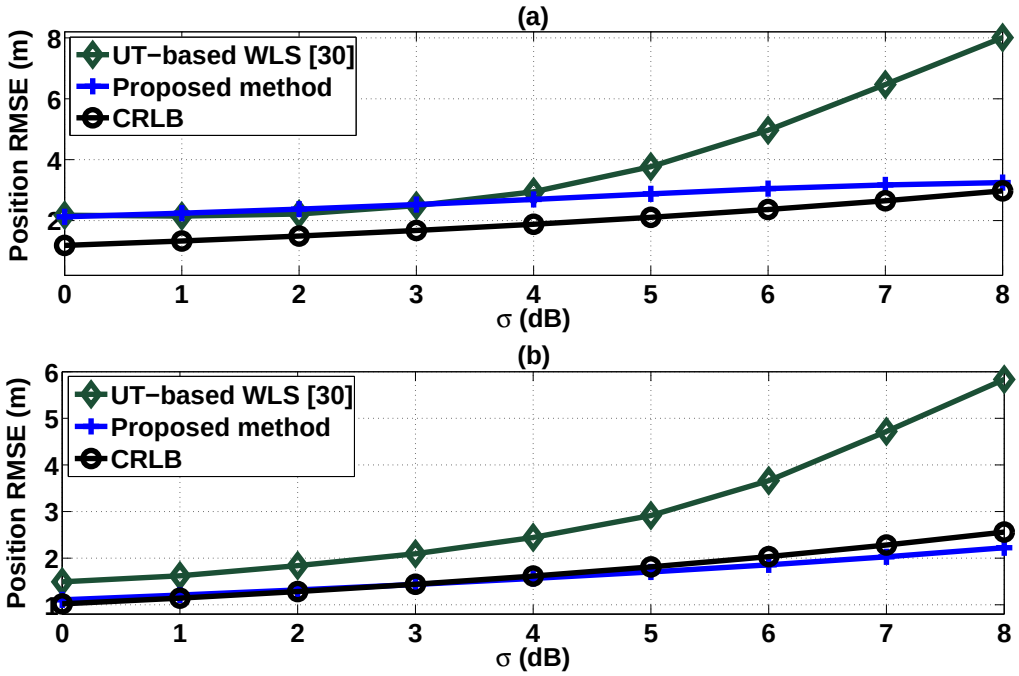

Figure 4.9: RMSE for the source location estimation with $\gamma = 2$ and (a) $N = 4$ sensors, and (b) $N = 7$ sensors.

$(15, 15)$, $(30, 15)$, and $(15, 30)$. The unknown source is located at $\mathbf{s} = (10, 6)$. The performance of the proposed method is compared with several well known RSSD based methods based on the root mean square error (RMSE) and the bias which can be obtained using the L_2 and L_1 norms, respectively. The proposed method was implemented using the CVX toolbox and SDPT3 solver [22]. Figure 4.8 illustrates the effect of the measurement noise standard deviation on the bias and RMSE of the proposed, standard LS [59], corrected LS [60], and NLS [61] methods. The Cramér-Rao lower bound (CRLB) is also shown. The standard LS and corrected LS methods perform achieves better performance due to the lower RMSE compare to the NLS while they receive larger bias.

The proposed method has superior performance with lower bias and RMSE. Figure 4.9 compares the proposed method with the recently developed UT-WLS [53] method for $M = 4$ and $M = 7$ sensors. These results shows a considerable improvement in performance with the proposed method when the noise is significant. For example, with $\sigma = 6$ dB, there is approximately 1.71 dB and 1.92 dB improvement in the position RMSE for $M = 4$ and $M = 7$, respectively. The effect of the path loss exponent α on the position RMSE is shown in Fig. 3.10. This indicates that an increased path loss exponent results in a decreased RMSE. For example, changing α

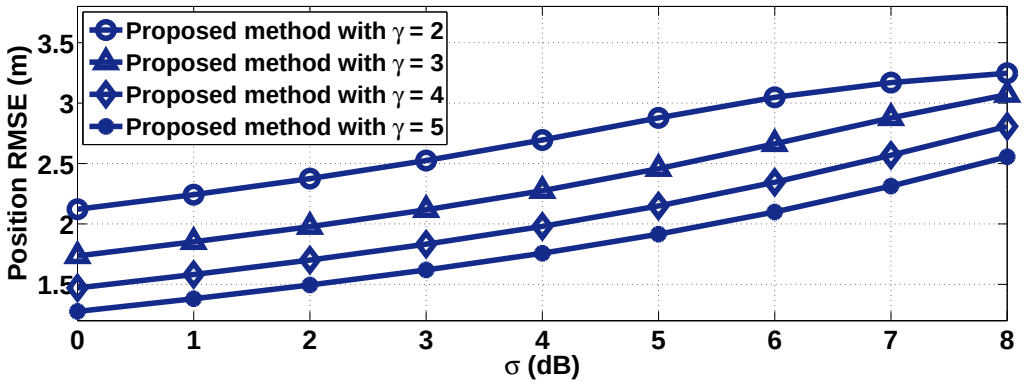

Figure 4.10: RMSE for the source location estimation with different path loss exponents γ and $N = 4$ sensors.

from 2 to 3 with $\sigma = 6$ dB results in a 0.94 dB decrease in position RMSE.

Chapter 5

ETLS-SDP method with System Parameter Error

In this chapter the nonlinear RSSD-based model is formulated for systems perturbed by noise. Solutions obtained using conventional least squares methods suffer from significant performance degradation as they only consider errors in the data vector. Thus an extended total least squares (ETLS) method is developed for blind localization which considers perturbations in the system parameters as well as the constraints imposed by the relation between the observation matrix and data vector. The nonlinear and nonconvex RSSD-based localization problem is then transformed to an ETLS problem with fewer constraints.

This is transformed to a convex semidefinite programming (SDP) problem using relaxation. The corresponding ETLS-SDP method is extended to the case with an unknown path loss exponent to jointly estimate the unknown source location and path loss exponent without resorting to transmit power estimation which is sensitive to errors. The mean squared error of the proposed ETLS method is obtained and the corresponding Cramér-Rao lower bound (CRLB) is derived as a performance benchmark. Performance results are presented which show that the RSSD-based ETLS-SDP method attains the CRLB for a sufficiently large signal to noise ratio (SNR).

5.1 ETLS Problem Formulation

In this section the RSSD measurements model for source localization with system parameter error is formulated The anchor nodes are assumed to be sensors with known positions and the target is a source with unknown location. Let $\mathbf{u} = [x, y]^T$ be the unknown source position to be determined in a two-dimensional (2D) space, and $\mathbf{u}_i = [x_i, y_i]^T$, $i = 1, 2, \ldots, N$ be the known coordinates of the N sensors where $(\ )^T$ denotes transpose. The source localization problem requires RSSD values from at least three anchor nodes.

The distance between the source and sensor i is given by

$$\begin{aligned} r_i &= \|\mathbf{u} - \mathbf{u}_i\| \\ &= \sqrt{(x - x_i)^2 + (y - y_i)^2}, \quad i = 1, 2, \ldots, N. \end{aligned} \tag{5.1}$$

The average received power P_i at the ith sensor can be expressed considering the log-normal distribution of P_i as [4],[43]

$$P_i(\text{dB}) - P_t(\text{dB}) = K_0(\text{dB}) - 10\gamma \log_{10}(\|\mathbf{u} - \mathbf{u}_i\|) + n_i, \tag{5.2}$$

where n_i is the measurement noise at the ith sensor which is assumed to be Gaussian distributed with zero mean and variance σ_i^2 so that $n_i \sim N(0, \sigma_i^2)$, P_t is the source transmit power, γ is the path loss exponent, and K_0 is the path loss for the reference distance which is normally taken as 1 m. The value of γ can vary from 1 to 6 [4] and is equal to 2 in free space which is assumed to be the a priori value for the RSSD measurements. Denote the RSSD between the first and ith sensor as $\Delta P_{1i} = P_1 - P_i$. From (5.2), this can be expressed as

$$\Delta P_{1i} = 10\gamma \log_{10}\left(\frac{\|\mathbf{u} - \mathbf{u}_i\|}{\|\mathbf{u} - \mathbf{u}_1\|}\right) + n_{1i}, \quad i = 1, 2, \ldots, N, \tag{5.3}$$

where $n_{1i} \sim N(0, \sigma_i^2 + \sigma_1^2)$ is the RSSD measurement noise. Therefore, the source localization problem is to estimate $\mathbf{u}$ from the ΔP_{1i}. From (5.3), the ith distance, $r_i = \|\mathbf{u} - \mathbf{u}_i\|$, is given by

$$r_i = 10^{\left(\frac{\Delta \tilde{P}_{1i}}{10\gamma}\right)} r_1, \quad i = 2, \ldots, N, \tag{5.4}$$

where $\Delta\tilde{P}_{1i}$ is the noise free RSSD measurement with respect to the first sensor. To convert the RSSD measurements into a set of linear equations, we introduce the intermediate variable

$$R^2 = x^2 + y^2. \tag{5.5}$$

Squaring both sides of (5.4) and substituting (5.1) yields

$$\begin{aligned} (1 - 10^{\frac{\Delta\tilde{P}_{1i}}{5\gamma}})(x^2 + y^2) + 2(x_1 10^{\frac{\Delta\tilde{P}_{1i}}{5\gamma}} - x_i)x + \\ 2(y_1 10^{\frac{\Delta\tilde{P}_{1i}}{5\gamma}} - y_i)y = 10^{\frac{\Delta\tilde{P}_{1i}}{5\gamma}}(x_1^2 + y_1^2) - (x_i^2 + y_i^2), \\ i = 2, \ldots, N. \end{aligned} \tag{5.6}$$

Define $c_{1i} = 10^{\frac{\Delta\tilde{P}_{1i}}{5\gamma}}$ which can be approximated using a first-order Taylor series for sufficiently small noise levels as $c_{1i} = \eta_{1i}\left(\frac{5\gamma}{\ln 10} + n_{i1}\right)$, where $\eta_{1i} = \frac{\ln 10}{5\gamma} 10^{\frac{\Delta P_{1i}}{5\gamma}}$. Then (5.6) can be expressed in matrix form as

$$\mathbf{A}\boldsymbol{\theta} = \mathbf{b}, \tag{5.7}$$

where

$$\mathbf{A} = \begin{bmatrix} 2(c_{12}x_1 - x_2) & 2(c_{12}y_1 - y_2) & 1 - c_{12} \\ \vdots & \vdots & \vdots \\ 2(c_{1N}x_1 - x_N) & 2(c_{1N}y_1 - y_N) & 1 - c_{1N} \end{bmatrix}, \tag{5.8}$$

$$\boldsymbol{\theta} = \begin{bmatrix} x & y & R^2 \end{bmatrix}^T, \tag{5.9}$$

and

$$\mathbf{b} = \begin{bmatrix} c_{12}(x_1^2 + y_1^2) - (x_2^2 + y_2^2) \\ \vdots \\ c_{1N}(x_1^2 + y_1^2) - (x_N^2 + y_N^2) \end{bmatrix}. \tag{5.10}$$

5.1.1 The TLS and CLS methods

Considering (5.7), data matrix $\mathbf{A}$ and observation vector $\mathbf{b}$ yield an overdetermined estimation problem which consists of more nonlinear equations than unknowns. Least squares is a conventional approach to solve this problem. Equations (5.3) and (5.7) can be used to obtain a source location estimate via minimization of the constrained

least squares (CLS) criterion which gives

$$\begin{array}{ll} \underset{x,y,R}{\text{minimize}} & \sum_{i=1}^{N} \left(\Delta P_{1i} - 10\gamma \log \frac{r_i}{r_1} \right)^2 \\ \text{subject to} & x^2 + y^2 = R^2. \end{array} \tag{5.11}$$

Note that the optimization problem given in (5.11) is a nonlinear and nonconvex problem which yields multiple local minima. Therefore, the global minimum solution is typically difficult to obtain. The CLS problem in (5.11) can be rewritten in matrix form as

$$\begin{array}{ll} \underset{\boldsymbol{\theta}}{\text{minimize}} & (\mathbf{A}\boldsymbol{\theta} - \mathbf{b})^T (\mathbf{A}\boldsymbol{\theta} - \mathbf{b}) \\ \text{subject to} & \mathbf{u}^T\mathbf{u} = R^2. \end{array} \tag{5.12}$$

Both $\mathbf{A}$ and $\mathbf{b}$ are perturbed by RSSD measurement noise which exists in the c_{1i}. Let $\mathbf{A} = \mathbf{A_0} + \boldsymbol{\delta}_\mathbf{A}$ and $\mathbf{b} = \mathbf{b_0} + \boldsymbol{\delta}_\mathbf{b}$ where $\mathbf{A_0}$ and $\mathbf{b_0}$ are the noise free components of $\mathbf{A}$ and $\mathbf{b}$, respectively, and $\boldsymbol{\delta}_\mathbf{A}$ and $\boldsymbol{\delta}_\mathbf{b}$ are the corresponding RSSD measurement noise terms. Then (5.7) can be expressed as

$$(\mathbf{A}_0\boldsymbol{\theta} - \mathbf{b}_0) + (\boldsymbol{\delta}_\mathbf{A}\boldsymbol{\theta} - \boldsymbol{\delta}_\mathbf{b}) = \mathbf{0}, \tag{5.13}$$

where

$$\mathbf{A}_0 = \begin{bmatrix} 2\left(\frac{5\eta_{12}}{\ln 10}\gamma x_1 - x_2\right) & 2\left(\frac{5\eta_{12}}{\ln 10}\gamma y_1 - y_2\right) & 1 - \frac{5\eta_{12}}{\ln 10}\gamma \\ \vdots & \vdots & \vdots \\ 2\left(\frac{5\eta_{1N}}{\ln 10}\gamma x_1 - x_N\right) & 2\left(\frac{5\eta_{1N}}{\ln 10}\gamma y_1 - y_N\right) & 1 - \frac{5\eta_{1N}}{\ln 10}\gamma \end{bmatrix},$$

$$\boldsymbol{\delta}_\mathbf{A} = \begin{bmatrix} 2\eta_{12}x_1 n_{21} & 2\eta_{12}y_1 n_{21} & -\eta_{12}n_{21} \\ \vdots & \vdots & \vdots \\ 2\eta_{1N}x_1 n_{N1} & 2\eta_{1N}y_1 n_{N1} & -\eta_{1N}n_{N1} \end{bmatrix},$$

$$\mathbf{b}_0 = \begin{bmatrix} \frac{5\eta_{12}}{\ln 10}\gamma R_1^2 - R_2^2 \\ \vdots \\ \frac{5\eta_{1N}}{\ln 10}\gamma R_1^2 - R_N^2 \end{bmatrix}, \quad \boldsymbol{\delta}_\mathbf{b} = R_1^2 \begin{bmatrix} \eta_{12}n_{21} \\ \vdots \\ \eta_{1N}n_{N1} \end{bmatrix}.$$

$\mathbf{A}_0 \in \Re^{(N-1)\times 3}$ and $\mathbf{b}_0 \in \Re^{(N-1)}$ are data matrices, $\delta_A \in \Re^{(N-1)\times 3}$ and $\delta_b \in \Re^{(N-1)}$ are perturbation matrices, and $R_i^2 = x_i^2 + y_i^2$. Equation (5.13) shows that error terms exist in both $\mathbf{A}$ and $\mathbf{b}$. Therefore, the standard LS approach which considers only errors in the observation vector $\mathbf{b}$ may not provide an optimal solution [24],[26].

Based on (5.13), this source localization problem can be solved by minimizing the

total error, which gives the following minimization problem

$$\begin{array}{ll} \text{minimize} & \left[\begin{array}{cc} \delta_{\mathbf{A}} & \delta_{\mathbf{b}} \end{array} \right] \\ \text{subject to} & \mathbf{A}\theta = \mathbf{b} \\ & \mathbf{u}^T\mathbf{u} = R^2 \end{array} \tag{5.14}$$

This is known as the total least squares (TLS) optimization problem [24]. Note that in this case, $\mathbf{b_0}$ is not in the range space of $\mathbf{A}_0$.

The total least squares (TLS) method takes into account perturbations in both $\mathbf{A}$ and $\mathbf{b}$ [28]. The TLS solution of (5.14) is $\boldsymbol{\theta}_{TLS}$ that satisfies

$$\left(\mathbf{A}_0 + \boldsymbol{\delta}_{\mathbf{A}}\right)\boldsymbol{\theta}_{TLS} - \left(\mathbf{b}_0 + \boldsymbol{\delta}_{\mathbf{b}}\right) = 0. \tag{5.15}$$

The TLS method can be applied to problems where the perturbations in $\mathbf{A}$ and $\mathbf{b}$ are independent and identically distributed (i.i.d.). Therefore, any linear dependencies between the error terms in the observation matrix $\mathbf{A}$ and data vector $\mathbf{b}$ require a transformation of the original TLS problem resulting in an extended total least squares (ETLS) method. Thus the proposed ETLS method considers dependencies between the data vector and observation matrix. This method is presented in the next section.

5.2 The ETLS Localization Method

Let $\boldsymbol{\Phi}_{\mathbf{o}} = [\ \mathbf{A}_0 \quad \mathbf{b}_0\ ]$ and $\boldsymbol{\Delta\Phi} = [\ \boldsymbol{\delta}_{\mathbf{A}} \quad \boldsymbol{\delta}_{\mathbf{b}}\ ]$ where $\boldsymbol{\Phi_0} \in \Re^{(N-1)\times 4}$ and $\boldsymbol{\Delta\Phi} \in \Re^{(N-1)\times 4}$ are matrices formed by the columns of $\mathbf{A_0}$,$\mathbf{b_0}$ and $\boldsymbol{\delta}_{\mathbf{A}}$,$\boldsymbol{\delta}_{\mathbf{b}}$, respectively. Then (5.15) can be written as

$$\boldsymbol{\Phi_0}\tilde{\boldsymbol{\theta}} + \boldsymbol{\Delta\Phi}\tilde{\boldsymbol{\theta}} = \mathbf{0}, \tag{5.16}$$

where $\tilde{\boldsymbol{\theta}} = \left[\begin{array}{cc} \boldsymbol{\theta} & -1 \end{array} \right]^T$. The extended total least squares (ETLS) estimate of $\boldsymbol{\theta}$ can be obtained by minimizing the constrained cost function

$$\underset{\boldsymbol{\Delta\Phi},\tilde{\boldsymbol{\theta}}}{\arg\min} \quad \|\boldsymbol{\Delta\Phi}\|_F^2 \tag{5.17}$$

$$\begin{array}{ll} \text{subject to :} & \boldsymbol{\Delta\Phi\Upsilon} = \mathbf{0} \\ & \boldsymbol{\Phi_0}\tilde{\boldsymbol{\theta}} + \boldsymbol{\Delta\Phi}\tilde{\boldsymbol{\theta}} = \mathbf{0} \\ & \tilde{\boldsymbol{\theta}}^T\mathbf{P}\tilde{\boldsymbol{\theta}} + \tilde{\boldsymbol{\theta}}^T\mathbf{q} = \mathbf{0} \end{array} \tag{5.18}$$

where $\mathbf{P} = diag\{1, 1, 0, 1\}$, $\boldsymbol{\Upsilon} = \begin{bmatrix} -y_1 & x_1 & R_1^2 & 1 \end{bmatrix}^T$, $\mathbf{q} = \begin{bmatrix} 0 & 0 & -1 & 1 \end{bmatrix}^T$, and $\|\boldsymbol{\Delta\Phi}\|_F^2$ denotes the Frobenius norm of $\boldsymbol{\Delta\Phi}$ which is given by

$$\|\boldsymbol{\Delta\Phi}\|_F = \sqrt{\sum_{i=1}^{N}\sum_{j=1}^{4} |\Delta\Phi_{ij}|^2} = \sqrt{\mathbf{Tr}\left\{\boldsymbol{\Delta\Phi}^T\boldsymbol{\Delta\Phi}\right\}}.$$

Minimizing (5.17) subject to (5.18) is equivalent to minimizing the Lagrangian cost function with Lagrange multipliers $\boldsymbol{\Lambda}$, $\boldsymbol{\alpha}$ and β, given by

$$\begin{aligned} L(\boldsymbol{\Delta\Phi}, \boldsymbol{\Lambda}, \boldsymbol{\alpha}, \beta) = \mathbf{Tr}\left\{\boldsymbol{\Delta\Phi}^T\boldsymbol{\Delta\Phi}\right\} + \boldsymbol{\Lambda}^T\left(\boldsymbol{\Phi}_0 + \boldsymbol{\Delta\Phi}\right)\tilde{\boldsymbol{\theta}} \\ + \boldsymbol{\alpha}^T\left(\boldsymbol{\Delta\Phi}\boldsymbol{\Upsilon}\right) + \beta\left(\tilde{\boldsymbol{\theta}}^T\mathbf{P}\tilde{\boldsymbol{\theta}} + \tilde{\boldsymbol{\theta}}^T\mathbf{q}\right), \end{aligned} \tag{5.19}$$

where $\boldsymbol{\Delta\Phi}$ is the optimization variable vector and $\mathbf{Tr}\{.\}$ denotes the trace of the matrix. Differentiating $L(\boldsymbol{\Delta\Phi}, \boldsymbol{\Lambda}, \boldsymbol{\alpha}, \beta)$ with respect to $\boldsymbol{\Delta\Phi}$ and equating it to zero gives

$$\boldsymbol{\Delta\Phi} = -\frac{1}{2}(\boldsymbol{\Lambda}\tilde{\boldsymbol{\theta}}^T + \boldsymbol{\alpha}\boldsymbol{\Upsilon}^T). \tag{5.20}$$

Substituting $\boldsymbol{\Delta\Phi}$ given by (5.20) into the minimization constraints in (5.18) gives the Lagrange multipliers

$$\boldsymbol{\Lambda} = \left(\sum_{i=1}^{4}\tilde{\boldsymbol{\theta}}_i^2\right)^{-1}\left(2\boldsymbol{\Phi}_0 - \boldsymbol{\alpha}\boldsymbol{\Upsilon}^T\right)\tilde{\boldsymbol{\theta}}, \tag{5.21}$$

and

$$\boldsymbol{\alpha} = -\boldsymbol{\Lambda}\tilde{\boldsymbol{\theta}}\boldsymbol{\Upsilon}^T(\boldsymbol{\Upsilon}^T\boldsymbol{\Upsilon})^{-1}. \tag{5.22}$$

$\boldsymbol{\Lambda}$ can be evaluated by substituting (5.22) into (5.21) which yields

$$\begin{aligned} \boldsymbol{\Lambda} &= \left(\sum_{i=1}^{4}\tilde{\boldsymbol{\theta}}_i^2\right)^{-1}\left(2\boldsymbol{\Phi}_0 + \left(\boldsymbol{\Lambda}\tilde{\boldsymbol{\theta}}^T\boldsymbol{\Upsilon}\left(\boldsymbol{\Upsilon}^T\boldsymbol{\Upsilon}\right)^{-1}\boldsymbol{\Upsilon}^T\right)\right)\tilde{\boldsymbol{\theta}} \\ &= 2\left(\sum_{i=1}^{4}\tilde{\boldsymbol{\theta}}_i^2\right)^{-1}\boldsymbol{\Phi}_0\tilde{\boldsymbol{\theta}} + \boldsymbol{\Lambda}\left(\sum_{i=1}^{4}\tilde{\boldsymbol{\theta}}_i^2\right)^{-1}\left(\tilde{\boldsymbol{\theta}}^T\widehat{\boldsymbol{\Upsilon}}\tilde{\boldsymbol{\theta}}\right) \\ &= 2\left(\sum_{i=1}^{4}\tilde{\boldsymbol{\theta}}_i^2 - \tilde{\boldsymbol{\theta}}^T\widehat{\boldsymbol{\Upsilon}}\tilde{\boldsymbol{\theta}}\right)^{-1}\boldsymbol{\Phi}_0\tilde{\boldsymbol{\theta}}, \end{aligned} \tag{5.23}$$

where $\widehat{\boldsymbol{\Upsilon}} = \boldsymbol{\Upsilon}\left(\boldsymbol{\Upsilon}^T\boldsymbol{\Upsilon}\right)^{-1}\boldsymbol{\Upsilon}^T$. From (5.23), $\boldsymbol{\alpha}$ can be obtained using (5.19) and (5.22) as

$$\boldsymbol{\alpha} = -2\left(\sum_{i=1}^{4}\tilde{\boldsymbol{\theta}}_i^2 - \tilde{\boldsymbol{\theta}}^T\widehat{\boldsymbol{\Upsilon}}\tilde{\boldsymbol{\theta}}\right)^{-1}\boldsymbol{\Phi}_0\tilde{\boldsymbol{\theta}}_0\tilde{\boldsymbol{\theta}}^T\boldsymbol{\Upsilon}\left(\boldsymbol{\Upsilon}^T\boldsymbol{\Upsilon}\right)^{-1}. \tag{5.24}$$

Substituting (5.23) and (5.24) in (5.20) results in

$$\begin{aligned}\boldsymbol{\Delta\Phi} &= \left(\tilde{\boldsymbol{\theta}}^T\widehat{\boldsymbol{\Upsilon}}\tilde{\boldsymbol{\theta}} - \left(\sum_{i=1}^{4}\tilde{\boldsymbol{\theta}}_i^2\right)\right)^{-1}\boldsymbol{\Phi}_0\tilde{\boldsymbol{\theta}}\tilde{\boldsymbol{\theta}}^T \\ &\quad + \left(\sum_{i=1}^{4}\tilde{\boldsymbol{\theta}}_i^2 - 2\tilde{\boldsymbol{\theta}}^T\widehat{\boldsymbol{\Upsilon}}\tilde{\boldsymbol{\theta}}\right)^{-1}\boldsymbol{\Phi}_0\tilde{\boldsymbol{\theta}}\tilde{\boldsymbol{\theta}}^T\boldsymbol{\Upsilon}\left(\boldsymbol{\Upsilon}^T\boldsymbol{\Upsilon}\right)^{-1}\boldsymbol{\Upsilon}^T \\ &= -\left(\tilde{\boldsymbol{\theta}}^T\widehat{\boldsymbol{\Upsilon}}\tilde{\boldsymbol{\theta}} - \left(\sum_{i=1}^{4}\tilde{\boldsymbol{\theta}}_i^2\right)\right)^{-1}\left(\boldsymbol{\Phi}_0\tilde{\boldsymbol{\theta}}\tilde{\boldsymbol{\theta}}^T - \boldsymbol{\Phi}_0\tilde{\boldsymbol{\theta}}\tilde{\boldsymbol{\theta}}^T\widehat{\boldsymbol{\Upsilon}}\right) \\ &= \left(\tilde{\boldsymbol{\theta}}^T\left(\mathbf{I} - \widehat{\boldsymbol{\Upsilon}}\right)\tilde{\boldsymbol{\theta}}\right)^{-1}\boldsymbol{\Phi}_0\tilde{\boldsymbol{\theta}}\tilde{\boldsymbol{\theta}}^T\left(\widehat{\boldsymbol{\Upsilon}} - \mathbf{I}\right).\end{aligned} \tag{5.25}$$

Considering $\widehat{\boldsymbol{\Upsilon}} = \boldsymbol{\Upsilon}\left(\boldsymbol{\Upsilon}^T\boldsymbol{\Upsilon}\right)^{-1}\boldsymbol{\Upsilon}^T$ gives

$$\begin{aligned}\left(\mathbf{I} - \widehat{\boldsymbol{\Upsilon}}\right)^2 &= \mathbf{I} + \boldsymbol{\Upsilon}\left(\boldsymbol{\Upsilon}^T\boldsymbol{\Upsilon}\right)^{-1}\boldsymbol{\Upsilon}^T\boldsymbol{\Upsilon}\left(\boldsymbol{\Upsilon}^T\boldsymbol{\Upsilon}\right)^{-1}\boldsymbol{\Upsilon}^T - 2\widehat{\boldsymbol{\Upsilon}} \\ &= \mathbf{I} + \boldsymbol{\Upsilon}\left(\boldsymbol{\Upsilon}^T\boldsymbol{\Upsilon}\right)^{-1}\boldsymbol{\Upsilon}^T - 2\widehat{\boldsymbol{\Upsilon}} = \left(\mathbf{I} - \widehat{\boldsymbol{\Upsilon}}\right).\end{aligned} \tag{5.26}$$

Therefore, the Frobenius norm of $\boldsymbol{\Delta\Phi}$ given in (5.17) can be calculated as

$$\begin{aligned}\|\boldsymbol{\Delta\Phi}\|_F^2 &= \mathbf{Tr}\left\{\left(\tilde{\boldsymbol{\theta}}^T\left(\mathbf{I} - \widehat{\boldsymbol{\Upsilon}}\right)\tilde{\boldsymbol{\theta}}\right)^{-2}\boldsymbol{\Phi}_0\tilde{\boldsymbol{\theta}}\tilde{\boldsymbol{\theta}}^T\left(\mathbf{I} - \widehat{\boldsymbol{\Upsilon}}\right)^2\tilde{\boldsymbol{\theta}}\tilde{\boldsymbol{\theta}}^T\boldsymbol{\Phi}_0^T\right\} \\ &= \mathbf{Tr}\left\{\boldsymbol{\Phi}_0\tilde{\boldsymbol{\theta}}\tilde{\boldsymbol{\theta}}^T\boldsymbol{\Phi}_0^T\left(\tilde{\boldsymbol{\theta}}^T\left(\mathbf{I} - \widehat{\boldsymbol{\Upsilon}}\right)\tilde{\boldsymbol{\theta}}\right)^{-1}\right\} \\ &= \left\{\tilde{\boldsymbol{\theta}}^T\widehat{\boldsymbol{\Phi}}_0\tilde{\boldsymbol{\theta}}\left(\tilde{\boldsymbol{\theta}}^T\left(\mathbf{I} - \widehat{\boldsymbol{\Upsilon}}\right)\tilde{\boldsymbol{\theta}}\right)^{-1}\right\},\end{aligned} \tag{5.27}$$

where $\widehat{\boldsymbol{\Phi}}_0 = \boldsymbol{\Phi}_0^T\boldsymbol{\Phi}_0$, and $\mathbf{Tr}\left\{\boldsymbol{\Phi}_0\tilde{\boldsymbol{\theta}}\tilde{\boldsymbol{\theta}}^T\boldsymbol{\Phi}_0^T\right\} = \tilde{\boldsymbol{\theta}}\widehat{\boldsymbol{\Phi}}_0\tilde{\boldsymbol{\theta}}^T$ which is derived in Appendix D. Then the constrained minimization problem defined in (5.17) and (5.18) can be simplified using (5.27) to

$$\begin{aligned}\underset{\tilde{\boldsymbol{\theta}}}{\arg\min} \quad & \tilde{\boldsymbol{\theta}}^T\widehat{\boldsymbol{\Phi}}_0\left(\tilde{\boldsymbol{\theta}}^T\left(\mathbf{I} - \widehat{\boldsymbol{\Upsilon}}\right)\tilde{\boldsymbol{\theta}}\right)^{-1}\tilde{\boldsymbol{\theta}} \\ \text{subject to} \quad & \tilde{\boldsymbol{\theta}}^{\mathrm{T}}\mathbf{P}\tilde{\boldsymbol{\theta}} + \tilde{\boldsymbol{\theta}}^{\mathrm{T}}\mathbf{q} = \mathbf{0}.\end{aligned} \tag{5.28}$$

This is an extended TLS (ETLS) constrained optimization problem which considers the error in all data.

5.2.1 Semidefinite Relaxation for RSSD Measurements

The problem given in (5.28) is nonconvex with nonlinear constraints, so obtaining the optimal solution is difficult. Therefore semidefinite relaxation (SDR) is used to convert (5.28) into a convex optimization problem. This transforms the ETLS optimization problem into an SDP optimization problem. First, define the auxiliary variable $t = \tilde{\boldsymbol{\theta}}^T \widehat{\boldsymbol{\Phi}}_0 (\tilde{\boldsymbol{\theta}}^T (\mathbf{I} - \widehat{\boldsymbol{\Upsilon}}) \tilde{\boldsymbol{\theta}})^{-1} \tilde{\boldsymbol{\theta}}$ and rewrite (5.28) as

$$\begin{aligned} &\underset{\tilde{\boldsymbol{\theta}}, t}{\text{minimize}}\ t \\ \text{subject to}: \quad & t - \tilde{\boldsymbol{\theta}}^T \widehat{\boldsymbol{\Phi}}_0 (\tilde{\boldsymbol{\theta}}^T (\mathbf{I} - \widehat{\boldsymbol{\Upsilon}}) \tilde{\boldsymbol{\theta}})^{-1} \tilde{\boldsymbol{\theta}} = 0 \\ & \tilde{\boldsymbol{\theta}}^T \mathbf{P} \tilde{\boldsymbol{\theta}} + \tilde{\boldsymbol{\theta}}^T \mathbf{q} = 0. \end{aligned} \tag{5.29}$$

Considering the trace of a matrix, (5.29) can be expressed as

$$\begin{aligned} &\underset{\tilde{\boldsymbol{\theta}}, t}{\text{minimize}}\ t \\ \text{subject to}: \quad & \Big(\mathbf{P}\tilde{\boldsymbol{\theta}}\Big)^T \Big(\mathbf{P}\tilde{\boldsymbol{\theta}}\Big) + \tilde{\boldsymbol{\theta}}^T \mathbf{q} = 0 \\ & t - \tilde{\boldsymbol{\theta}}^T \widehat{\boldsymbol{\Phi}}_0 \Big(\mathbf{Tr}\Big\{(\mathbf{I} - \widehat{\boldsymbol{\Upsilon}}) \tilde{\boldsymbol{\theta}} \tilde{\boldsymbol{\theta}}^T\Big\}\Big)^{-1} \tilde{\boldsymbol{\theta}} = 0. \end{aligned} \tag{5.30}$$

The cost function in (5.30) is linear and convex, but the constraints are still nonconvex due to the presence of $\tilde{\boldsymbol{\theta}} \tilde{\boldsymbol{\theta}}^T$. Thus, the next step is to relax the nonconvex constraints in (5.30) to obtain convex constraints. Define the auxiliary variable

$$\mathbf{Q} = \tilde{\boldsymbol{\theta}} \tilde{\boldsymbol{\theta}}^{\mathbf{T}},$$

which can be used to reformulate the constraints in (5.30) as linear and convex. This leads to nonconvex equality constraints that can be relaxed using the SDR method as

$$\begin{aligned} \mathbf{Q} - \tilde{\boldsymbol{\theta}} \tilde{\boldsymbol{\theta}}^T &\succeq 0 \\ \Big(\mathbf{P}\tilde{\boldsymbol{\theta}}\Big)^T \Big(\mathbf{P}\tilde{\boldsymbol{\theta}}\Big) + \tilde{\boldsymbol{\theta}}^T \mathbf{q} &\succeq 0 \end{aligned} \tag{5.31}$$

and

$$t - \Big(\boldsymbol{\Phi}_0 \tilde{\boldsymbol{\theta}}\Big)^T \boldsymbol{\Phi}_0 \tilde{\boldsymbol{\theta}} \Big(\mathbf{Tr}\Big\{(\mathbf{I} - \widehat{\boldsymbol{\Upsilon}}) \mathbf{Q}\Big\}\Big)^{-1} \succeq 0, \tag{5.32}$$

where for a symmetric matrix $\mathbf{S}$, $\mathbf{S} \succeq \mathbf{0}$ denotes that $\mathbf{S}$ is positive semidefinite. The inequality constraints given in (5.31) and (5.32) can be written as linear matrix inequalities (LMI) based on Schur's Complement Lemma [66] given below.

Lemma 1: Consider the symmetric matrix

$$\mathbf{\Xi} = \begin{bmatrix} \mathbf{Z}_1 & \mathbf{Z}_2 \\ \mathbf{Z}_2^T & \mathbf{Z}_3 \end{bmatrix},$$

where $\mathbf{Z}_3$ is a positive definite matrix ($\mathbf{Z}_3 \succ 0$). Then the Schur complement of $\mathbf{Z}_3$ defined as

$$\tilde{\mathbf{Z}}_3 = \mathbf{Z}_1 - \mathbf{Z}_2 {\mathbf{Z}_3}^{-1} \mathbf{Z}_2^T,$$

is positive semi-definite ($\tilde{\mathbf{Z}}_3 \succeq \mathbf{0}$) if and only if $\mathbf{\Xi}$ is positive semi-definite ($\mathbf{\Xi} \succeq \mathbf{0}$).

Considering Lemma 1, the inequality constraints in (5.31) and (5.32) can be written as

$$\begin{bmatrix} t & \tilde{\boldsymbol{\theta}}^T {\mathbf{\Phi}_0}^T \\ \mathbf{\Phi}_0 \tilde{\boldsymbol{\theta}} & \mathbf{Tr}\left\{(\mathbf{I} - \widehat{\mathbf{\Upsilon}})\mathbf{Q}\right\} \end{bmatrix} \succeq 0$$

$$\begin{bmatrix} \mathbf{Q} & \tilde{\boldsymbol{\theta}} \\ \tilde{\boldsymbol{\theta}}^T & 1 \end{bmatrix} \succeq 0, \quad \begin{bmatrix} \tilde{\mathbf{q}}^T \tilde{\boldsymbol{\theta}} & \tilde{\boldsymbol{\theta}}^T \mathbf{P}^T \\ \mathbf{P}\tilde{\boldsymbol{\theta}} & \mathbf{I}_4 \end{bmatrix} \succeq 0, \tag{5.33}$$

respectively where $\tilde{\mathbf{q}} = [0, 0, 1, -1]^T$. Therefore, the nonconvex optimization problem given in (5.30) can be transformed to a convex problem using (5.31), (5.32) and Lemma 1. Hence, (5.30) can be reformulated into a standard SDP problem by applying (5.33) which gives

$$\begin{aligned} & \underset{\mathbf{Q}, \tilde{\boldsymbol{\theta}}, t}{\text{minimize}}\ t \\ \text{subject to :} \quad & \begin{bmatrix} \mathbf{Q} & \tilde{\boldsymbol{\theta}} \\ \tilde{\boldsymbol{\theta}}^T & 1 \end{bmatrix} \succeq 0 \\ & \begin{bmatrix} \tilde{\mathbf{q}}^T \tilde{\boldsymbol{\theta}} & \left(\mathbf{P}\tilde{\boldsymbol{\theta}}\right)^T \\ \mathbf{P}\tilde{\boldsymbol{\theta}} & \mathbf{I}_4 \end{bmatrix} \succeq 0 \\ & \begin{bmatrix} t & \left(\mathbf{\Phi}_0 \tilde{\boldsymbol{\theta}}\right)^T \\ \mathbf{\Phi}_0 \tilde{\boldsymbol{\theta}} & (\mathbf{I} - \widehat{\mathbf{\Upsilon}}) \bullet \mathbf{Q} \end{bmatrix} \succeq 0 \end{aligned} \tag{5.34}$$

where $\{\bullet\}$ denotes the inner product of symmetric matrices $\mathbf{S_{n\times n}}$ and $\mathbf{V_{n\times n}}$ given by

$$\mathbf{S} \bullet \mathbf{V} = \mathbf{Tr}\left\{\mathbf{SV}\right\} = \sum_{i=1}^{n}\sum_{j=1}^{n} s_{ij}v_{ij},$$

in which s_{ij} and v_{ij} are the ijth elements of $\mathbf{S}$ and $\mathbf{V}$, respectively. The problem given in (5.34) is a convex optimization problem for which a globally optimum solution can be obtained efficiently using SDP solvers such as SeDuMi and SDPT3 [22]-[23] that apply the interior point method [20]-[21].

Remark 1: Note that $\left(\sum_{i=1}^{4}\tilde{\boldsymbol{\theta}}_i^2 - \tilde{\boldsymbol{\theta}}^T\widehat{\boldsymbol{\Upsilon}}\tilde{\boldsymbol{\theta}}\right)^{-1}$ and $\left(\mathbf{Tr}\left\{(\mathbf{I}-\widehat{\boldsymbol{\Upsilon}})\mathbf{Q}\right\}\right)^{-1}$ in (5.23) and (5.32), respectively, are nonzero. This is shown in Appendix E.

5.2.2 Extension to the Unknown Path Loss Exponent Case

Deterministic PLE

The path loss exponent (PLE) typically lies in the interval $\gamma_{\min} \leq \gamma \leq \gamma_{\max}$, where $\gamma_{\min} = 1$ and $\gamma_{\max} = 6$ [4]. In free space, $\gamma = 2$. Calculating the PLE requires significant experimental results which can be time consuming and costly. An efficient alternative approach is considered in this section to jointly estimate the unknown path loss exponent and source location based on RSSD measurements. For simplicity, the term deterministic PLE is denoted as PLE in the remainder of the section.

The optimization problem given in (5.11) is linear with respect to the path loss exponent after location estimation, so it can be simply solved using the linear least squares method. However, to increase the accuracy, the weighted least squares solution can be employed which results in the following optimization problem

$$\underset{\gamma_j}{\text{minimize}} \quad \sum_{i=2}^{N}\frac{1}{\sigma_{1i}^2}\left(\Delta P_{1i} - 10\gamma_j \log\frac{\|\mathbf{u}_i - \hat{\mathbf{u}}_{j-1}\|}{\|\mathbf{u}_1 - \hat{\mathbf{u}}_{j-1}\|}\right)^2, \tag{5.35}$$

where $\hat{\mathbf{u}}_{j-1}$ is the estimated source location in the $(j-1)$th iteration, and γ_j is the estimated path loss exponent in the jth iteration. Note that the initial estimate of the path loss exponent γ_0 can be obtained based on empirical values such as those reported in [4].

The minimization problem in (5.35) can be rewritten in matrix form as

$$\underset{\gamma_j}{\text{minimize}} \quad \left(\hat{\mathbf{A}}_{j-1}\gamma_j - \hat{\mathbf{b}}_{j-1}\right)\mathbf{W}^{-1}\left(\hat{\mathbf{A}}_{j-1}\gamma_j - \hat{\mathbf{b}}_{j-1}\right)^T, \tag{5.36}$$

where

$$\hat{\mathbf{A}}_{j-1} = \begin{bmatrix} 10\log\frac{\hat{r}_{2_{(j-1)}}}{\hat{r}_{1_{(j-1)}}} \\ \vdots \\ 10\log\frac{\hat{r}_{N_{(j-1)}}}{\hat{r}_{1_{(j-1)}}} \end{bmatrix}, \quad \hat{\mathbf{b}}_{j-1} = \begin{bmatrix} \Delta P_{12} \\ \vdots \\ \Delta P_{1N} \end{bmatrix},$$

and

$$\hat{r}_{i_{(j-1)}} = \|\mathbf{u}_i - \hat{\mathbf{u}}_{j-1}\|, \quad \mathbf{W} = diag\left\{\sigma_{12}^2, \ldots, \sigma_{1N}^2\right\}.$$

Note that in the optimization problem given by (5.36), there are perturbation errors only in the observation vector $\hat{\mathbf{b}}_{(j-1)}$. Therefore, the WLS method can be used to

Algorithm 2 RSSD-based ETLS-SDP method with unknown transmit power and path loss exponent

1: Set $j = 0$ and $\gamma_0 = 2$ as the initial path loss exponent estimate.
2: Calculate $\tilde{\boldsymbol{\theta}}_0$ and $\hat{\mathbf{u}}_0$ using (5.28) and (5.34).
3: **repeat**
4: Set $j = j + 1$.
5: Calculate $\hat{\mathbf{A}}_{(j-1)}$, $\hat{\mathbf{b}}_{(j-1)}$ and $\hat{r}_{i_{(j-1)}}$ defined in (5.36) for $i = 1, \ldots, N$.
6: Set $\gamma_j = \left(\hat{\mathbf{A}}_{(j-1)}^T\mathbf{W}^{-1}\hat{\mathbf{A}}_{(j-1)}\right)\hat{\mathbf{A}}_{(j-1)}^T\mathbf{W}^{-1}\hat{\mathbf{b}}_{(j-1)}$.
7: Substitute γ_j into (5.13) and form the ETLS problem in (5.28).
8: Solve the SDP problem in (5.34) to obtain $\tilde{\boldsymbol{\theta}}_j$ and $\hat{\mathbf{u}}_j$.
9: Calculate t_j in (5.34) as the value of the ETLS-SDP cost function.
10: **until** $\left(\left|\frac{t_j}{t_{j-1}} - 1\right| < \varepsilon\right)$ **or** $(\gamma_{\min} \leq \gamma_j \leq \gamma_{\max})$
11: **if** $\gamma_j \in [\gamma_{\min}, \gamma_{\max}]$ **then**
12: $\tilde{\boldsymbol{\theta}}_j$ and γ_j are the location and path loss estimates.
13: **else**
14: $\tilde{\boldsymbol{\theta}}_{j-1}$ and γ_{j-1} are the location and path loss estimates.
15: **end if**

obtain a closed form solution of (5.35) or equivalently (5.36) as

$$\gamma_j = \left(\hat{\mathbf{A}}_{(j-1)}^T\mathbf{W}^{-1}\hat{\mathbf{A}}_{(j-1)}\right)^{-1}\hat{\mathbf{A}}_{(j-1)}^T\mathbf{W}^{-1}\hat{\mathbf{b}}_{(j-1)}. \tag{5.37}$$

The source location estimate in the jth iteration, $\tilde{\boldsymbol{\theta}}_j$, or correspondingly $\hat{\mathbf{u}}_j$, can then be obtained by substituting (5.37) into (5.28). This iterative method continues until

the stopping condition $\left|\frac{t_j}{t_{j-1}} - 1\right| < \varepsilon$ is satisfied, where t_j and t_{j-1} are the values of the cost function in (5.34) in the jth and $(j-1)$th iterations, respectively, and ϵ is a small number typically chosen as 10^{-3} [68], [69]. Note that (5.37) should satisfy $\gamma_{\min} \leq \gamma_j \leq \gamma_{\max}$. If this condition is violated, the algorithm is terminated and the previous estimate, γ_{j-1}, is used.

Random PLE

As mentioned in Section II, the path loss exponent γ varies in the range $\gamma \in [1, 6]$ for indoor and outdoor environments [4]. This can be consider a priori information regarding γ in the blind localization case. Further, the empirical results in [70] suggest that the path loss exponent can be considered as a random variable $\gamma \sim N\left(\mu_\gamma, \sigma_\gamma^2\right)$ with variance σ_γ^2 and mean μ_γ. Therefore, the maximum a posteriori (MAP) estimator can be developed [54]-[55] based on the a priori information of γ as the following optimization problem

$$\overset{(j)}{\underset{MAP}{\gamma}} = \arg\max_{\gamma} \left\{\ln \mathbf{g}\left(\gamma|\mathbf{\Delta P}\right)\right\}, \tag{5.38}$$

where $\overset{(j)}{\underset{MAP}{\gamma}}$ is the jth PLE MAP estimate, $\mathbf{g}\left(.\right)$ denotes the probability density function and $\mathbf{\Delta P}$ is the known vector of RSSD measurements. Using Bayes' theorem, (5.38) can be rewritten [54] as

$$\overset{(j)}{\underset{MAP}{\gamma}} = \arg\max_{\gamma} \left\{\ln \mathbf{g}(\gamma) + \ln \mathbf{g}\left(\mathbf{\Delta P}|\gamma\right)\right\} \tag{5.39}$$

Define $\Xi = \ln \mathbf{g}(\gamma) + \ln \mathbf{g}\left(\Delta \mathbf{P}|\gamma\right)$. Considering the joint Gaussian distribution of $\mathbf{g}\left(\Delta \mathbf{P}|\gamma\right)$, Ξ can be formulated as

$$\Xi = \tilde{k}_{MAP} - \frac{\left(\gamma - \mu_\gamma\right)^2}{2\sigma_\gamma^2} - \sum_{i=2}^{N} \frac{\left(\Delta P_{1i} - 10\gamma \log \frac{\hat{r}_{i_{(j-1)}}}{\hat{r}_{1_{(j-1)}}}\right)^2}{2\sigma_{1i}^2}, \tag{5.40}$$

where

$$\tilde{k}_{MAP} = \ln \frac{1}{\sqrt{2\pi}\sigma_\gamma} + \sum_{i=2}^{N} \ln\left(\frac{1}{\sqrt{2\pi}\sigma_{1i}}\right). \tag{5.41}$$

Differentiating (5.40) with respect to the unknown parameter γ yields

$$\frac{\partial \Xi}{\partial \gamma} = \frac{\mu_\gamma - \gamma}{\sigma_\gamma^2} + \sum_{i=2}^{N} \frac{10 \log \frac{\hat{r}_{i_{(j-1)}}}{\hat{r}_{1_{(j-1)}}} \left(\Delta P_{1i} - 10\gamma \log \frac{\hat{r}_{i_{(j-1)}}}{\hat{r}_{1_{(j-1)}}} \right)}{\sigma_{1i}^2}, \tag{5.42}$$

and then equating this to zero, $\frac{\partial \Xi}{\partial \gamma} = 0$, gives the MAP estimate of the path loss exponent γ in (5.39) as

$$\overset{(j)}{\underset{MAP}{\gamma}} = \arg\max_{\gamma} \Xi = \frac{\mu_\gamma + \sum_{i=2}^{N} \tilde{x}_i \Delta P_{1i}}{1 + 10 \sum_{i=2}^{N} \tilde{x}_i \log \frac{\hat{r}_{i_{(j-1)}}}{\hat{r}_{1_{(j-1)}}}}, \tag{5.43}$$

where

$$\tilde{x}_i = 10 \left(\frac{\sigma_\gamma}{\sigma_{1i}} \right)^2 \log \frac{\hat{r}_{i_{(j-1)}}}{\hat{r}_{1_{(j-1)}}}, \quad i = 2, \ldots, N. \tag{5.44}$$

Note that the estimated PLE in the jth iteration satisfies $\gamma_{\min} \leq \gamma_j \leq \gamma_{\max}$.

Remark 2: To obtain the MAP estimate of the PLE, Algorithm 1 can be modified by changing lines 5 and 6 as follows *Remark 3*: Algorithm 1 is an RSSD-based method,

---

1: Calculate $\hat{r}_{i_{(j-1)}} = \|\mathbf{u}_i - \hat{\mathbf{u}}_{j-1}\|$ for $i = 1, \ldots, N$.

2: Set $\gamma_j = \overset{(j)}{\underset{MAP}{\gamma}}$ given in (5.43).

---

so the transmit power does not have to be estimated as with existing methods. This increases the path loss accuracy and decreases the computational complexity. In addition, an accurate estimate of the transmit power can be obtained after the source location and path loss exponent have been estimated (when Algorithm 1 has terminated).

5.3 ETLS Performance Evaluation

5.3.1 Mean Squared Error Analysis

The mean squared error (MSE) of the proposed ETLS method is considered in this section. Let $\boldsymbol{\theta} = \boldsymbol{\theta}_0 + \boldsymbol{\Delta\theta}_{ETLS}$ where $\boldsymbol{\theta}_0$ and $\boldsymbol{\theta}$ denote the true and estimated values, respectively, and $\boldsymbol{\Delta\theta}_{ETLS}$ is the ETLS estimation error. Therefore, the MSE can be

written as

$$\begin{aligned} \text{MSE} &= E\left\{(\boldsymbol{\theta}-\boldsymbol{\theta}_0)^T(\boldsymbol{\theta}-\boldsymbol{\theta}_0)\right\} \\ &= \mathbf{Tr}\left\{E\left(\boldsymbol{\Delta\theta}_{ETLS}\boldsymbol{\Delta\theta}_{ETLS}^T\right)\right\}, \end{aligned} \tag{5.45}$$

where $E\{.\}$ denotes expected value. Note that $\boldsymbol{\theta}=\boldsymbol{\theta}_0+\boldsymbol{\Delta\theta}_{ETLS}$ can also be formulated as $\tilde{\boldsymbol{\theta}}=\tilde{\boldsymbol{\theta}}_0+\boldsymbol{\Delta}\tilde{\boldsymbol{\theta}}_{ETLS}$ where $\tilde{\boldsymbol{\theta}}_0=\begin{bmatrix}\boldsymbol{\theta}_0 & -1\end{bmatrix}^T$ and $\boldsymbol{\Delta}\tilde{\boldsymbol{\theta}}_{ETLS}=\begin{bmatrix}\boldsymbol{\Delta\theta}_{ETLS} & 0\end{bmatrix}^T$. Denote the ETLS cost function in (5.28) as

$$\boldsymbol{\Psi}(\tilde{\boldsymbol{\theta}})=\tilde{\boldsymbol{\theta}}^T\widehat{\boldsymbol{\Phi}}_0\tilde{\boldsymbol{\theta}}\left(\tilde{\boldsymbol{\theta}}^T\left(\mathbf{I}-\widehat{\boldsymbol{\Upsilon}}\right)\tilde{\boldsymbol{\theta}}\right)^{-1}. \tag{5.46}$$

Setting the gradient of (5.46) equal to zero yields

$$\frac{\partial\left(\tilde{\boldsymbol{\theta}}^T\boldsymbol{\Phi}_0^T\right)}{\partial\boldsymbol{\theta}}=\mathbf{A}_0, \tag{5.47}$$

and

$$\frac{\partial\mathbf{G}^{-1}}{\partial\boldsymbol{\theta}}=-\mathbf{G^{-1}}\left(2\mathbf{V}^T\left(\mathbf{I}-\widehat{\boldsymbol{\Upsilon}}\right)\boldsymbol{\theta}\right)\mathbf{G^{-1}}, \tag{5.48}$$

where $\mathbf{V}$ is a 4×3 diagonal matrix and $\mathbf{G}=\tilde{\boldsymbol{\theta}}^T\left(\mathbf{I}-\widehat{\boldsymbol{\Upsilon}}\right)\tilde{\boldsymbol{\theta}}$, the gradient of the ETLS cost function with respect to $\boldsymbol{\theta}$, is

$$\begin{aligned} \frac{\partial\boldsymbol{\Psi}(\tilde{\boldsymbol{\theta}})}{\partial\boldsymbol{\theta}} = 2\Big\{&\mathbf{A}_0^T\mathbf{G}^{-1}\left(\mathbf{A}_0\boldsymbol{\theta}-\mathbf{b}_0\right)-\mathbf{G}^{-1} \\ &\times\left(\tilde{\boldsymbol{\theta}}^T\left(\mathbf{I}-\widehat{\boldsymbol{\Upsilon}}\right)\mathbf{V}\right)^T\mathbf{G}^{-1}\Big\}. \end{aligned} \tag{5.49}$$

Substituting $\boldsymbol{\theta}=\boldsymbol{\theta}_0+\boldsymbol{\Delta\theta}_{ETLS}$ into (5.49) and setting $\frac{\partial\boldsymbol{\Psi}}{\partial\boldsymbol{\theta}}=0$, the following approximation for $\boldsymbol{\Delta\theta}_{ETLS}$ can be obtained by ignoring the second order error terms as

$$\boldsymbol{\Delta\theta}_{ETLS}=\tilde{\mathbf{G}}^{-1}\mathbf{A}_0^T\mathbf{G}^{-1}\boldsymbol{\Delta\Phi}\tilde{\boldsymbol{\theta}}_0, \tag{5.50}$$

where $\tilde{\mathbf{G}}=\mathbf{A}_0^T\mathbf{G}^{-1}\mathbf{A}_0$. A detailed derivation of (5.50) is given in Appendix F. This shows that $E\{\boldsymbol{\Delta\theta}_{ETLS}\}=0$ for small perturbations, so it is an unbiased estimate of $\boldsymbol{\theta}$. The effect of ignoring the second order error term on the bias is given in Appendix G.

For simplicity, let $\mathbf{E}_{ETLS} \triangleq E\left\{\boldsymbol{\Delta\theta}_{ETLS}\boldsymbol{\Delta\theta}_{ETLS}{}^{T}\right\}$. From (5.50), we obtain

$$\begin{aligned}\mathbf{E}_{ETLS} &= E\left\{\tilde{\mathbf{G}}^{-1}\mathbf{A}_0^T\mathbf{G}^{-1}\boldsymbol{\Delta\Phi}\tilde{\boldsymbol{\theta}}\tilde{\boldsymbol{\theta}}^T\boldsymbol{\Delta\Phi}^T\mathbf{G}^{-T}\mathbf{A}_0\tilde{\mathbf{G}}^{-T}\right\} \\ &= \tilde{\mathbf{G}}^{-1}\mathbf{A}_0^T\mathbf{G}^{-1}E\left\{\boldsymbol{\Delta\Phi}\tilde{\boldsymbol{\theta}}\left(\boldsymbol{\Delta\Phi}\tilde{\boldsymbol{\theta}}\right)^T\right\}\mathbf{G}^{-1}\mathbf{A}_0\tilde{\mathbf{G}}^{-1}.\end{aligned} \tag{5.51}$$

Defining $\mathbf{F} = \begin{bmatrix} 2x_1 & 2y_1 & -1 & R_1^2 \end{bmatrix}\tilde{\boldsymbol{\theta}}_0$, $\boldsymbol{\eta} = diag\left\{\eta_{12}, \ldots, \eta_{1N}\right\}$ and $\boldsymbol{\xi} = \boldsymbol{\eta}\begin{bmatrix} n_{21} & \ldots & n_{N1} \end{bmatrix}^T$ gives $\boldsymbol{\Delta\Phi}\tilde{\boldsymbol{\theta}} = \mathbf{F}\boldsymbol{\xi}$ so that (5.51) can be simplified to

$$\begin{aligned}\mathbf{E}_{ETLS} &= \tilde{\mathbf{G}}^{-1}\mathbf{A}_0^T\mathbf{G}^{-1}E\left\{\mathbf{F}\boldsymbol{\xi}\boldsymbol{\xi}^T\mathbf{F}^T\right\}\mathbf{G}^{-1}\mathbf{A}_0\tilde{\mathbf{G}}^{-1} \\ &= \mathbf{B}^T\tilde{\boldsymbol{\xi}}\mathbf{B},\end{aligned} \tag{5.52}$$

where

$$\begin{aligned}\mathbf{B} &= (\mathbf{F}\boldsymbol{\eta})^T\mathbf{G}^{-1}\mathbf{A}_0\tilde{\mathbf{G}}^{-1} \\ \tilde{\boldsymbol{\xi}} &= diag\left\{\sigma_2^2, ..., \sigma_N^2\right\}.\end{aligned}$$

Note that if the noise variances are equal, $\sigma_i^2 = \sigma^2$ for $2 \leq i \leq N$, (5.52) can be simplified as

$$\mathbf{E}_{ETLS} = \sigma^2\mathbf{B}^T\mathbf{B}. \tag{5.53}$$

Finally, the MSE can be found from (5.45) and (5.52) as $\text{MSE} = \mathbf{Tr}\left\{\mathbf{E}_{ETLS}\mathbf{E}_{ETLS}^T\right\}$. If $\tilde{\mathbf{G}^{-1}}$ is positive definite, the MSE can be simplified as follows.

Proposition 1: Let λ_k be the kth eigenvalue of $\tilde{\mathbf{G}}$ and $\mathbf{L}$ the corresponding eigenvector matrix. If $\tilde{\mathbf{G}^{-1}}$ is symmetric and $\tilde{\mathbf{G}} \succ 0$, then the MSE defined in (5.45) is given by

$$\text{MSE} = \sum_{k=1}^{K}\lambda_k^{-2}E\left\{h_k^2\right\}, \tag{5.54}$$

where $K = rank(\tilde{\mathbf{G}})$ and h_k is the kth element of the column vector

$$\tilde{\mathbf{h}} = \mathbf{L}^T\mathbf{A}_0^T\mathbf{G}^{-1}\boldsymbol{\Delta\Phi}\tilde{\boldsymbol{\theta}}_0. \tag{5.55}$$

Proof. Considering $\boldsymbol{\Delta\theta}_{ETLS}$ defined in (5.50), the mean squared error can be rewrit-

ten as

$$\begin{aligned}\text{MSE} &= E\left\{\boldsymbol{\Delta\theta}_{ETLS}{}^{T}\boldsymbol{\Delta\theta}_{ETLS}\right\}\\ &= E\left\{\left(\tilde{\mathbf{G}}^{-1}\mathbf{A}_0^T\mathbf{G}^{-1}\boldsymbol{\Delta\Phi}\tilde{\boldsymbol{\theta}}_0\right)^T\left(\tilde{\mathbf{G}}^{-1}\mathbf{A}_0^T\mathbf{G}^{-1}\boldsymbol{\Delta\Phi}\tilde{\boldsymbol{\theta}}_0\right)\right\}\\ &= E\left\{\tilde{\boldsymbol{\theta}}_0^T\boldsymbol{\Delta\Phi}^T\mathbf{G}^{-1}\mathbf{A}_0\tilde{\mathbf{G}}^{-2}\mathbf{A}_0^T\mathbf{G}^{-1}\boldsymbol{\Delta\Phi}\tilde{\boldsymbol{\theta}}_0\right\},\end{aligned} \tag{5.56}$$

where

$$\tilde{\mathbf{G}}^{-T}\tilde{\mathbf{G}}^{-1} = \left(\mathbf{A}_0^T\mathbf{G}^{-1}\mathbf{A}_0\right)^T\left(\mathbf{A}_0^T\mathbf{G}^{-1}\mathbf{A}_0\right) = \tilde{\mathbf{G}}^{-2}. \tag{5.57}$$

Since $\tilde{\mathbf{G}} \succ 0$ from Proposition 1, it has eigenvalue-eigenvector decomposition

$$\tilde{\mathbf{G}} = \mathbf{LHL}^T, \tag{5.58}$$

where

$$\begin{aligned}\mathbf{H} &= diag\left\{\lambda_1, \ldots, \lambda_K\right\}\\ \mathbf{L} &= \left[l_1, \ldots, l_K\right],\end{aligned}$$

in which l_k denotes the kth eigenvector corresponding to eigenvalue λ_k, and $K = rank(\tilde{\mathbf{G}})$. As $\tilde{\mathbf{G}} \succ 0$, it follows that $\tilde{\mathbf{G}}^{-1} \succ 0$ [20]. Therefore, $\tilde{\mathbf{G}}^{-2}$ can be decomposed using (5.58) as $\tilde{\mathbf{G}}^{-2} = \mathbf{LH}^{-2}\mathbf{L}^T$. Substituting $\tilde{\mathbf{G}}^{-2}$ into (5.56) yields

$$\begin{aligned}\text{MSE} &= E\left\{\left(\boldsymbol{\Delta\Phi}\tilde{\boldsymbol{\theta}}\right)^T\mathbf{G}^{-1}\mathbf{A}_0\mathbf{LH}^{-2}(\mathbf{A}_0\mathbf{L})^T\mathbf{G}^{-1}\boldsymbol{\Delta\Phi}\tilde{\boldsymbol{\theta}}\right\}\\ &= E\left\{\tilde{\mathbf{h}}^T\mathbf{H}^{-2}\tilde{\mathbf{h}}\right\} = \sum_{k=1}^{K}\lambda_k^{-2}E\left\{h_k^2\right\},\end{aligned} \tag{5.59}$$

where $K = rank(\tilde{\mathbf{G}})$ and h_k denotes the kth element of the column vector $\tilde{\mathbf{h}} = (\mathbf{A}_0\mathbf{L})^T\mathbf{G}^{-1}\boldsymbol{\Delta\Phi}\tilde{\boldsymbol{\theta}}_0$. □

5.3.2 Cramer-Rao Lower Bound Analysis

The Cramer-Rao Lower Bound (CRLB) of the proposed RSSD-based solution using the ETLS-SDP method is derived in this section. The CRLB provides a lower limit on the covariance matrix of an unbiased estimator which can be defined as

$$\text{cov}(\hat{\mathbf{u}}) \geq \tilde{\mathbf{F}}^{-1}, \tag{5.60}$$

where $\tilde{\mathbf{F}}$ denotes the Fisher Information Matrix (FIM) [55], and cov( ) is the covariance matrix of the unknown vector $\hat{\mathbf{u}}$. Let

$$\mathbf{\Delta P} = \begin{bmatrix} \Delta P_{12} & \cdots & \Delta P_{1N} \end{bmatrix}^T,$$

be the vector of $(N-1)$ measured signal strength differences between the first and ith sensor, ΔP_{1i}, as defined in (5.4). Assuming the Gaussian noise is independent and identically distributed (i.i.d.) with zero mean and variance σ_{1i}^2 ($n_{i1} \sim N(0, \sigma_i^2 + \sigma_1^2)$), i.e., ignoring the correlation between the measurements, the joint probability density function (pdf) of $\mathbf{\Delta P}$ can be written as

$$\begin{aligned} \mathbf{g}\left(\mathbf{\Delta P}|\mathbf{u}\right) = \prod_{i=2}^{N} \frac{1}{\sqrt{2\pi(\sigma_i^2+\sigma_1^2)}} \exp\Bigg\{ -\frac{1}{(\sigma_i^2+\sigma_1^2)} \\ \left(\Delta P_{1i} - 10\gamma \log_{10}\left(\frac{\|\mathbf{u}-\mathbf{u}_i\|}{\|\mathbf{u}-\mathbf{u}_1\|}\right)\right)^2 \Bigg\}, \end{aligned} \tag{5.61}$$

where $\mathbf{g}\left(\mathbf{\Delta P}|\mathbf{u}\right)$ denotes the joint pdf of the measured RSSD vector $\mathbf{\Delta P}$ conditioned on $\mathbf{u}$. Based on (5.61), the log-likelihood function of the proposed unknown location vector, $\ln\left(\mathbf{g}\left(\mathbf{\Delta P}|\mathbf{u}\right)\right)$, can be expressed as

$$\tilde{\mathbf{g}}\left(\mathbf{u}\right) = \sum_{i=2}^{N} \left(\frac{10\gamma}{\sigma_{1i}^2} \log_{10}\left(\frac{\|\mathbf{u}-\mathbf{u}_i\|}{\|\mathbf{u}-\mathbf{u}_1\|}\right)^2 - \nu_i \right), \tag{5.62}$$

where

$$\nu_i = \frac{5\gamma}{\sigma_{1i}^2}\Delta P_{1i} + \frac{1}{2}\ln\left(2\pi\sigma_{1i}^2\right).$$

The FIM components in (5.60) are obtained using the log-likelihood function $\tilde{\mathbf{g}}\left(\mathbf{u}\right)$ which yields

$$\left[\tilde{\mathbf{F}}\right]_{m,n} = -E\left\{ \frac{\partial^2 \tilde{\mathbf{g}}\left(\mathbf{u}\right)}{\partial \mathbf{u}^{(m)} \partial \mathbf{u}^{(n)}} \right\}, \quad m,n = 1,2, \tag{5.63}$$

where $\mathbf{u}^{(m)}$ denotes the mth element of $\mathbf{u}$. Therefore, the FIM components can be derived from (5.62) and (5.63) as

$$\left[\tilde{\mathbf{F}}\right]_{xx} = \sum_{i=2}^{N} \left(\frac{10\gamma}{\sigma_{1i}\ln 10}\right)^2 \left(\frac{x-x_1}{\|\mathbf{u}-\mathbf{u}_1\|^2} + \frac{x_i - x}{\|\mathbf{u}_i - \mathbf{u}\|^2}\right)^2,$$

$$\left[\tilde{\mathbf{F}}\right]_{yy} = \sum_{i=2}^{N} \left(\frac{10\gamma}{\sigma_{1i}\ln 10}\right)^2 \left(\frac{y-y_1}{\|\mathbf{u}-\mathbf{u}_1\|^2} + \frac{y_i-y}{\|\mathbf{u}_i-\mathbf{u}\|^2}\right)^2,$$

$$\begin{aligned}\left[\tilde{\mathbf{F}}\right]_{xy} &= \sum_{i=2}^{N} \left(\frac{10\gamma}{\sigma_{1i}\ln 10}\right)^2 \left\{ \left(\frac{(x-x_1)\|\mathbf{u}_i-\mathbf{u}\|^2}{\|\mathbf{u}-\mathbf{u}_1\|^4} \right.\right. \\ &\quad \left.\left. + \frac{(x_i-x)}{\|\mathbf{u}-\mathbf{u}_1\|^2}\right) \left(\frac{(y-y_1)\|\mathbf{u}_i-\mathbf{u}\|^2}{\|\mathbf{u}_i-\mathbf{u}\|^4} + \frac{(y_i-y)}{\|\mathbf{u}_i-\mathbf{u}\|^2}\right)\right\}. \\ &= \left[\tilde{\mathbf{F}}\right]_{yx}\end{aligned} \tag{5.64}$$

The CRLB is then obtained by substituting the FIM components from (5.64) into (5.60). Based on (5.64), the CRLB will depend on the sensor geometry, number of sensors and the propagation model (path loss exponent). Equations (5.60) and (5.64) show that increasing the path loss exponent or number of sensors leads to a decrease in the CRLB.

5.3.3 CRLB with Correlated Measurement Noise

In this section, the effect of the correlated measurement noise on the CRLB is considered in order to derive generalized CRLB as a tight bound for comparison with the simulation results [71]-[72]. Let $\mathbf{C} \in \Re^{(\mathbf{N-1})\times(\mathbf{N-1})}$ be the covariance matrix of the RSSD-based correlated measurement noise. The matrix elements C_{ij}, $i, j = 2, 3, \ldots, N$, can be written as [55]

$$C_{ij} = \begin{cases} \sigma_{1i}^2 = \sigma_1^2 + \sigma_i^2 & i = j \\ \rho_{ij}\sigma_{1i}\sigma_{1j} & i \neq j \end{cases}, \tag{5.65}$$

where $\rho\sigma_{1i}\sigma_{1j}$ denotes $\mathrm{cov}(n_{1i}, n_{1j})$ and ρ_{ij} is the correlation coefficient between n_{1i} and n_{1j}. For simplicity and without lose of generality, we consider the correlation coefficients to be identical so that $\rho_{ij} = \rho$. Therefore, the diagonal and off diagonal elements of $\mathbf{C}$ are σ_{1i}^2 and $\rho\sigma_{1i}\sigma_{1j}$, respectively.

Considering the i.i.d. and Gaussian RSSD measurement noise with zero mean and variance σ_{1i}^2, the joint probability density function with correlated measurement noise $\mathbf{g}_\rho(\mathbf{\Delta P}|\mathbf{u})$ can be written as

$$\begin{aligned}\mathbf{g}_\rho(\mathbf{\Delta P}|\mathbf{u}) =& (2\pi)^{-(N-1)/2}|\mathbf{C}|^{-1/2}\times \\ & \exp\left(-\frac{1}{2}(\mathbf{\Delta P}-\boldsymbol{\mu}_{\mathbf{\Delta P}})^T\mathbf{C}^{-1}(\mathbf{\Delta P}-\boldsymbol{\mu}_{\mathbf{\Delta P}})\right),\end{aligned} \tag{5.66}$$

where $\boldsymbol{\mu}_{\mathbf{\Delta P}} \in \Re^{(N-1)\times 1}$ is the mean of the measurement vector that can be obtained using (5.3) and the fact that $E\left(n_{1i}\right) = 0$ as

$$\mu_{\mathbf{\Delta P}} = 10\gamma \left[\log \frac{\|\mathbf{u}-\mathbf{u}_2\|}{\|\mathbf{u}-\mathbf{u}_1\|}, \ldots, \log \frac{\|\mathbf{u}-\mathbf{u}_N\|}{\|\mathbf{u}-\mathbf{u}_1\|}\right]^T. \tag{5.67}$$

Defining $\tilde{\mathbf{g}}_\rho(\mathbf{u}) = \ln\left(\mathbf{g}_\rho\left(\mathbf{\Delta P}|\mathbf{u}\right)\right)$, the log likelihood of the joint pdf given in (5.66) can be obtained as

$$\tilde{\mathbf{g}}_\rho\left(\mathbf{u}\right) = \tilde{\nu} - \frac{1}{2}(\mathbf{\Delta P} - \boldsymbol{\mu}_{\mathbf{\Delta P}})^T \mathbf{C}^{-1}\left(\mathbf{\Delta P} - \boldsymbol{\mu}_{\mathbf{\Delta P}}\right), \tag{5.68}$$

where

$$\tilde{\nu} = -\frac{1}{2}\ln\left\{(2\pi)^{(N-1)}\left|\mathbf{C}\right|\right\}.$$

Considering (5.60), the FIM is required to evaluate the CRLB of the proposed estimator. Using (5.63), the FIM with correlated measurement noise $\tilde{\mathbf{F}}_\rho$ can be obtained by substituting (5.68) in (5.66) which gives

$$\tilde{\mathbf{F}}_\rho = -E\left\{\frac{\partial^2 \tilde{\mathbf{g}}_\rho\left(\mathbf{u}\right)}{\partial \mathbf{u} \partial \mathbf{u}^T}\right\} = \left(\frac{\partial \boldsymbol{\mu}_{\mathbf{\Delta P}}}{\partial \mathbf{u}}\right)^T \mathbf{C}^{-1}\left(\frac{\partial \boldsymbol{\mu}_{\mathbf{\Delta P}}}{\partial \mathbf{u}}\right), \tag{5.69}$$

where the ijth component of the matrix $\left(\frac{\partial \boldsymbol{\mu}_{\mathbf{\Delta P}}}{\partial \mathbf{u}}\right) \in \Re^{(N-1)\times 2}$ can be expressed as

$$\left(\frac{\partial \boldsymbol{\mu}_{\mathbf{\Delta P}}}{\partial \mathbf{u}}\right)_{ij} = \begin{cases} \frac{\partial \mu^{[i]}_{\mathbf{\Delta P}}}{\partial x} & j = 1, \\ \frac{\partial \mu^{[i]}_{\mathbf{\Delta P}}}{\partial y} & j = 2, \end{cases} \quad i = 1, 2, \ldots, N-1, \tag{5.70}$$

where $\mu^{[i]}_{\mathbf{\Delta P}}$ denotes the ith element of the vector $\boldsymbol{\mu}_{\mathbf{\Delta P}}$ in (5.67). Substituting (5.67) into (5.70) gives

$$\frac{\partial \boldsymbol{\mu}_{\mathbf{\Delta P}}}{\partial \mathbf{u}} = \left(\frac{10\gamma}{\ln 10}\right) \begin{bmatrix} \frac{(\mathbf{u}-\mathbf{u}_2)^T}{\|\mathbf{u}-\mathbf{u}_2\|^2} - \frac{(\mathbf{u}-\mathbf{u}_1)^T}{\|\mathbf{u}-\mathbf{u}_1\|^2} \\ \vdots \\ \frac{(\mathbf{u}-\mathbf{u}_N)^T}{\|\mathbf{u}-\mathbf{u}_N\|^2} - \frac{(\mathbf{u}-\mathbf{u}_1)^T}{\|\mathbf{u}-\mathbf{u}_1\|^2} \end{bmatrix}. \tag{5.71}$$

Then the new FIM $\tilde{\mathbf{F}}_\rho \in \Re^{2\times 2}$ can be obtained by substituting (5.65) and (5.71) into (5.69) resulting in

$$\tilde{\mathbf{F}}_\rho = \left(\frac{10\gamma}{\ln 10}\right)^2 \sum_{j=2}^{N} \left[\left(\sum_{i=2}^{N}\left(\tilde{\mathbf{u}}_i - \tilde{\mathbf{u}}_1\right)\right)\left(\tilde{\mathbf{u}}_j^T - \tilde{\mathbf{u}}_1^T\right)\right], \tag{5.72}$$

where $\tilde{\mathbf{u}}_m$ is defined as

$$\tilde{\mathbf{u}}_m \triangleq \frac{(\mathbf{u}-\mathbf{u}_m)}{\|\mathbf{u}-\mathbf{u}_m\|^2}.$$

Equation (5.72) provides a tight CRLB when there is correlated measurement noise. Note that the FIM given in (5.72) can easily be changed to the case of non identical correlation coefficients by substituting $\rho \neq \rho_{ij}$ in (5.72).

5.3.4 ETLS-SDP Complexity Analysis

In this section, the computational complexity of the proposed method is considered based on the number of floating point operations (flops). A flop is an addition, subtraction, multiplication or division in the algorithm [67]. The ETLS-SDP method is compared with the complexity of several other well known algorithms. In each iteration of this method, the path loss exponent γ_j in (5.37) and the SDP in (5.34) are updated.

From (5.37), the number of flops required to compute γ in an iteration is

$$\gamma_j = \overbrace{\underbrace{\left(\hat{\mathbf{A}}_{(j-1)}^T \mathbf{W}^{-1} \hat{\mathbf{A}}_{(j-1)}\right)^{-1}}_{(3N-4)} \underbrace{\hat{\mathbf{A}}_{(j-1)}^T \mathbf{W}^{-1} \hat{\mathbf{b}}_{(j-1)}}_{(4N-5)}}^{\text{Complexity} \simeq \mathbf{O}(N)}, \tag{5.73}$$

so a total of $7N-9$ flops are required. Thus, for K iterations the computational complexity is $O(KN)$. Since each iteration has bounded complexity $O\left(\log\left(\frac{1}{\varepsilon}\right) N^{1/2}\right)$,

Table 5.1: Computational Complexity Of Six Methods for N Sensors

Algorithm	Number of Flops	Time (ms)
NLS [61]	$O\left(KN^3\right)$	31.2
Improved LLS [51]	$O\left(K18N+87\right)$	0.62
WLS-UT [53]	$O\left(N^{2.5}\left(N+1\right)\log\left(\frac{1}{\varepsilon}\right)\right)$	46.8
LCJE [50]	$O\left(KN^2\right)$	9.8
GTRS [64]	$O\left(34N+36K\right)$	1.34
ETLS-SDP	$O\left(N\left(\tilde{K}N^{3.5}+7\right)-9\right)$	53

the worst case computational complexity in solving the ETLS-SDP problem in (5.34) is

$$\text{Complexity}_{\text{SDP}} = O\left(K \log\left(\frac{1}{\varepsilon}\right) N^{4.5}\right). \tag{5.74}$$

Hence, the worst case complexity of the ETLS-SDP method with unknown path loss exponent can be obtained from (5.73) and (5.74) as $O\left(\bar{K}N^{4.5} + N\right)$ in which $\bar{K} = K \log\left(\frac{1}{\varepsilon}\right)$.

Table 5.2: Summary of the Methods used for Performance Comparison

Method Name	Description
Standard LS [59]	RSSD-based LS method with known PLE
ILLS [51]	RSS-based improved LLS with known transmit power and unknown PLE
Improved LS [60]	RSSD-based weighted LS method with known PLE
NLS [61]	RSSD-based nonlinear LS method with known PLE
UT-WLS [53]	RSS-based WLS with unscented transform for unknown transmit power and PLE
ML-SDR [62],[63]	RSS-based ML-SDR with unknown transmit power and PLE
LCJE [50]	RSS-based LCJE with known transmit power and unknown PLE
GTRS [64]	RSS-based GTRS with unknown transmit power and PLE
ETLS-SDP	The proposed RSSD-based method with unknown transmit power and unknown PLE

The ML and NLS estimators are two nonlinear estimators which employ an iterative method such as steepest-descent or Newton with a suitable initial point to estimate the unknown parameter [54]-[55]. The complexity of these algorithms is $O(KN^3)$ where K is the number of iterations. The LCJE and improved LLS methods are two low complexity linear estimators with computational complexities $O(N^2)$ and $O(N)$, respectively. However, the performance of these linear estimators is poor at low signal to noise ratios compared to the proposed method as will be shown in the next section. The GTRS method is another low complexity algorithm which has better performance than the LCJE and improved LLS techniques under mild conditions [64].

Table 5.1 compares the complexity and average running time of six received signal strength based techniques. Note that the number of iterations K for the ML and NLS estimators depends on the initial point and iterative method chosen. This choice will also affect the accuracy of the solution. Further, the number of SDP iterations K depends on the required accuracy specified by ϵ in the algorithm. From Table 5.1, the complexity of the proposed ETLS-SDP method is higher than that of the LS-based algorithms, but the proposed method provides more accurate solutions, as will be shown in the next section. Table 5.1 also shows the CPU time in milliseconds required to execute the algorithms on a computer with a 2.5 GHz Intel Core i5 processor and 6 GB of memory. These results indicate that the improved LLS and LCJE methods have low computational complexity, but as will be shown in the next section, they also have poor performance in terms of the source location estimate and bias in the path loss exponent estimate. The CPU time of the WLS-UT method is very close to that of the proposed ETLS-SDP method, but the proposed method has superior performance.

5.4 Performance Evaluation

In this section, the performance of the proposed RSSD-based ETLS-SDP localization method is evaluated via simulation. A 2D geometry is considered with $N = 9$ sensors at the known coordinates (5,5), (0,15), (15,0), (30,0), (0,30), (15,15), (15,30), (30,15), and (30,30) in meters. These sensors are used to estimate an unknown source which is located at (24,16). The performance of the proposed method is compared with several well known methods with both known and unknown path loss exponent (PLE). Table 5.2 provides a brief summary of these techniques. The proposed SDP method is

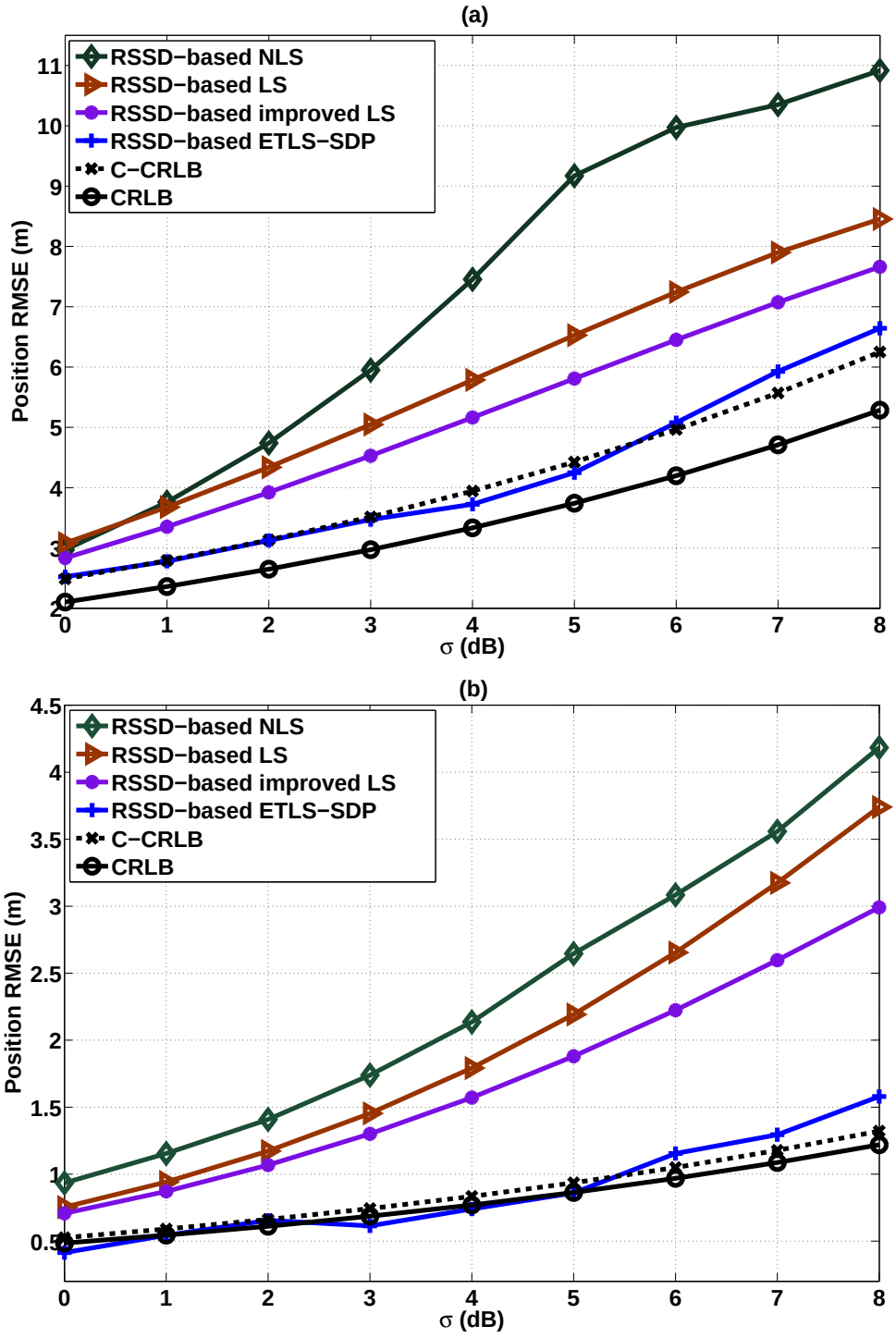

Figure 5.1: RMSE of the source position estimate versus σ for several RSSD-based methods with $\gamma = 2$, (a) $N = 5$ and (b) $N = 9$ sensors.

implemented using the CVX toolbox with the self-dual-minimization (SeDuMi) solver [23].

5.4.1 ETLS-SDP versus other RSSD-based Methods

In this section, the performance of the proposed RSSD-based method is evaluated and compared with the performance of the RSSD-based NLS [61], standard LS [59] and improved LS [60] methods. The corresponding CRLB is used as a benchmark for comparison. We consider the case with known path loss exponent and unknown transmit power. Figure 5.1 illustrates the effect of the measurement noise standard deviation σ on the root mean squared error (RMSE) of the source position estimate for $N = 5$ and $N = 9$ sensors. The path loss exponent is $\gamma = 2$, $\rho = 0.5$ and $N = 5$ denotes the first five sensors in the list above. These results show that the ETLS-SDP method provides the best performance compared to the other methods, and is closest to the CRLB.

Note that a large noise variance results in a small signal to noise ratio (SNR) which results in poor performance with the proposed method, as shown in Fig. 5.1. A degradation in performance may also occur if the error in the first order Taylor series approximation of c_{1i} is large. However, for a sufficiently large SNR, this approximation has been shown to be a good approximation [62], [63]-[64]. In addition, increasing the number of sensors to $N = 9$ improves the performance so that the proposed method achieves the CRLB for $\sigma \leq 5$. At $\sigma = 5$ dB, there is approximately a 0.48 m improvement with respect to the CRLB when N is increased from 5 to 9. The

Table 5.3: Performance of the ETLS-SDP Method With Unknown PLE for Various γ_0 with $k = 5$ Iterations

	Estimated PLE ($\hat{\gamma}$)				Average	Average	Average
σ (dB)	$\gamma_0 = 2.5$	$\gamma_0 = 3$	$\gamma_0 = 3.5$	$\gamma_0 = 4$	$\hat{\gamma}$	RMSE (m)	PLE Bias $\Delta\gamma$
2	2.01	2.01	2.02	2.03	2.02	0.67	0.02
5	1.95	1.94	1.94	1.92	1.94	0.98	0.06
7	1.93	1.92	1.92	1.9	1.92	1.22	0.08
8	1.92	1.92	1.91	1.91	1.91	1.66	0.09

poor performance of the standard LS algorithm is due to not employing constraints in the optimization problem as well as not considering errors in the observation data

matrix. For example, at $\sigma = 5$ dB there is approximately a 3.0 m and 1.3 m difference with respect to the CRLB for $N = 5$ and $N = 9$, respectively. The improved LS algorithm in [60] employs a weighting matrix which provides a significant improvement in performance. This improvement over the standard LS algorithm is approximately 0.72 m and 0.33 m at $\sigma = 5$ dB for $N = 5$ and $N = 9$, respectively. Note that the NLS method given in [61] provides the worst performance.

The RMSE of the source position estimate with the proposed and other RSSD-based methods versus the path loss exponent γ is given in Fig. 5.2 for $\sigma = 2$ dB and $\sigma = 6$ dB, and $N = 9$ sensors. This shows that the localization accuracy improves with increasing path loss exponent, which is also indicated by the CRLB analysis. As an example, increasing the path loss exponent from $\gamma = 2$ to $\gamma = 4$ provides a 44% and 53% reduction in the RMSE with the proposed method for $\sigma = 2$ dB and $\sigma = 6$ dB, respectively. Moreover, the performance of the LS and improved LS methods converge for larger path loss exponents. At $\gamma = 2$, there is approximately a 1.1 m and 1.37 m reduction in RMSE with the proposed method compared to the LS and improved LS methods, respectively, when $\sigma = 6$ dB. Note that the variance of the RMSE with respect to the path loss exponent is lowest with the ETLS-SDP method. Thus, the proposed method provides a considerable improvement in performance compared to the other RSSD-based methods, and is significantly more robust to changes in the path loss exponent.

5.4.2 ETLS-SDP with Unknown PLE

In this section, the performance of the ETLS-SDP method is evaluated for the case when both the transmit power and path loss exponent (PLE) are unknown. The actual PLE is set to $\gamma = 2$, and the initial PLE is considered to be in the range $\gamma_0 \in [2.5 - 4]$. Figure 5.3 illustrates the effect of γ_0 on the RMSE of the source position estimate for different values of σ after $k = 5$ iterations. This shows that increasing the number of iterations significantly decreases the RMSE dependence on γ_0. The bias of the PLE estimate denoted as $\Delta\gamma = (|\hat{\gamma} - \gamma|)$ is given in Table 5.3. Figure 5.3 and Table 5.3 show that there is a negligible change in the RMSE and PLE bias for different choices of γ_0. In addition, increasing σ increases the RMSE but has little effect on the PLE bias. For example, increasing σ from 2 to 8 dB with $\gamma_0 = 4$ results in a 0.95 m and 0.07 increase in the RMSE and PLE bias, respectively. The average PLE estimate $\hat{\gamma}$ and average RMSE of the source position estimate are also

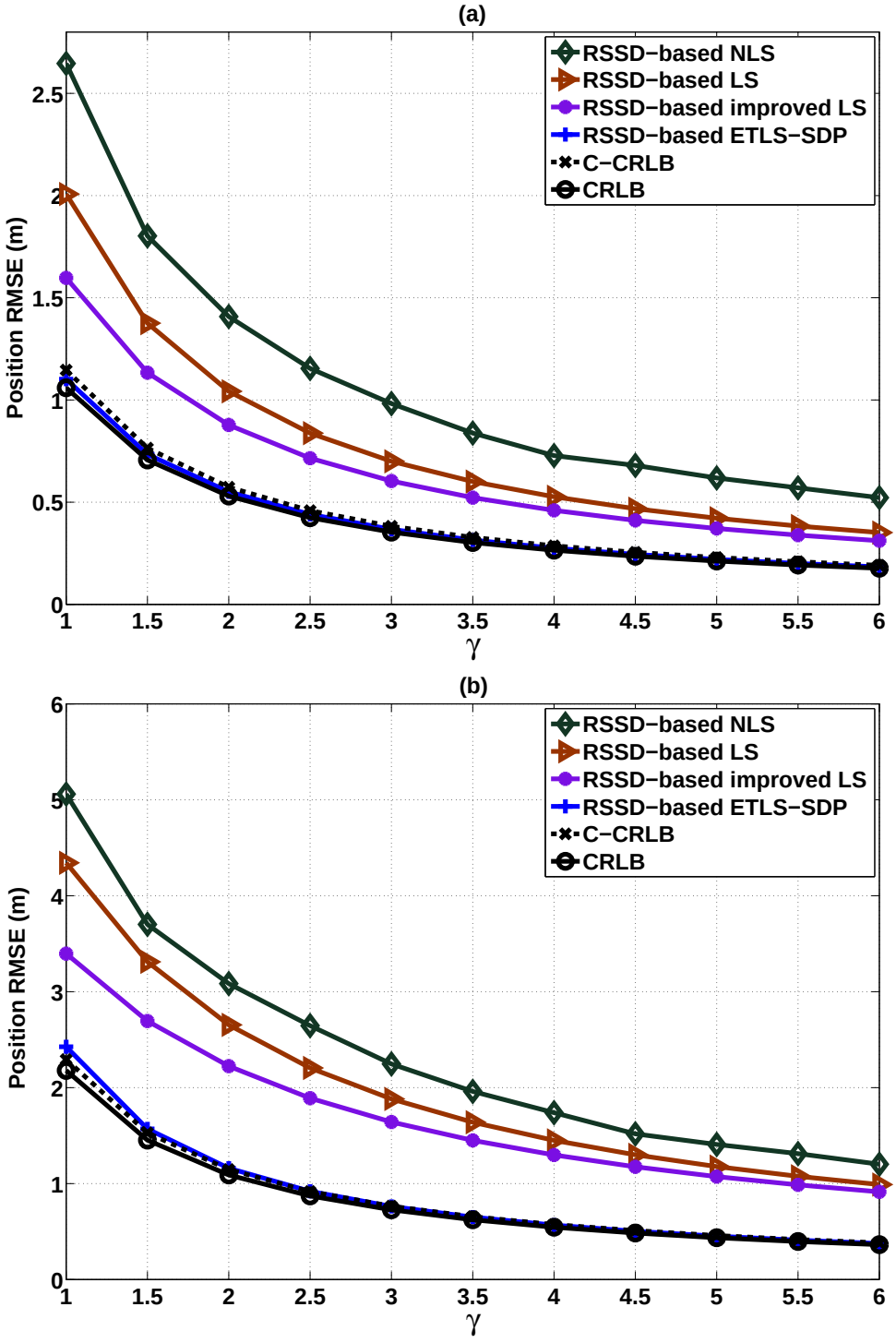

Figure 5.2: RMSE of the source position estimate versus γ with $N = 9$ sensors for several RSSD-based methods, (a) $\sigma = 2$ dB, and (b) $\sigma = 6$ dB.

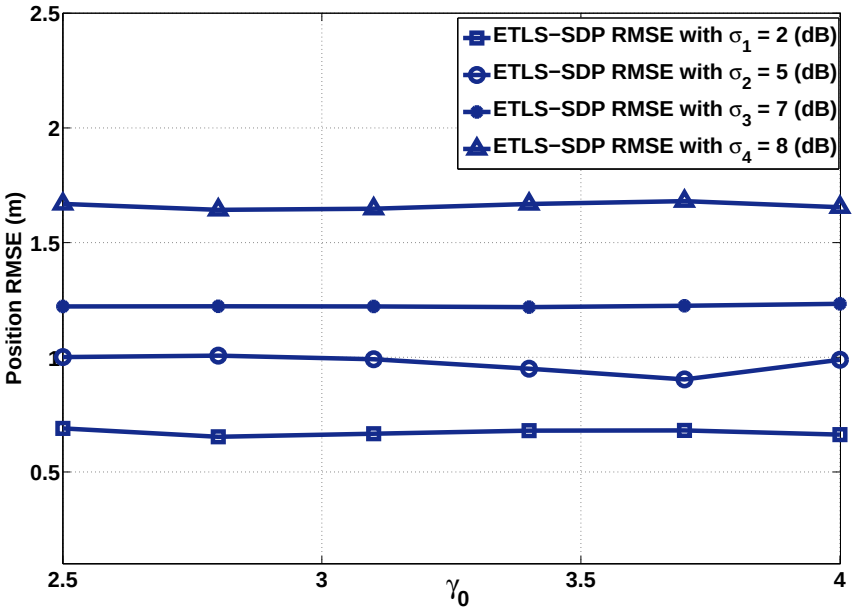

Figure 5.3: RMSE of the source position with the ETLS-SDP method versus the initial PLE with $N = 9$ sensors and $k = 5$ iterations for different σ.

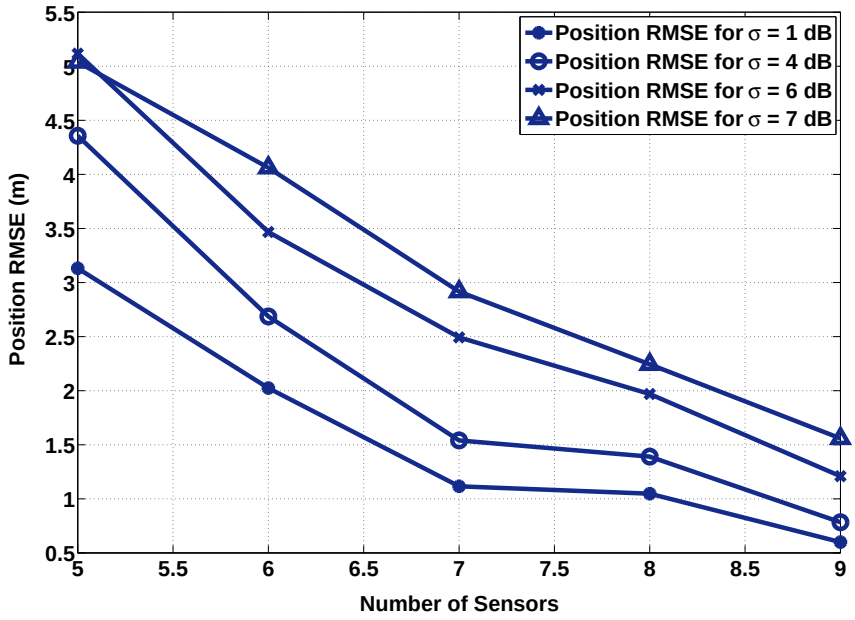

Figure 5.4: RMSE of the source position estimate versus the number of sensors for different σ with initial PLE estimate $\gamma_0 = 4$ and $k = 5$ iterations.

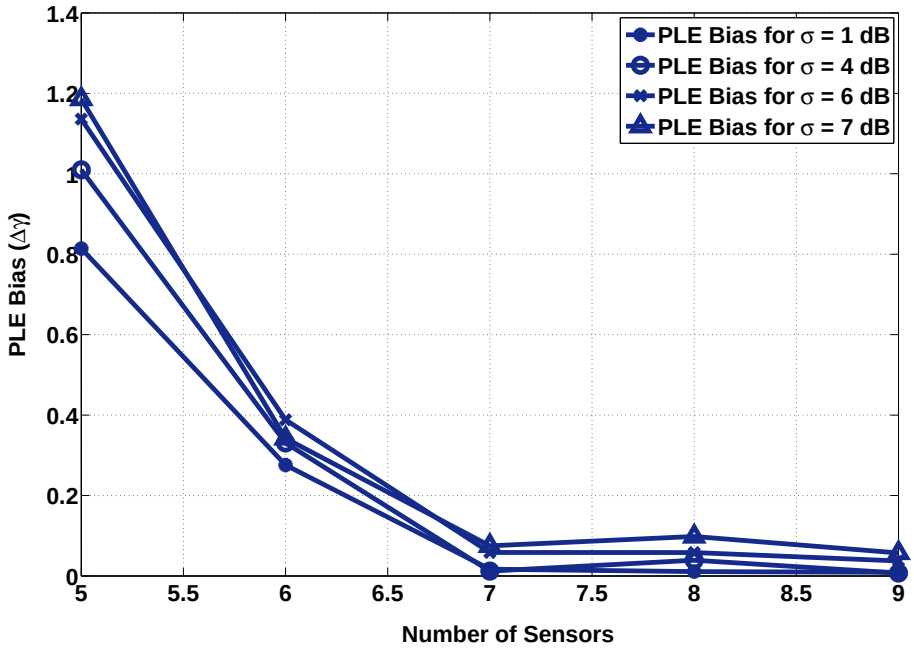

Figure 5.5: Path loss exponent bias versus the number of sensors for different σ with initial PLE estimate $\gamma_0 = 4$ and $k = 5$ iterations.

given in Table 5.3 for path loss exponents in the range $\gamma_0 \in [2.5 - 4]$.

Table 5.4: RMSE of the Source Position Estimate and PLE Bias with the ETLS-SDP Method for Different Numbers of Iterations

Iteration	RMSE (m)		PLE Bias $\Delta\gamma$	
Number k	$\sigma = 2$ (dB)	$\sigma = 6$ (dB)	$\sigma = 2$ (dB)	$\sigma = 6$ (dB)
2	0.64	1.27	0.07	0.11
3	0.56	1.24	0.03	0.10
5	0.49	1.22	0.02	0.07
7	0.49	1.21	0.02	0.06

Table 5.4 illustrates the change in the RMSE of the source position estimate as well as the PLE bias for different numbers of iterations with $\sigma = 2$ dB and $\sigma = 6$ dB, and $\gamma_0 = 4$. This shows that increasing the number of iterations improves the performance, as expected. However, after $k = 5$ iterations there is very little change in the RMSE and PLE bias.

The effect of the number of sensors on the RMSE of the source position estimate and the PLE bias for different σ is presented in Figs. 5.4 and 5.5. These results show that increasing the number of the sensors improves the performance significantly. As

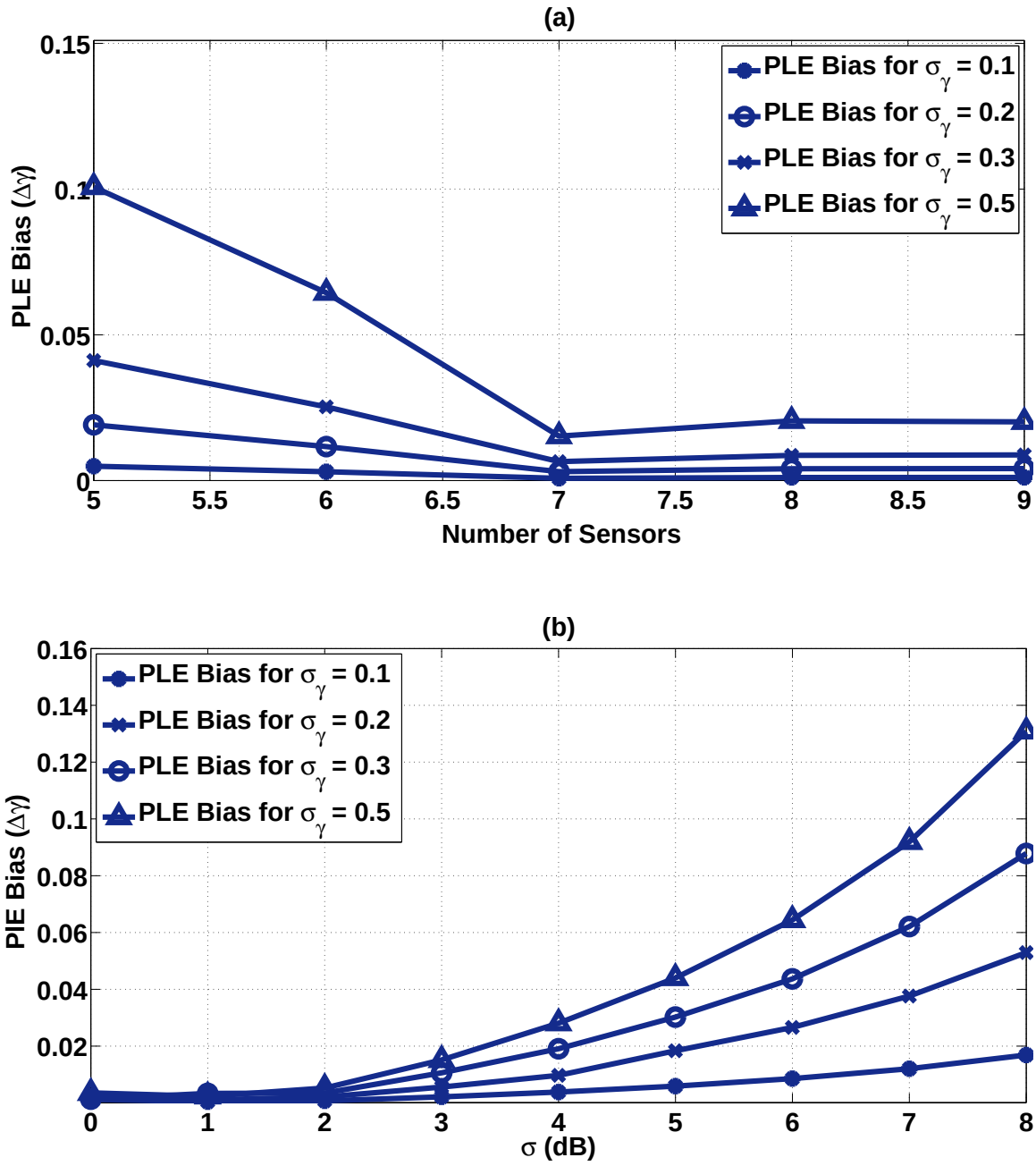

Figure 5.6: Path loss exponent (PLE) bias with an unknown PLE for different σ_γ and $k = 5$ iterations versus (a) number of sensors, and (b) σ (dB).

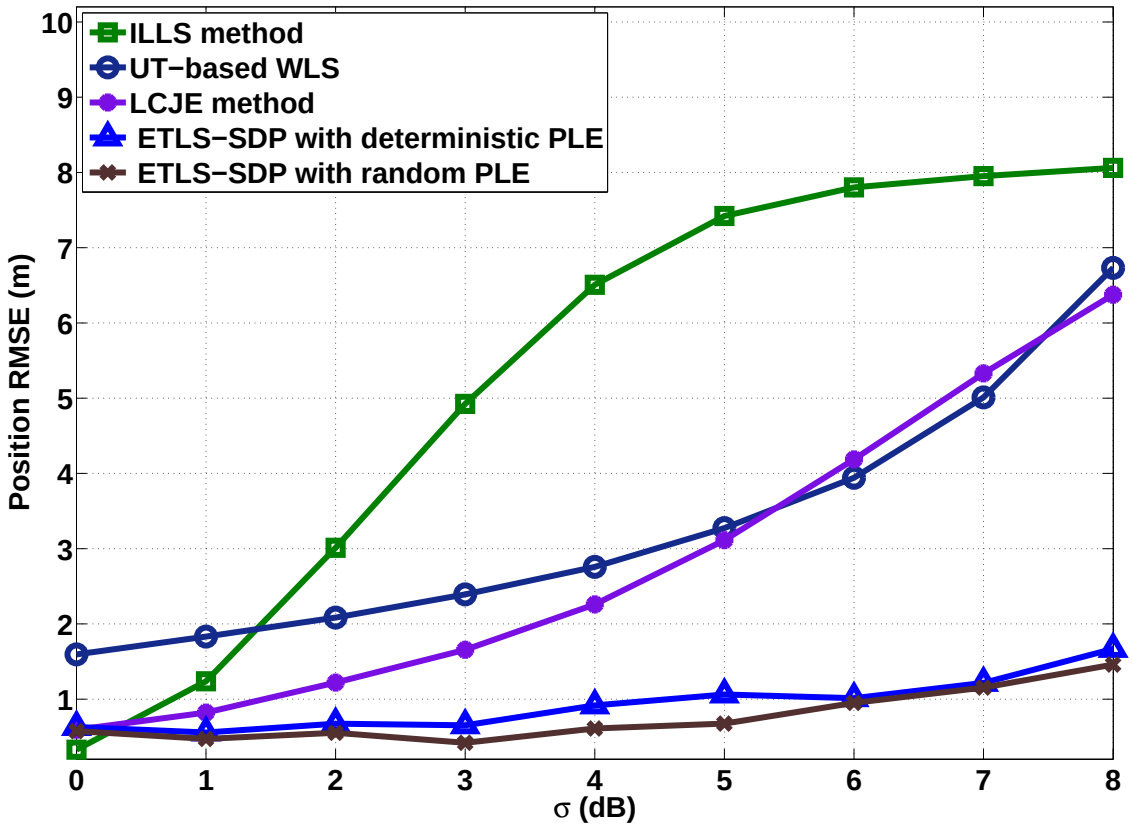

Figure 5.7: RMSE of the source position estimate versus σ for several unknown PLE methods with $N = 9$ sensors and initial PLE estimate $\gamma_0 = 4$.

an example, changing the number of sensors from $N = 5$ to 7 provides a 2.65 m and 1.11 m improvement in the RMSE and PLE bias for $\sigma = 6$ dB. Note that the PLE estimate is almost exact with $N = 7$ sensors, but the RMSE is improved by increasing N further. For example, there is a 1.28 m improvement in the RMSE by increasing the number of sensors from $N = 7$ to $N = 9$ for $\sigma = 6$ dB, but the corresponding improvement in the PLE bias is only 0.02.

Figure 5.6 shows the effect of the number of sensors and σ (dB) on the path loss exponent (PLE) bias for the random PLE case with different σ_γ. These results indicate that increasing the number of sensors or decreasing σ_γ will improve the PLE bias.

The performance of the proposed ETLS-SDP method is now compared with the performance of the unknown path loss exponent algorithms LCJE [53], UT-WLS [50] and improved linear LS (ILLS) [51]. Figure 5.7 presents the RMSE of the source location estimate versus σ for $k = 5$ iterations and $\gamma_0 = 4$. This shows that the

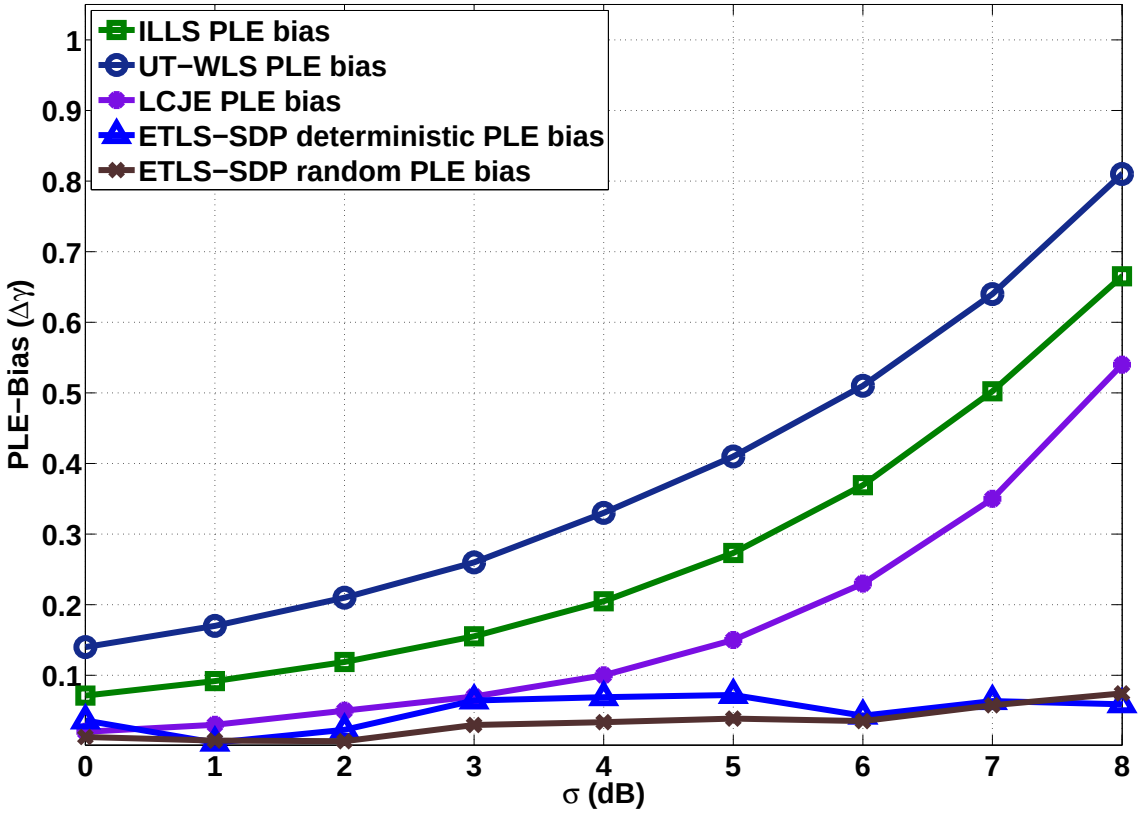

Figure 5.8: Comparison of path loss exponent bias versus σ for different unknown PLE methods with $N = 9$ sensors and initial PLE $\gamma_0 = 4$.

ETLS-SDP method provides a significant improvement in performance over the other methods, particularly for large σ. The poor performance of the ILLS method is due to errors in approximating the data vector as well as ignoring the error terms due to the assumptions employed to reduce the complexity [51]. The UT-WLS method provides good performance due to the use of the unscented transformation which does not require estimation of the data vector. For example, at $\sigma = 6$ dB there is approximately a 4.2 m improvement in the RMSE over the ILLS method. The LCJE method provides very good performance for very small values of σ. However, the performance is similar to that of the UT-WLS technique when σ is higher. Thus the degradation in performance is still considerable. Thus the ETLS-SDP method has the best performance for most values of σ. For example, the proposed method provides a 2.3 m and 2.1 m improvement in RMSE at $\sigma = 5$ dB over the UT-WLS and LCJE techniques, respectively.

Figure 5.8 shows the bias of the PLE estimate versus σ with $\gamma_0 = 4$ and $k = 5$

iterations. The largest bias is produced by the ILLS method, while the proposed ETLS-SDP method has the lowest bias. For example, at $\sigma = 5$ dB the ILLS bias is approximately 0.41, while the bias with the UT-WLS and LCJE methods is 0.14 and 0.26 lower, respectively. The proposed method has a bias of only 0.06 with respect to the actual path loss exponent $\gamma = 2$, which is an impprovement of 0.1 over the LCJE method. Thus the proposed ETLS-SDP method provides the best performance with respect to the PLE bias. Note that although the UT-WLS and LCJE methods have similar RMSE performance, for higher σ the LCJE method has a lower PLE bias.

5.4.3 ETLS-SDP versus Joint RSS Methods

In this section, the proposed ETLS-SDP method is compared with the ML-SDR method [62],[63] and the generalized trust region subproblem (GTRS) solution [64], which are recently proposed joint RSS estimators. In [62], the authors developed an RSS-based joint estimator using relaxation which provides good performance with respect to the previous methods. This approach was improved using the GTRS solution in [64]. To provide a fair comparison, a random source location is considered. Figure 5.9 compares the proposed ETLS-SDP method with these methods for the case of known and unknown path loss exponents. This shows that for a sufficiently large SNRs, the GTRS and ML-SDR methods have performance comparable to the proposed method. However for small SNRs, the proposed method provides better performance, particularly for the unknown path loss exponent case. For example, at $\sigma = 6$ dB and $N = 9$ there is approximately a 0.67 dB and 0.96 dB improvement in RMSE compared to the GTRS and ML-SDP methods, respectively, for the known PLE case. The corresponding improvements for the unknown PLE case are 0.63 dB and 0.49 dB. While the GTRS method has the lowest complexity compared to the other two methods [64], the corresponding performance is the worst, particularly with an unknown PLE.

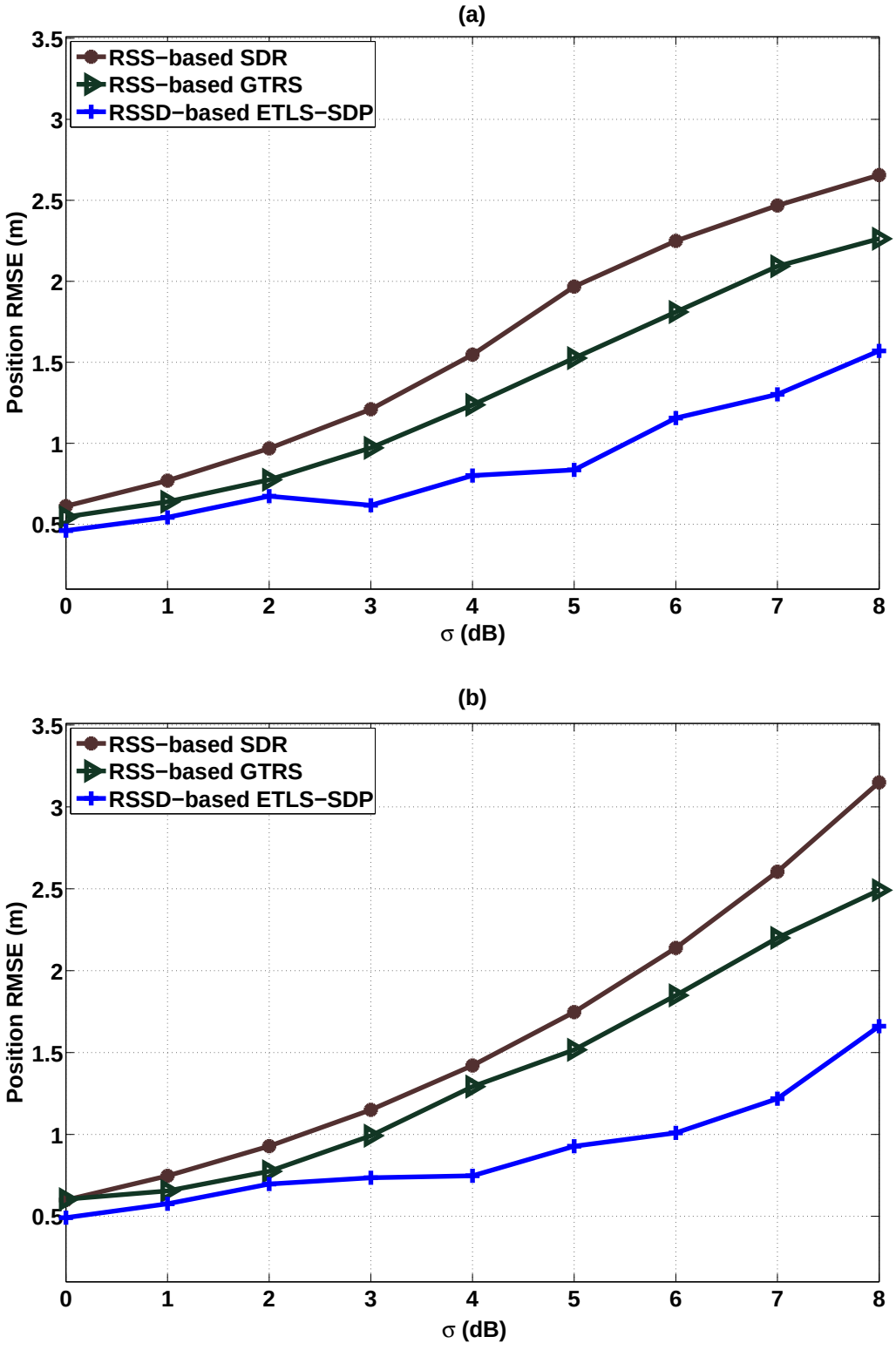

Figure 5.9: RMSE of the source position estimate versus σ for different joint estimation methods with $N = 9$ sensors and initial PLE estimate $\gamma_0 = 4$, (a) known PLE and (b) unknown PLE.

Chapter 6

Conclusions

In this dissertation, a received signal strength difference (RSSD) based source localization technique was proposed for the case when the transmit power is unknown and there is uncertainty in the sensor locations. Two methods were considered for the proposed problem. First, the constrained weighted least squares (CWLS) method was used to estimate the initial source location, which is considered as an initial point for the Newton method. This initial source estimation technique was also compared with other popular methods in terms of the accuracy of the final estimate. The improvement using the maximum likelihood (ML) technique compared to the CWLS approach is minimal, but the ML complexity is much higher. Further, the CWLS method provides a significant improvement over other RSSD-based methods. The effect of sensor uncertainty was illustrated for different path loss exponents, sensor position error variances, and number of sensors for both the near field and far field cases. Results were presented which show a significant degradation in the CRLB due to sensor uncertainty. Therefore this uncertainly should be considered when employing localization techniques.

Next, a linear estimator was developed for sufficient SNR which employs minimax optimization to solve the corresponding MSE optimization problem. Semidefinite relaxation was applied to the resulting nonlinear and nonconvex optimization problem to convert it into a convex optimization problem. The unknown source location estimate was then obtained as an optimal solution of the corresponding semidefinite programming problem which can be solved efficiently. Performance results were presented which confirm the effectiveness of the proposed method for sufficiently large signal to noise ratios (SNRs).

Finally, The extended total least squares (ETLS) method was developed in order

to obtain an optimization cost function which considers errors in both the observation matrix and data vector. Semidefinite relaxation (SDR) was used to obtain a convex cost function in a form which can be used with semidefinite programming (SDP). The proposed ETLS-SDP method was extended to the case with unknown path loss exponent so that the exponent and source location are jointly estimated. The mean squared error (MSE) was analysed and compared with the corresponding CRLB. The ETLS-SDP method was also compared with several well-known methods in terms of the estimation accuracy and complexity. Simulation results were presented which show a significant improvement in the location estimate over conventional least squares methods which do not consider errors in the observation matrix. Further, the proposed ETLS-SDP method was shown to achieve the CRLB at sufficient signal to noise ratios.

Chapter 7

Future Work

The problem of blind RSSD based source localization can be formulated as a non-SDP or an SDP-based optimization problem. In this dissertation, the non-SDP model based on the CWLS framework was considered first and the location estimate obtained by developing a new method denoted as LSIE-NM. Then, a minimax SDP based approach was derived to improve the performance with the corresponding CRLB as a benchmark. In addition, the effect of the sensor uncertainty on the location estimate and the proposed CRLB was evaluated.

Although the proposed methods have advantages over conventional blind energy based techniques, there are still improvements that can be considered as well as extensions that can be done for both non-cooperative and cooperative source localization. These include improved estimation accuracy, computational complexity, robustness for a sufficiently large SNR as well as the extension to unknown path loss exponent and cooperative source localization cases. Towards this end, four main research directions are planned for future work as outlined below.

7.1 ETLS with Sensor Position Uncertainty

The mean squared error of the proposed ETLS method will be obtained and the corresponding Cramér-Rao lower bound (CRLB) derived as a performance benchmark. Due to the accuracy of *a priori* sensor position information, the source location estimate obtained can vary significantly regardless of the localization method used. In fact, to the best of our knowledge, in the literature the sensor positions are assumed to be known exactly, which is not reasonable in practice. Therefore, sensor position

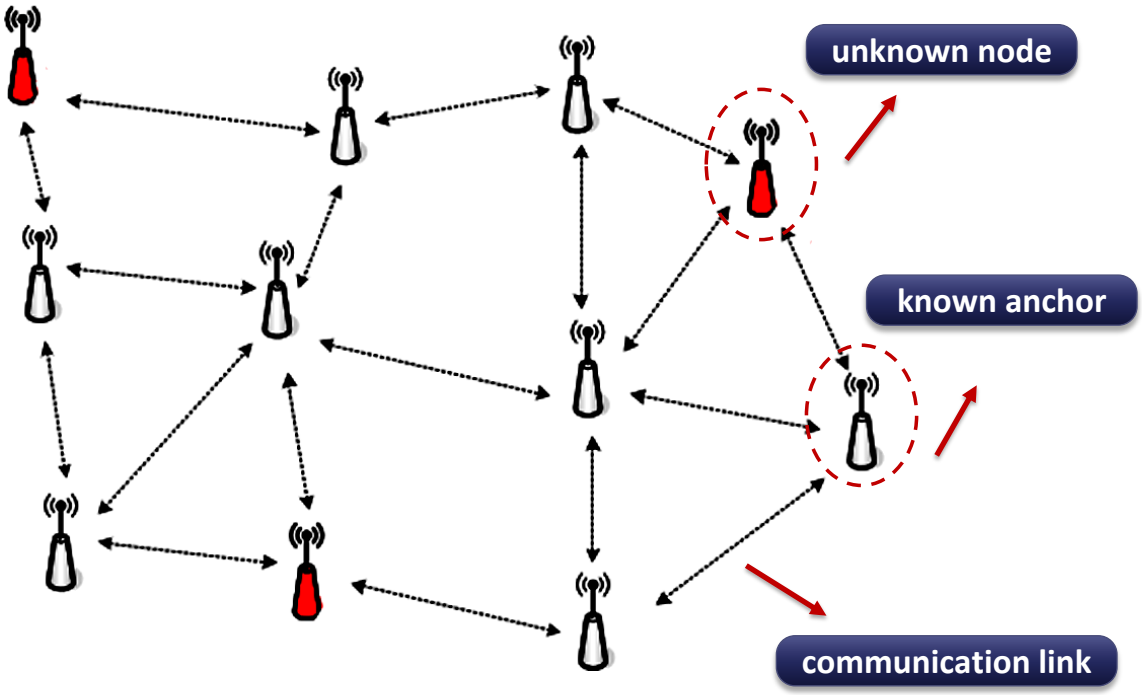

Figure 7.1: Cooperative source localization scenario in wireless network of sensors.

uncertainty should be considered when developing practical location estimation techniques. Thus, the proposed ETLS-SDP method will be extended in the presence of sensor position uncertainty.

7.2 Regularized and Recursive ETLS Methods

The proposed ETLS method solved the RSSD-based localization problem via minimizing the Frobenius norm of the system parameter errors. However, noise perturbation may cause numerical ill conditioning. Therefore, a regularized technique should be considered for robust estimation. Hence, a regularized version of the proposed ETLS method will be developed to reduce the estimation error. Perturbation analysis of the regularized ETLS method should be performed to show the statistical characteristics of the solution. In addition, the proposed ETLS method which is solved based on the SDP problem can be solved recursively to obtain a new recursive computationally efficient method.

7.3 Extension to the Kernel Recursive Total Least Square

The proposed Minimax-SDP method considered an MSE estimator with a known PLE. In future, this will be extended to the case of an unknown PLE with a random observation matrix instead of a deterministic matrix. In addition, a nonlinear version of the total recursive least squares algorithm can be developed which performs linear regression in a high-dimensional feature space induced by a new kernel. This can be used to recursively construct minimum mean squared error solutions to nonlinear least squares problems that are frequently encountered in signal processing applications.

7.4 ETLS Method in a Cooperative Environment

Sensor localization is generally divided into two cases: non-cooperative and cooperative. In a non-cooperative scenario, the source can communicate only with the sensors (anchor nodes). Every source needs to communicate with several sensors which requires a high density of sensors. Thus, the lack of accessible sensors as well as limited connectivity lead to the emergence of cooperative localization in which sources are able to communicate with both sensors and other sources. Since the sensors and other sources can receive the signal energy from the corresponding source, cooperative localization can result in improved estimation. Figure 7.1 presents a typical cooperative source localization scenario in a wireless sensor network. Hence, the proposed non-cooperative RSSD based model will be formulated for the cooperative case and the ETLS-SDP method will be extended to the cooperative case to improve the location estimation. The MSE of the cooperative ETLS-SDP will also be obtained and the CRLB will be calculated as benchmarks for comparison purposes.

Chapter 8

Appendices

8.1 Appendix A

The second order error term is obtained by substituting $\tilde{\mathbf{u}}_i = \Delta\mathbf{u}_i + \mathbf{u}_i$ into (4.8) which gives

$$\delta'_i = (\Delta\mathbf{u}_i - \Delta\mathbf{u}_1)^T(\Delta\mathbf{u}_1 - \Delta\mathbf{u}_i),\ i = 2, \ldots, N \tag{8.1}$$

Let $\boldsymbol{\delta}' = [\delta'_2, \delta'_3, \ldots, \delta'_N]^T$. Considering

$$\begin{aligned} E\{(\Delta x_i - \Delta x_1)^4\} &= 3\sigma^4_{(\Delta x_i - \Delta x_1)} = 3(\sigma^2_{\Delta x_i} + \sigma^2_{\Delta x_1})^2, \\ E\{(\Delta y_i - \Delta y_1)^4\} &= 3\sigma^4_{(\Delta y_i - \Delta y_1)} = 3(\sigma^2_{\Delta y_i} + \sigma^2_{\Delta y_1})^2, \end{aligned} \tag{8.2}$$

and

$$\begin{aligned} &E\{(\Delta x_i - \Delta x_1)^2(\Delta y_i - \Delta y_1)^2\} = \\ &\sigma^2_{(\Delta x_i - \Delta x_1)}\sigma^2_{(\Delta y_i - \Delta y_1)} = (\sigma^2_{\Delta x_i} + \sigma^2_{\Delta x_1})(\sigma^2_{\Delta y_i} + \sigma^2_{\Delta y_1}), \end{aligned} \tag{8.3}$$

the covariance matrix of $\boldsymbol{\delta}'$ can be written as

$$\boldsymbol{\Sigma} = cov(\boldsymbol{\delta}') = E\left[\boldsymbol{\delta}'\boldsymbol{\delta}'^T\right], \tag{8.4}$$

where Σ_{ij}, $i, j = 2, \ldots, N$, is given as

$$\Sigma_{ij} = \begin{cases} \frac{1}{2}\left\{5\left(\sigma^4_{(\Delta x_i - \Delta x_1)} + \sigma^4_{(\Delta y_i - \Delta y_1)}\right) + \left(\sigma^2_{(\Delta x_i - \Delta x_1)} + \sigma^2_{(\Delta y_i - \Delta y_1)}\right)^2\right\} & i = j \\ \left\{\left(\sigma^2_{(\Delta x_i - \Delta x_1)} + \sigma^2_{(\Delta y_i - \Delta y_1)}\right)\left(\sigma^2_{(\Delta x_j - \Delta x_1)} + \sigma^2_{(\Delta y_j - \Delta y_1)}\right)\right\} & i \neq j \end{cases} \tag{8.5}$$

Therefore, the weighting matrix given by (4.18) with the second order error term can be written using (4.14) and (8.5) as

$$\widehat{\mathbf{\Phi}}^{-1} = (\mathbf{\Sigma} + \mathbf{C}\mathbf{Q}_{\mathbf{\Delta u}}\mathbf{C}^T)^{-1} = (\mathbf{\Sigma} + \mathbf{\Phi})^{-1}, \tag{8.6}$$

which results in an initial estimate of the source location different than that given by (4.23). The difference between $\widehat{\mathbf{\Phi}}^{-1}$ and $\mathbf{\Phi}^{-1}$ using (8.6) can be obtained [67] as

$$\left|\widehat{\mathbf{\Phi}}^{-1} - \mathbf{\Phi}^{-1}\right| = \frac{1}{1 + tr\left\{\mathbf{\Sigma}\mathbf{\Phi}^{-1}\right\}}\mathbf{\Phi}^{-1}\mathbf{\Sigma}\mathbf{\Phi}^{-1} \tag{8.7}$$

where $tr\{\}$ denotes the trace of the matrix. Equation (8.9) shows that small sensor location error variances give $\left|\widehat{\mathbf{\Phi}}^{-1} - \mathbf{\Phi}^{-1}\right| \approx 0$, so that $\widehat{\mathbf{\Phi}}^{-1} \approx \mathbf{\Phi}^{-1}$. Defining $\mathbf{\Upsilon} = \widehat{\mathbf{\Phi}}^{-1} + \widehat{\mathbf{\Phi}}^{-T}$, (4.29) can be evaluated with the second order error term to obtain the new weighting matrix from (8.6) as

$$\widetilde{\mathbf{s}}_k = \widetilde{\mathbf{s}}_{k-1} - \left\{\left(\alpha^T\Upsilon\mathbf{A}_3 + 2\mu\Upsilon\mu^T\right)^{-1}\mu\Upsilon\alpha\right\} \tag{8.8}$$

where

$$\Upsilon_{ij} = \begin{cases} 2\widehat{\Phi}_{ii} & i = j \\ \widehat{\Phi}_{ij} + \widehat{\Phi}_{ji} & i \neq j \end{cases}.$$

8.2 Appendix B

The Hessian matrix $\mathbf{H}_k$ can be modified using a technique such as the Gaussian elimination method to reduce the likelihood of a singular matrix. With this approach, a positive definite matrix $\hat{\mathbf{H}}_k$ is obtain as

$$\hat{\mathbf{H}}_{k-1} = \mathbf{L}^{-1}\hat{\mathbf{D}}\mathbf{L}^{-T}, \tag{8.9}$$

where $\mathbf{L}$ and $\hat{\mathbf{D}}$ are given by

$$\mathbf{L} = \begin{bmatrix} l_{11} & 0 \\ l_{21} & l_{22} \end{bmatrix},$$

and

$$\hat{\mathbf{D}} = diag\{\hat{d}_{11}, \hat{d}_{22}\}.$$

The elements of $\hat{\mathbf{D}}$ and $\mathbf{L}$ are obtained using Algorithm 2.

Algorithm 3 Hessian Matrix Modification

Input $\mathbf{H}_{k-1}$ for the kth modification iteration
Initialize $\mathbf{L}_{2\times2} = \mathbf{0}_{2\times2}$, $\hat{\mathbf{D}}_{2\times2} = \mathbf{0}_{2\times2}$
if $h_{11} > 0$ **then**
  $temp = h_{11}$
else
  $h_{11} = temp = 1$
end if
Set $l_{21} = -h_{21}/h_{11}$, $h_{21} = 0$
Set $h_{22} = h_{22} + l_{21}h_{12}$
if $h_{22} < 0$ **then**
  $h_{22} = temp$
end if
for $1 \leq i \leq 2$ **do**
  $l_{ii} = 1$, $\hat{d}_{ii} = h_{ii}$
end for

In Algorithm 2, $\mathbf{H}_{k-1}$ is first transformed into an upper triangular matrix. If the diagonal elements of the resulting matrix are positive, these are assigned to the diagonal elements of $\hat{\mathbf{D}}$, otherwise 1 is assigned. Thus, if both h_{11} and h_{22} after the transformation are negative, $\hat{\mathbf{D}}$ will be an identity matrix, $\mathbf{I}_{2\times2}$. Then from (8.9), the

modified Hessian matrix $\hat{\mathbf{H}}_{k-1}$ is

$$\hat{\mathbf{H}}_{k-1} = \mathbf{L}^{-1}\mathbf{L}^{-T} = \begin{bmatrix} 1 & \frac{h_2}{h_1} \\ \frac{h_2}{h_1} & 1 + \left(\frac{h_2}{h_1}\right)^2 \end{bmatrix}. \tag{8.10}$$

8.3 Appendix C

The FIM $\tilde{F}$ is a $2N \times 2N$ square matrix that consists of three submatrices $\tilde{F}_{\mathbf{uu}}$, $\tilde{F}_{\mathbf{uu_s}}$ and $\tilde{F}_{\mathbf{u_s u_s}}$ where $\tilde{F}_{\mathbf{uu_s}} = (\tilde{F}_{\mathbf{u_s u}})^T$. From (3.16)-(3.18), these submatrices can be obtained by taking the partial derivatives

$$\frac{\partial \Delta \mathbf{P}}{\partial \mathbf{u}} = [D_{12}, D_{13}, \ldots, D_{1N}]^T, \tag{8.11}$$

and

$$\frac{\partial \Delta \mathbf{P}}{\partial \mathbf{u_s}} = [C_{12}, C_{13}, \ldots, C_{1N}]^T, \tag{8.12}$$

where

$$D_{1i} = \left[\frac{\partial P_{1i}}{\partial x}, \frac{\partial P_{1i}}{\partial y}\right], \quad i = 2, 3, \ldots, N \tag{8.13}$$

and

$$C_{1i} = \left[\frac{\partial P_{1i}}{\partial x_1}, \frac{\partial P_{1i}}{\partial y_1}, \ldots, \frac{\partial P_{1i}}{\partial x_N}, \frac{\partial P_{1i}}{\partial y_N}\right]. \tag{8.14}$$

The elements of (8.13) and (8.14) are given by

$$\frac{\partial P_{1i}}{\partial x} = \eta \left(\frac{x(d_i - d_1) + x_i d_1 - x_1 d_i}{d_1 d_i}\right),$$

$$\frac{\partial P_{1i}}{\partial y} = \eta \left(\frac{y(d_i - d_1) + y_i d_1 - y_1 d_i}{d_1 d_i}\right),$$

and

$$\begin{bmatrix} \frac{\partial P_{1i}}{\partial x_j} & \frac{\partial P_{1i}}{\partial y_j} \end{bmatrix} = \begin{cases} M_{1i} = \eta \begin{bmatrix} \frac{x_i - x}{d_i} & \frac{y_i - y}{d_i} \end{bmatrix} & i = j \\ \mathbf{0} & i \neq j \end{cases},$$

where $\mathbf{0}$ denotes a (1×2) zero matrix. The second and third submatrices $\tilde{F}_{\mathbf{uu_s}}$ and $\tilde{F}_{\mathbf{u_s u_s}}$ can then be obtained using

$$\left(\frac{\partial \Delta \mathbf{P}}{\partial \mathbf{u}}\right)^T Q_v^{-1} \left(\frac{\partial \Delta \mathbf{P}}{\partial \mathbf{u_s}}\right) = [H_{12}, H_{13}, \ldots, H_{1N}], \tag{8.15}$$

and

$$\left(\frac{\partial \Delta \mathbf{P}}{\partial \mathbf{u_s}}\right)^T Q_v^{-1} \left(\frac{\partial \Delta \mathbf{P}}{\partial \mathbf{u_s}}\right) = diag\,(F_{12}, F_{13}, \ldots, F_{1N}) \tag{8.16}$$

where

$$H_{1i} = \frac{1}{(\sigma_1^2 + \sigma_i^2)} D_{1i}^T M_{1i},$$

and

$$F_{1i} = \frac{1}{(\sigma_1^2 + \sigma_i^2)} \begin{bmatrix} \frac{\partial^2 P_{1i}}{\partial x} & \frac{\partial P_{1i}}{\partial x \partial y} \\ \frac{\partial P_{1i}}{\partial y \partial x} & \frac{\partial^2 P_{1i}}{\partial y} \end{bmatrix}.$$

8.4 Appendix D

In this appendix, it is shown that $\mathbf{Tr}\left\{\mathbf{\Phi}_0\tilde{\boldsymbol{\theta}}\tilde{\boldsymbol{\theta}}^T\mathbf{\Phi}_0^T\right\} = \tilde{\boldsymbol{\theta}}\widehat{\mathbf{\Phi}}_0\tilde{\boldsymbol{\theta}}^T$. Considering $\mathbf{\Phi}_0$ and $\tilde{\boldsymbol{\theta}}$ defined in 5.16, one can obtain

$$\left[\mathbf{\Phi}_0\tilde{\boldsymbol{\theta}}\right]_{j1} = \sum_{i=1}^{4}\tilde{\boldsymbol{\theta}}_i(\mathbf{\Phi}_0)_{ji}, \tag{8.17}$$

and

$$\left[\tilde{\boldsymbol{\theta}}^T\mathbf{\Phi}_0^T\right]_{1k} = \sum_{i=1}^{4}\left(\mathbf{\Phi}_0^T\right)_{ik}\tilde{\boldsymbol{\theta}}_i^T, \tag{8.18}$$

where $1 \leq j \leq N-1$ and $1 \leq k \leq N-1$. Define

$$\mathbf{\Gamma} = \mathbf{Tr}\left\{\mathbf{\Phi}_0\tilde{\boldsymbol{\theta}}\tilde{\boldsymbol{\theta}}^T\mathbf{\Phi}_0^T\right\}, \tag{8.19}$$

and substitute (8.17) and (8.18) into (8.19) to obtain

$$\begin{aligned}\mathbf{\Gamma} &= \mathbf{Tr}\left\{\left[\mathbf{\Phi}_0\tilde{\boldsymbol{\theta}}\right]_{j1}\left[\tilde{\boldsymbol{\theta}}^T\mathbf{\Phi}_0^T\right]_{1k}\right\} \\ &= \left\{\sum_{i=1}^{4}\tilde{\boldsymbol{\theta}}_i(\mathbf{\Phi}_0)_{ji}\sum_{i=1}^{4}\left(\mathbf{\Phi}_0^T\right)_{ik}\tilde{\boldsymbol{\theta}}_i^T\right\}_{k=j}.\end{aligned} \tag{8.20}$$

Simplifying (8.20) yields

$$\begin{aligned}\mathbf{\Gamma} &= \sum_{n=1}^{N}\left\{\sum_{i=1}^{4}\tilde{\boldsymbol{\theta}}_i(\mathbf{\Phi}_0)_{ni}\sum_{i=1}^{4}\left(\mathbf{\Phi}_0^T\right)_{in}\tilde{\boldsymbol{\theta}}_i^T\right\} \\ &= \sum_{i=1}^{4}\tilde{\boldsymbol{\theta}}_i\left\{\sum_{n=1}^{N}\left(\mathbf{\Phi}_0^T\right)_{in}(\mathbf{\Phi}_0)_{ni}\right\}\tilde{\boldsymbol{\theta}}_i^T \\ &= \sum_{j=1}^{4}\tilde{\boldsymbol{\theta}}_j^T\left\{\sum_{i=1}^{4}\tilde{\boldsymbol{\theta}}_i\sum_{n=1}^{N}\left(\mathbf{\Phi}_0^T\right)_{in}(\mathbf{\Phi}_0)_{ni}\right\} \\ &= \tilde{\boldsymbol{\theta}}^T\left\{\sum_{i=1}^{4}\sum_{n=1}^{N}\left(\mathbf{\Phi}_0^T\right)_{in}(\mathbf{\Phi}_0)_{ni}\right\}\tilde{\boldsymbol{\theta}}\end{aligned} \tag{8.21}$$

Now, defining $\widehat{\mathbf{\Phi}}_0 = \mathbf{\Phi}_0^T \mathbf{\Phi}_0$ and considering

$$\mathbf{\Phi}_0^T \mathbf{\Phi}_0 = \sum_{i=1}^{4} \sum_{n=1}^{N} \left(\mathbf{\Phi}_0^T\right)_{in} (\mathbf{\Phi}_0)_{ni}, \tag{8.22}$$

the result in (8.21) can be obtained as

$$\begin{aligned} \mathbf{Tr}\left\{\mathbf{\Phi}_0 \tilde{\boldsymbol{\theta}} \tilde{\boldsymbol{\theta}}^T \mathbf{\Phi}_0^T\right\} &= \tilde{\boldsymbol{\theta}}^T \left\{\mathbf{\Phi}_0^T \mathbf{\Phi}_0\right\} \tilde{\boldsymbol{\theta}} \\ &= \tilde{\boldsymbol{\theta}} \widehat{\mathbf{\Phi}}_0 \tilde{\boldsymbol{\theta}}. \end{aligned} \tag{8.23}$$

8.5 Appendix E

In this appendix, it is shown that $\sum_{i=1}^{4} \tilde{\boldsymbol{\theta}}_i^2 - \tilde{\boldsymbol{\theta}}^T \widehat{\boldsymbol{\Upsilon}} \tilde{\boldsymbol{\theta}} \neq 0$ and $\mathbf{Tr}\left\{(\mathbf{I} - \widehat{\boldsymbol{\Upsilon}})\mathbf{Q}\right\} \neq 0$. First let $\Omega = \sum_{i=1}^{4} \tilde{\boldsymbol{\theta}}_i^2 - \tilde{\boldsymbol{\theta}}^T \widehat{\boldsymbol{\Upsilon}} \tilde{\boldsymbol{\theta}}$, which is the difference of $\sum_{i=1}^{4} \tilde{\boldsymbol{\theta}}_i^2$ and $\tilde{\boldsymbol{\theta}}^T \widehat{\boldsymbol{\Upsilon}} \tilde{\boldsymbol{\theta}}$. Hence, $\Omega \neq 0$ implies that

$$\sum_{i=1}^{4} \tilde{\boldsymbol{\theta}}_i^2 \neq \tilde{\boldsymbol{\theta}}^T \widehat{\boldsymbol{\Upsilon}} \tilde{\boldsymbol{\theta}}. \tag{8.24}$$

Using $\sum_{i=1}^{4} \tilde{\boldsymbol{\theta}}_i^2 = \tilde{\boldsymbol{\theta}}^T \mathbf{I}_{4\times 4} \tilde{\boldsymbol{\theta}}$, (8.24) can be rewritten as

$$\tilde{\boldsymbol{\theta}}^T \mathbf{I} \tilde{\boldsymbol{\theta}} \neq \tilde{\boldsymbol{\theta}}^T \widehat{\boldsymbol{\Upsilon}} \tilde{\boldsymbol{\theta}} \;\Rightarrow\; \widehat{\boldsymbol{\Upsilon}} \neq \mathbf{I}_{4\times 4}. \tag{8.25}$$

Therefore, in order to prove that $\Omega \neq 0$, it is sufficient to show that $\widehat{\boldsymbol{\Upsilon}} \neq \mathbf{I}_{4\times 4}$. Since $\boldsymbol{\Upsilon} = \begin{bmatrix} -y_1 & x_1 & R_1^2 & 1 \end{bmatrix}^T$, the symmetric matrix $\widehat{\boldsymbol{\Upsilon}} \in \Re^{4\times 4}$ given by $\widehat{\boldsymbol{\Upsilon}} = \boldsymbol{\Upsilon}\left(\boldsymbol{\Upsilon}^T\boldsymbol{\Upsilon}\right)^{-1}\boldsymbol{\Upsilon}^T$ can be expressed as

$$\widehat{\boldsymbol{\Upsilon}} = \begin{bmatrix} y_1^2 & -x_1y_1 & -y_1R_1^2 & -y_1 \\ -x_1y_1 & x_1^2 & x_1R_1^2 & x_1 \\ x_1^2 & x_1R_1^2 & R_1^4 & R_1^2 \\ -y_1 & x_1 & R_1^2 & 1 \end{bmatrix}. \tag{8.26}$$

Note that the term $\left(\boldsymbol{\Upsilon}^T\boldsymbol{\Upsilon}\right) \neq 0$ in $\widehat{\boldsymbol{\Upsilon}} = \boldsymbol{\Upsilon}\left(\boldsymbol{\Upsilon}^T\boldsymbol{\Upsilon}\right)^{-1}\boldsymbol{\Upsilon}^T$ since $\boldsymbol{\Upsilon}^T\boldsymbol{\Upsilon} = R_1^4 + R_1^2 + 1 > 0$.

To prove that $\widehat{\boldsymbol{\Upsilon}} \neq \mathbf{I}_{4\times 4}$, one can normalize the diagonal elements of $\widehat{\boldsymbol{\Upsilon}}$ in (8.26) to 1 which yields that $x_1 = \pm 1$, $y_1 = \pm 1$ and $R_1^4 = R_1^2 = 1$. In this case, x_1, y_1 and R_1^2 are non zero, so the off diagonal elements cannot be zero. Therefore, $\widehat{\boldsymbol{\Upsilon}} \neq \mathbf{I}$ which implies $\Omega \neq 0$, and the first result is proven.

For the second case, define $\mathrm{Z} = \mathbf{Tr}\left\{(\mathbf{I} - \widehat{\boldsymbol{\Upsilon}})\mathbf{Q}\right\}$, which can be expressed as

$$\mathrm{Z} = \mathbf{Tr}\left\{\left(\mathbf{I} - \widehat{\boldsymbol{\Upsilon}}\right)\left(\tilde{\boldsymbol{\theta}}\tilde{\boldsymbol{\theta}}^{\mathrm{T}}\right)\right\} = \tilde{\boldsymbol{\theta}}^{\mathrm{T}}\left(\mathbf{I} - \widehat{\boldsymbol{\Upsilon}}\right)\tilde{\boldsymbol{\theta}}. \tag{8.27}$$

Simplifying (8.27) gives

$$\mathrm{Z} = \tilde{\boldsymbol{\theta}}^T\boldsymbol{\theta} - \tilde{\boldsymbol{\theta}}^T\widehat{\boldsymbol{\Upsilon}}\tilde{\boldsymbol{\theta}} = \sum_{i=1}^{4} \tilde{\boldsymbol{\theta}}_i^2 - \tilde{\boldsymbol{\theta}}^T\widehat{\boldsymbol{\Upsilon}}\tilde{\boldsymbol{\theta}} = \Omega, \tag{8.28}$$

and from the previous result $\Omega \neq 0$, so that $Z \neq 0$, which proves that $\mathbf{Tr}\left\{(\mathbf{I} - \widehat{\boldsymbol{\Upsilon}})\mathbf{Q}\right\} \neq 0$.

8.6 Appendix F

$\boldsymbol{\Delta\theta}_{ETLS}$ in (5.50) is derived in this appendix. Using (5.33), the cost function $\boldsymbol{\Psi}(\tilde{\boldsymbol{\theta}})$ can be rewritten as

$$\boldsymbol{\Psi}(\tilde{\boldsymbol{\theta}}) = \tilde{\boldsymbol{\theta}}^T {\boldsymbol{\Phi}_0}^T \Big(\tilde{\boldsymbol{\theta}}^T \left(\mathbf{I} - \widehat{\boldsymbol{\Upsilon}}\right) \tilde{\boldsymbol{\theta}}\Big)^{-1} \boldsymbol{\Phi}_0 \tilde{\boldsymbol{\theta}}. \tag{8.29}$$

The gradient of (8.29) can be found by taking the partial derivative

$$\begin{aligned} \frac{\partial \boldsymbol{\Psi}(\tilde{\boldsymbol{\theta}})}{\partial \boldsymbol{\theta}} = 2 \frac{\partial \left(\tilde{\boldsymbol{\theta}}^T \boldsymbol{\Phi}_0^T\right)}{\partial \boldsymbol{\theta}} \Big(\tilde{\boldsymbol{\theta}}^T \left(\mathbf{I} - \widehat{\boldsymbol{\Upsilon}}\right) \tilde{\boldsymbol{\theta}}\Big)^{-1} \boldsymbol{\Phi}_0 \tilde{\boldsymbol{\theta}} + \Big(\boldsymbol{\Phi}_0 \tilde{\boldsymbol{\theta}}\Big)^T \\ \times \frac{\partial \left\{ \Big(\tilde{\boldsymbol{\theta}}^T \left(\mathbf{I} - \widehat{\boldsymbol{\Upsilon}}\right) \tilde{\boldsymbol{\theta}}\Big)^{-1} \right\}}{\partial \boldsymbol{\theta}} \boldsymbol{\Phi}_0 \tilde{\boldsymbol{\theta}}. \end{aligned} \tag{8.30}$$

Considering the RHS of (8.30), there are two partial derivatives that must be calculated. The first is

$$\frac{\partial \left(\tilde{\boldsymbol{\theta}}^T \boldsymbol{\Phi}_0^T\right)}{\partial \boldsymbol{\theta}} = \left\{ \frac{\partial \left(\boldsymbol{\Phi}_0 \tilde{\boldsymbol{\theta}}\right)}{\partial \boldsymbol{\theta}} \right\}^T = \left\{ \frac{\partial}{\partial \boldsymbol{\theta}} \left(\mathbf{A}_0 \boldsymbol{\theta} - \mathbf{b}_0\right) \right\}^T = \mathbf{A}_0^T, \tag{8.31}$$

and the second is the derivative of a matrix inverse

$$\begin{aligned} \frac{\partial \boldsymbol{\Psi}(\tilde{\boldsymbol{\theta}})}{\partial \boldsymbol{\theta}} &= 2 \Big\{ \mathbf{A}_0^T \mathbf{G}^{-1} - \mathbf{G}^{-1} \Big(\tilde{\boldsymbol{\theta}}^T \left(\mathbf{I} - \widehat{\boldsymbol{\Upsilon}}\right) \mathbf{V}\Big)^T \\ &\quad \times \mathbf{G}^{-1} \Big(\boldsymbol{\Phi}_0 \tilde{\boldsymbol{\theta}}\Big)^T \Big\} \left(\mathbf{A}_0 \boldsymbol{\theta} - \mathbf{b}_0\right) \\ &= 2 \mathbf{A}_0^T \mathbf{G}^{-1} \boldsymbol{\Phi}_0 \tilde{\boldsymbol{\theta}} - 2 \mathbf{G}^{-1} \mathbf{V}^T \Big(\mathbf{I} - \widehat{\boldsymbol{\Upsilon}}\Big) \tilde{\boldsymbol{\theta}} \mathbf{G}^{-1} \tilde{\boldsymbol{\theta}}^T \widehat{\boldsymbol{\Phi}}_0 \tilde{\boldsymbol{\theta}}, \end{aligned} \tag{8.32}$$

where $\mathbf{G} = \tilde{\boldsymbol{\theta}}^T \left(\mathbf{I} - \widehat{\boldsymbol{\Upsilon}}\right) \tilde{\boldsymbol{\theta}}$ and v_{ij} denotes the ijth component of $\mathbf{V}$ given by

$$v_{ij} = \begin{cases} 1 & i = j \\ 0 & i \neq j \end{cases}.$$

Substituting (8.31) and (8.32) in (8.30) and setting this to zero yields

$$\Big\{ \mathbf{A}_0^T \mathbf{G}^{-1} + \mathbf{G}^{-1} \mathbf{V}^T \left(\mathbf{I} - \widehat{\boldsymbol{\Upsilon}}\right) \tilde{\boldsymbol{\theta}} \mathbf{G}^{-1} \tilde{\boldsymbol{\theta}}^T \boldsymbol{\Delta} \boldsymbol{\Phi}^T \Big\} \boldsymbol{\Phi}_o \tilde{\boldsymbol{\theta}} = 0. \tag{8.33}$$

Substituting $\boldsymbol{\theta} = \boldsymbol{\theta}_0 + \boldsymbol{\Delta\theta}_{ETLS}$ in (8.33) and ignoring the higher order error terms gives

$$\mathbf{A}_0^T\mathbf{G}^{-1}\boldsymbol{\Delta\Phi}\tilde{\boldsymbol{\theta}}_0 - \mathbf{A}_0^T\mathbf{G}^{-1}\mathbf{A}_0\boldsymbol{\Delta\theta}_{ETLS} \approx 0, \tag{8.34}$$

where $\boldsymbol{\Phi}_0\tilde{\boldsymbol{\theta}}$ in (8.30) is simplified to

$$\boldsymbol{\Phi}_0\tilde{\boldsymbol{\theta}} = \mathbf{A}_0\boldsymbol{\theta} - \mathbf{b}_0 = \mathbf{A}_0\boldsymbol{\Delta\theta}_{ETLS} - \boldsymbol{\Delta\Phi}\tilde{\boldsymbol{\theta}}_0.$$

Then, $\boldsymbol{\Delta\theta}_{ETLS}$ is obtained in closed form using (8.34) as given in (5.50).

8.7 Appendix G

The effect of ignoring the second order error terms on the estimation bias $E\{\boldsymbol{\Delta\theta}_{ETLS}\}$ is calculated in this appendix. Considering the second order error terms in (5.49), one obtains

$$\begin{aligned}\frac{\partial\boldsymbol{\Psi}(\tilde{\boldsymbol{\theta}})}{\partial\boldsymbol{\theta}} &= \mathbf{A}_0^T\mathbf{G}^{-1}\mathbf{A}_0\boldsymbol{\Delta\theta}_{ETLS} + \mathbf{G}^{-1}\mathbf{V}^T\left(\mathbf{I}-\widehat{\boldsymbol{\Upsilon}}\right)\tilde{\boldsymbol{\theta}}\mathbf{G}^{-1}\tilde{\boldsymbol{\theta}}^T \\ &\quad\times\boldsymbol{\Delta\Phi}^T\boldsymbol{\Phi}_0\tilde{\boldsymbol{\theta}} - \mathbf{A}_0^T\mathbf{G}^{-1}\boldsymbol{\Delta\Phi}\tilde{\boldsymbol{\theta}}_0.\end{aligned} \tag{8.35}$$

Substituting $\boldsymbol{\theta} = \boldsymbol{\theta}_0 + \boldsymbol{\Delta\theta}_{ETLS}$ in (8.35) gives

$$\begin{aligned}\frac{\partial\boldsymbol{\Psi}(\tilde{\boldsymbol{\theta}})}{\partial\boldsymbol{\theta}} &= \mathbf{A}_0^T\mathbf{G}^{-1}\mathbf{A}_0\boldsymbol{\Delta\theta}_{ETLS} - \mathbf{G}^{-2}\mathbf{V}^T\left(\mathbf{I}-\widehat{\boldsymbol{\Upsilon}}\right) \\ &\quad\times\tilde{\boldsymbol{\theta}}_0\tilde{\boldsymbol{\theta}}_0^T\boldsymbol{\Delta\Phi}^T\boldsymbol{\Delta\Phi}\tilde{\boldsymbol{\theta}}_0 - \mathbf{A}_0^T\mathbf{G}^{-1}\boldsymbol{\Delta\Phi}\tilde{\boldsymbol{\theta}}_0 \\ &= \tilde{\mathbf{G}}\boldsymbol{\Delta\theta}_{ETLS} - \left(\mathbf{G}^{-2}\mathbf{V}^T\left(\mathbf{I}-\widehat{\boldsymbol{\Upsilon}}\right)\tilde{\boldsymbol{\theta}}_0\tilde{\boldsymbol{\theta}}_0^T\boldsymbol{\Delta\Phi}^T\right. \\ &\quad\left.+\,\mathbf{A}_0^T\mathbf{G}^{-1}\right)\boldsymbol{\Delta\Phi}\tilde{\boldsymbol{\theta}}_0.\end{aligned} \tag{8.36}$$

Therefore, $\boldsymbol{\Delta\theta}_{ETLS}$ can be obtained by setting $\frac{\partial\boldsymbol{\Psi}(\tilde{\boldsymbol{\theta}})}{\partial\boldsymbol{\theta}} = 0$ in (8.36) as

$$\begin{aligned}\boldsymbol{\Delta\theta}_{ETLS} &= \tilde{\mathbf{G}}^{-1}\left(\mathbf{A}_0^T\mathbf{G}^{-1}\boldsymbol{\Delta\Phi} + \mathbf{G}^{-2}\mathbf{V}^T\left(\mathbf{I}-\widehat{\boldsymbol{\Upsilon}}\right)\right. \\ &\quad\left.\times\,\tilde{\boldsymbol{\theta}}_0\tilde{\boldsymbol{\theta}}_0^T\boldsymbol{\Delta\Phi}^T\boldsymbol{\Delta\Phi}\right)\tilde{\boldsymbol{\theta}}_0.\end{aligned} \tag{8.37}$$

Taking the expectation of $\boldsymbol{\Delta\theta}_{ETLS}$ gives the bias of the estimate considering the second order error term as

$$\begin{aligned}E\{\boldsymbol{\Delta\theta}_{ETLS}\} &= \tilde{\mathbf{G}}^{-1}\left(\mathbf{A}_0^T\mathbf{G}^{-1}E\{\boldsymbol{\Delta\Phi}\} + \mathbf{G}^{-2}\mathbf{V}^T\left(\mathbf{I}-\widehat{\boldsymbol{\Upsilon}}\right)\right. \\ &\quad\left.\times\,\tilde{\boldsymbol{\theta}}_0\tilde{\boldsymbol{\theta}}_0^T E\left\{\boldsymbol{\Delta\Phi}^T\boldsymbol{\Delta\Phi}\right\}\right)\tilde{\boldsymbol{\theta}}_0 \\ &= \mathbf{G}^{-2}\mathbf{V}^T\left(\mathbf{I}-\widehat{\boldsymbol{\Upsilon}}\right)\tilde{\boldsymbol{\theta}}_0\tilde{\boldsymbol{\theta}}_0^T\tilde{\mathbf{R}}\tilde{\boldsymbol{\theta}}_0,\end{aligned} \tag{8.38}$$

where $\tilde{\mathbf{R}}$ denotes $E\left\{\boldsymbol{\Delta\Phi}^T\boldsymbol{\Delta\Phi}\right\}$.

Bibliography

[1] S. Gezici, "A survey on wireless position estimation," *Wireless Personal Commun.*, vol. 44, no. 3, pp. 263–282, Feb. 2008.

[2] I. F. Akyildiz, W. Su, Y. Sankarasubramaniam, and E. Cayirci, "A survey on sensor networks," *IEEE Commun. Mag.*, vol. 40, no. 8, pp. 102–114, Aug. 2002.

[3] Y. Zhao, "Standardization of mobile phone positioning for 3G systems," *IEEE Commun. Mag.*, vol. 40, no. 7, pp. 108–116, Jul. 2002.

[4] T. Rappaport, *Wireless Communications Principles and Practice.* Englewood Cliffs, NJ: Prentice-Hall, 1999.

[5] N. Patwari, J. N. Ash, S. Kyperountas, A. O. Hero, III, R. L. Moses and N. S. Correal, "Locating the nodes: Cooperative localization in wireless sensor networks," *IEEE Signal Process. Mag.*, vol. 22, no. 4, pp. 54–69, Jul. 2005.

[6] A. J. Weiss and J. S. Picard, "Network localization with biased range measurements," *IEEE Trans. Wireless Commun.*, vol. 7, no. 1, pp. 298-304, Jan. 2008.

[7] T. S. Rappaport, J. H. Reed, and B. D. Woerner, "Position location using wireless communications on highways of the future," *IEEE Commun. Mag.*, vol. 14, no. 10, pp. 33-41, Oct. 1996.

[8] K. Martinez, J. K. Hart, and R. Ong, "Environmental sensor networks," *IEEE Computer*, vol. 37, no. 8, pp. 50-56, Aug. 2004.

[9] Y. Qi, H. Kobayashi, and H. Suda, "Analysis of wireless geolocation in a non-line-of-sight environment," *IEEE Trans. Wireless Commun.*, vol. 5, no. 3, pp. 672-681, Mar. 2006.

[10] N. Bulusu, J. Heidemann, and D. Estrin, "GPS-less low cost outdoor localization for very small devices," *IEEE Personal Commun. Mag.*, vol. 7, no. 5, pp. 28–34, Oct. 2000.

[11] J. J. Caffery, Jr., *Wireless Location in CDMA Cellular Radio Systems.* Norwell, MA: Kluwer, 2000.

[12] F. Gustafsson and F. Gunnarsson, "Mobile positioning using wireless network," *IEEE Signal Process. Mag.*, vol. 22, no. 4, pp. 41–53, Jul. 2005.

[13] H. Whitehead, *Sperm Whales: Social Evolution in the Ocean*, The University of Chicago Press, Chicago, IL, 2003.

[14] K. Fristrup and G. Harbison, "How do sperm whales catch squids?," *Marine Mammal Sci.*, vol. 18, no. 1, pp. 42–54, Jan. 2002.

[15] A. Thode, J. Skinner, P. Scott, J. Roswell, J. Straley J, and K. Folkert, "Tracking sperm whale with a towed acoustic vector sensor," *J. Acoust. Soc. Am.*, vol. 128, no. 5, pp. 2681–2694, Nov. 2010.

[16] P. M. Baggenstoss, "Seperation of sperm whale click-trains for multipath rejection," *J. Acoust. Soc. Am.*, vol. 129, no. 6, pp. 3598–3609, Jun. 2011.

[17] H. Lohrasbipeydeh, T. Dakin, T. A. Gulliver, and A. Zielinski, "Characterization of sperm whale vocalization energy based on echolocation signals", in *Proc. IEEE Oceans Conf.*, San Diego, CA. USA, pp. 1–5, Sep. 2013.

[18] H. Lohrasbipeydeh, S. Mosayyebpour, and T. A. Gulliver, "Single hydrophone passive acoustic sperm whale range and depth estimation," in *Proc. IEEE Int. Conf. on Acoustics, Speech and Signal Process.*, Vancouver, BC, pp. 754–757, Nov. 2012.

[19] C. O. Tiemann, A. M. Thode, V. O'Connell, and K. Folkert, "Three-dimensional localization of sperm whales using a single hydrophone," *J. Acoust. Soc. Am.*, vol. 120, no. 4, pp. 2355–2365, Oct. 2006.

[20] S. Boyd and L. Vandenberghe, *Convex Optimization*, Cambridge, UK: Cambridge Univ. Press, 2004.

[21] L. A. Vandenberghe and S. B. Boyd, "Semidefinite programming," *SIAM Rev.*, vol. 38, no. 1, pp. 49-95, Mar. 1996.

[22] K. C. Toh, M. J. Todd, and R. H. Tutuncu, "SDPT3A MATLAB software package for semidefinite programming," *Optim. Methods Softw.*, vol. 11, pp. 545-581, 1999.

[23] J. F. Sturm, Using SeDuMi 1.02, a MATLAB Toolbox for Optimization Over Symmetric Cones, 1998.

[24] G. H. Golub and C. F. Van Loan, "An analysis of the total least squares problem," *SIAM J. Numer. Anal.*, vol. 17, no. 6, pp. 883–893, Dec. 1980

[25] T. J. Abatzoglou, J. M. Mendel, and G. A. Harada, "The constrained total least squares technique and its applications to harmonic super resolution," *IEEE Trans. Signal Process.*, vol. 39, no. 5, pp. 1070–1087, May 1991.

[26] I. Markovsky and S. V. Huffel, "Overview of total least-squares methods," *Signal Process.*, vol. 59, no. 8, pp. 4035–4040, Oct. 2007.

[27] M. A. Rahman and K.-B. Yu, "Total least square approach for frequency estimation using linear prediction," *IEEE Trans. Acoust., Speech, Signal Process.*, vol. 35, no. 10, pp. 1440-1454, Oct. 1987.

[28] S. Van Huffel and J. Vanderwalle, *The Total Least Squares Problem: Computational Aspects and Analysis. SIAM Frontiers in Applied Mathematics*, vol. 9, Philadelphia, PA: SIAM, 1991.

[29] X. Li and K. Pahlavan, "Super-resolution TOA estimation with diversity for indoor geolocation," *IEEE Trans. Wireless Commun.*, vol. 3, no. 1, pp. 224–234, Jan. 2004.

[30] I. Guvenc and C. C. Chong, "A survey on TOA based wireless localizzation and NLOS mitigation techniques," *IEEE Commun. Surveys Tutor.*, vol. 11, no. 3, pp. 107–124, Jan. 2009.

[31] C. Mensing and S. Plass, "Positioning algorithms for cellular networks using TDOA," in Proc. *IEEE Int. Conf. Acoust., Speech, Signal Process.*, Toulouse, France, May 2006, pp. 513–516.

[32] X. Li, "Collaborative localization with received-signal strength in wireless sensor networks," *IEEE Trans. Vehic. Tech.*, vol. 56, no. 6, pp. 3807–3817, Nov. 2007.

[33] H. C. So, W. K. Ma, and Y. T. Chan, "Least squares algorithms for time-of-arrival based mobile location," *IEEE Trans. Signal Process.*, vol. 52, no. 4, pp. 1121-1128, Apr. 2004.

[34] L. Yang and K. C. Ho, "An asymptotically efficient estimator for TDOA and FDOA positioning of multiple disjoint sources in the presence of sensor location uncertainties," *IEEE Trans. Signal Process.*, vol. 59, no. 7, pp. 3434-3440, Jul. 2011.

[35] A. Catovic and Z. Sahinoglu, "The Cramer-Rao bounds of hybrid TOA/RSS and TDOA/RSS location estimation schemes," *IEEE Commun. Lett.*, vol. 8, no. 10, pp. 626–628, Oct. 2004.

[36] H. Yu, G. Huang, J. Gao, and B. Liu, "An efficient constrained weighted least squares algorithm for moving source location using TDOA and FDOA measurements," *IEEE Commun. Lett.*, vol. 11, no. 1, pp 44–47, Jan. 2012.

[37] L. Yang and K. C. Ho, "An approximately efficient TDOA localization algorithm in closed-form for locating multiple disjoint sources with erroneous sensor positions," *IEEE Trans. Signal Process.*, vol. 57, no. 12, pp. 4598-4615, Dec. 2009.

[38] A. Kangas and T. Wigren, "Angle of arrival localization in LTE using MIMO pre-coder index feedback" *IEEE Commun. Lett.*, vol. 17, no. 8, pp. 1584–1587, Aug. 2013.

[39] L. Cong and W. Zhuang, "Hybrid TDOA/AOA mobile user location for wideband CDMA cellular systems," *IEEE Trans. Wireless Commun.*, vol. 1, no. 3, pp. 439-447, Jul. 2002.

[40] L. Taponecco, A. A. D'Amico, and U. Mengali, "Joint TOA and AOA estimation for UWB localization applications," *IEEE Trans. Wireless Commun.*, vol. 10, no. 7, pp. 2207–2217, Jul. 2011.

[41] M. C. Vanderveen, C. B. Papadias, and A. Paulraj, "Joint angle and delay estimation (JADE) for multipath signals arriving at an antenna array," *IEEE Commun. Lett.*, vol. 1, no. 1, pp. 12-14, Jun. 1997.

[42] W. D. Wang and Q. X. Zhu, "RSS-based Monte Carlo localisation for mobile sensor networks," *IET Commun.*, vol. 2, no. 5, pp. 673–681, May. 2008.

[43] N. Patwari et al., "Relative location estimation in wireless sensor networks," *IEEE Trans. Signal Process.*, vol. 51, no. 8, pp. 2137–2148, Aug. 2003.

[44] C. T. Huang, C. H. Wu, Y. N. Lee, and J. T. Chen, "A novel indoor RSS based position location algorithm using factor graphs," *IEEE Trans. Wireless Commun.*, vol. 8, no. 6, pp. 3050-3058, Jun. 2009.

[45] Y. Huang et al., "Real-time passive source localization: A practical linear-correction least-squares approach," *IEEE Trans. Speech Audio Process.*, vol 9, no. 8, pp. 943–956, Nov. 2001.

[46] S. D. Chitte, S. Dasgupta, and Z. Ding, "Distance estimation from received signal strength under log-normal shadowing: Bias and variance," *IEEE Signal Process. Lett.*, vol. 16, no. 3, pp. 216–218, Mar. 2009.

[47] A. Coluccia and F. Ricciato, "On ML estimation for automatic RSS based indoor localization," in *Proc. IEEE Int. Symp. Wireless Pervasive Comput.*, Modena, Italy, May 2010, pp. 495–502.

[48] P. Pivato, L. Palopoli, and D. Petri, "Accuracy of RSS-based centroid localization algorithms in an indoor environment," *IEEE Trans. Instrum. Meas.*, vol. 60, no. 10, pp. 3451–3460, Oct. 2011.

[49] X. Li, "RSS-based location estimation with unknown path loss model," *IEEE Trans. Wireless Commun.*, vol. 5, no. 12, pp. 3626–3633, Dec. 2006.

[50] N. Salman, M. Ghogho, and A. Kemp, "On the joint estimation of the RSS-based location and path loss exponent," *IEEE Commun. Lett.*, vol. 1, no. 1, pp. 34–37, Feb. 2012.

[51] H. C. So and L. Lin, "Linear least squares approach for accurate received signal strength based source localization," *IEEE Trans. Signal Process.*, vol. 59, no. 8, pp. 4035–4040, Aug. 2011.

[52] G. Wang and K. Yang, "A new approach to sensor node localization using RSS measurements in wireless sensor networks," *IEEE Trans. Wireless Commun.*, vol. 10, no. 5, pp. 1389–1395, May 2011.

[53] G. Wang, H. Chen, Y. Li, and M. Jin, "On received-signal-strength based localization with unknown transmit power and path loss exponent," *IEEE Commun. Lett.*, vol. 1, no. 5, pp. 536–539, Oct. 2012.

[54] H. L. Van Trees, *Detection, Estimation, and Modulation Theory Part IV: Optimum Array Processing*. New York, NY: Wiley, 2002.

[55] S. M. Kay, *Fundamentals of Statistical Signal Processing: Estimation Theory*. Englewood Cliffs, NJ: Prentice-Hall, 1993.

[56] J. O. Smith and J. S. Abel, "Closed-form least-squares source location estimation from range-difference measurements," *IEEE Trans. Acoustics, Speech, Signal Process.*, vol. 35, no. 12, pp. 1661–1669, Dec. 1987.

[57] K. C. Ho and M. Sun, "An accurate algebraic closed-form solution for energy-based source localization," *IEEE Trans. Audio, Speech, Lang. Process.*, vol. 15, no. 8, pp. 2542–2550, Nov. 2007.

[58] F. K. W. Chan, H. C. So, J. Zheng, and K. W. K. Lui, "Best linear unbiased estimator approach for time-of-arrival based localization," *IET Signal Process.*, vol. 2, no. 2, pp. 156–162, Jun. 2008.

[59] B. C. Liu, K. H. Lin, and J. C. Wu, "Analysis of hyperbolic and circular positioning algorithms using stationary signal strength difference measurements in wireless communication," *IEEE Trans. Vehic. Tech.*, vol. 55, no. 2, pp. 499–509, Mar. 2006.

[60] B. C. Liu and K. H. Lin, "Distance difference error correction by least square for stationary signal-strength-difference-based hyperbolic location in cellular communication," *IEEE Trans. Vehic. Tech.*, vol. 57, no. 1, pp. 227–238, Jan. 2008.

[61] S. Wang and R. Inkol, "A near-optimal least squares solution to received signal strength difference based geolocation," in *Proc. IEEE Int. Conf. on Acoustics, Speech and Signal Process.*, Prague, Czech Republic, May 2011, pp. 2600–2603.

[62] R. M. Vaghefi, M. R. Gholami, and E. G. Strom, "RSS-based sensor localization with unknown transmit power," in *Proc. IEEE Int. Conf. Acoust., Speech, Signal Process.*, Prague, Czech Republic, May 2011, pp. 2480–2483.

[63] R. M. Vaghefi, M. R. Gholami, R. Buehrer, and E. Strom, "Cooperative received signal strength-based sensor localization with unknown transmit powers," *IEEE Trans. Signal Process.*, vol. 61, no. 6, pp. 1389-1403, Mar. 2013.

[64] M. R. Gholami, R. M. Vaghefi, and E. G. Strom, "RSS-based sensor localization in the presence of unknown channel parameters," *IEEE Trans. Signal Process.*, vol. 61, no. 15, pp. 3752–3759, Aug. 2013.

[65] A. Beck, P. Stoica, and J. Li, "Exact and approximate solutions of source localization problems," *IEEE Trans. Signal Process.*, vol. 56, no. 5, pp. 1770–1778, May 2008.

[66] R. A. Horn and C. R. Johnson, *Matrix Analysis*. Cambridge, UK: Cambridge Univ. Press, 1985.

[67] G. Golub and C. F. V. Loan, *Matrix Computations*. 3rd ed. Baltimore, MD: Johns Hopkins Univ. Press, 1996.

[68] W. Sun and Y.-X. Yuan, *Optimization Theory and Methods*. New York, NY: Springer, 2006.

[69] A. Antoniou and W.-S. Lu, *Practical Optimization: Algorithms and Engineering Applications*. New York, NY: Springer, 2007.

[70] S. S. Ghassemzadeh, R. Jana, C. W. Rice, W. Turin, and V. Tarokh, "A statistical path loss model for in-home UWB channels," in *Proc. IEEE Conf. Ultra Wideband Syst. Technol.*, Baltimore, MD, May 2002, pp. 59–64.

[71] S. Park, E. Serpedin, and K. Qaraqe, "Gaussian Assumption: The least favorable but the most useful," *IEEE Signal Process. Mag.*, vol. 30, pp. 183–186, Apr. 2013.

[72] S. N. Diggavi and T. M. Cover,, "The worst additive noise under a covariance constraint," *IEEE Trans. Inform Theory.*, vol. 47, no. 7, pp. 3072–3081, Nov. 2001.